Materials Science & Engineering R 142 (2020) 100580

Contents lists available at ScienceDirect

Materials Science & Engineering R

journal homepage: www.elsevier.com/locate/mser

Three-dimensional interconnected networks for thermally conductive polymer composites: Design, preparation, properties, and mechanisms

Fei Zhang[a], Yiyu Feng[a,b], Wei Feng[a,b,c,*]

[a] School of Materials Science and Engineering, Tianjin University, Tianjin Key Laboratory of Composite and Functional Materials, Tianjin 300072, PR China
[b] Collaborative Innovation Center of Chemical Science and Engineering, Tianjin 300072, PR China
[c] Key Laboratory of Advanced Ceramics and Machining Technology, Ministry of Education, Tianjin 300072, PR China

ARTICLE INFO

Keywords:
Thermal conductivity
Polymer composite
Graphene
Three-dimensional interconnected network

ABSTRACT

With the development of science and technology, microelectronic components have evolved to become increasingly integrated and miniaturized. As a result, thermal management, which can seriously impact the function, reliability, and lifetime of such components, has become a critical issue. Recently, the use of polymer-based thermal interface materials (TIMs) in thermal management systems has attracted considerable attention in view of the superior comprehensive properties of the former. Compared with designing and fabricating a polymer with an intrinsically high thermal conductivity, a more effective and widely used strategy for improving the heat conductivity is to fill a polymer matrix with a thermally conductive filler. Specifically, three-dimensional (3D) interconnected heat-conductive networks can increase the thermal conductivity (k) of polymers more effectively than dispersed fillers can, owing to their intrinsic continuous structures. In this review, we first introduce the heat conduction mechanisms and the problems associated with polymer-based TIMs fabricated using engineering polymer chains and traditional filling methods. Next, we discuss the advantages and mechanisms of 3D interconnected heat-conductive networks for preparing thermally conductive polymer-based composites. In addition, we highlight new advancements in the design and fabrication of 3D thermally conductive networks as well as their application in improving the k of polymers. Our exhaustive review of 3D interconnected networks includes graphene, carbon nanotubes, boron nitride, metal and other 3D hybrid architectures. The key structural parameters and control methods for improving the thermal properties of polymer composites are outlined. Finally, we summarize some effective strategies and possible challenges for the development of polymer-based thermally conductive composites via integration with 3D interconnected networks.

1. Introduction

Advances in science and technology have been accompanied by the evolution of microelectronic devices toward miniaturization, high levels of integration, and high power, thus imposing new requirements on and posing new challenges for traditional heat conductors. Owing to the augmentation of the frequencies and powers of semiconductor chips and the dense packing of integrated circuits, electronic devices and their components emit a considerable amount of heat energy to their surroundings during operation. Unless the generated heat can be dissipated effectively, it will be concentrated in some small areas. Such local hotspots with extremely high temperatures will strongly influence the performance and service life of microelectronic devices. Consequently, efficient heat management systems are essential for lowering the temperature of the local hotspots in high-power electronics [1–3]. As the critical component of heat management systems, thermal interface materials (TIMs) play an important role in dissipating heat in electronic devices. Undoubtedly, overheated environments have limited the development of microelectronics and integrated circuits with higher powers and levels of integration. Thus, efficient thermal

---

Abbreviations: TIMs, thermal interface materials; 3D, three-dimensional; CVD, chemical vapor deposition; GF, graphene foam; CNTs, carbon nanotubes; BN, boron nitride; AlN, aluminum nitride; PCM, phase change material; 1D, one-dimensional; 2D, two-dimensional; EMT, effective medium theory; MWCNTs, multiwalled carbon nanotubes; SWCNTs, single-walled carbon nanotubes; VACNTs, vertically aligned carbon nanotubes; rGO, reduced graphene oxide; PDMS, polydimethylsiloxane; GO, graphene oxide; PVA, polyvinyl alcohol; SEM, scanning electron microscopy; PU, polyurethane; TEM, transmission electron microscopy; PMMA, poly(methyl methacrylate); PP, polypropylene; PVDF, Polyvinylidene fluoride

[*] Corresponding author at: School of Materials Science and Engineering, Tianjin University, Tianjin Key Laboratory of Composite and Functional Materials, Tianjin 300072, PR China.

E-mail address: weifeng@tju.edu.cn (W. Feng).

https://doi.org/10.1016/j.mser.2020.100580
Received 28 February 2020; Received in revised form 20 June 2020; Accepted 30 July 2020

management systems are now emerging as a critical factor in realizing next-generation electronic devices.

Thermal management systems have become an integral part of the electronics and aerospace industries. As TIMs are the core components of thermal management systems, the thermal conductivity (k) of such a material directly determines the quality of the entire system. The excellent properties of organic polymers, such as electrical insulation, high flexibility, low weight, low cost, outstanding mechanical properties, and machinability, have enabled their wide use in various application fields over the past few decades [4]. However, multiple factors, including the amorphous arrangement and vibrations of the molecular chains, cause polymers to exhibit poor thermal conduction [5]. For most polymers, phonon thermal conduction is the dominant thermal conduction pathway. As the amorphous structure and vibrations of the macromolecular chains in polymers can induce massive phonon scattering, the vast majority of neat polymers are heat insulators or relatively poor heat conductors (k values of 0.1–0.5 W m^{-1} K^{-1}) [6–8]. Therefore, pure polymers cannot facilitate heat dissipation to accelerate the minimization and integration of components in the modern electronics industry.

Phonons, being the quantized collective modes of crystal lattice vibrations, are the primary thermal energy carriers in insulators [9,10]. Heat transfer in materials with high crystallinity can be realized through lattice vibrations within the material [1,11]. As shown in Fig. 1a, the conduction of thermal energy in a polymer matrix can be regarded as a phonon transfer process. Because of the high disorder of polymer chains, the phonon scattering phenomenon is quite pronounced in polymers, resulting in ultralow k values. The scattering of phonons mainly occurs via collisions between phonons and at interfaces between impurities and lattice defects. To address the low thermal conduction of polymers caused by their disordered molecular chains and improve their thermal conduction capability, two strategies can be implemented: (i) engineer the morphology of the polymer chains or (ii) fill the polymer matrix with a highly thermally conductive filler [12,13]. Improving the orientation and crystallinity of the polymer chains can decrease the disorder of the polymer molecules and thus effectively reduce phonon scattering (Fig. 1b). Similarly, compounding with thermally conductive fillers can effectively improve the heat transfer properties of a polymer. The thermally conductive fillers connect to each other to form a continuous three-dimensional (3D) network in the polymer matrix, which provides a high-speed channel for the transmission of phonons. Thus, heat transfer can be accelerated along the 3D network with decreased phonon scattering (Fig. 1c). Compared with the morphological design of polymer molecular chains, compounding polymers with thermally conductive fillers is a more efficient and convenient approach.

Over the past few decades, considerable research has been dedicated to the fabrication of polymer-based TIMs by compounding with dispersed filler particles. However, owing to the huge interfacial thermal resistance at filler–filler and filler–matrix interfaces, the resulting polymer composites only exhibited moderate improvements in k, even with large filler ratios. Additionally, the poor particle dispersibility and large loading levels of dispersed fillers severely degrade the polymer properties. These factors have prevented conductive fillers from reaching their full potential for enhancing the heat conduction of polymers. Recently, more attention has been focused on the construction of thermally conductive networks. As shown in Fig. 2, compared with dispersed filler particles, a preconstructed 3D thermally conductive architecture is a good candidate for creating high-performance polymer-based TIMs because it ensures good filler distribution and forms an interconnected network in the polymer matrix, both of which minimize the unfavorable effect of interfacial thermal resistance at filler–filler interfaces. Moreover, with such architectures, the improvement can be maximized with a minimal filling ratio. The construction methods for 3D continuous thermally conductive networks include in situ chemical vapor deposition (CVD) growth, sol–gel methods, self-assembly, and template methods. Almost all thermally conductive fillers can form 3D thermally conductive frameworks, and the most widely used include graphene foams (GFs), carbon nanotube (CNT) frameworks, boron nitride (BN) networks, and hybrid architectures of several fillers [2,14,15]. The popularity of these materials is primarily due to their inherently good thermally conductivities, low weights, large specific surface areas, and excellent comprehensive performance. A percolated skeletal network provides sufficient phonon transfer pathways with abundant interfacial contact points, which can effectively weaken phonon interface scattering. As a result, constructing a continuous 3D architecture as the thermal enhancer in a polymer matrix is an effective strategy for preparing high-performance TIMs, and hence, has become a current research trend.

Herein, we review numerous studies pertaining to the preparation of heat-conductive polymers and polymer composites with high k values by filling with thermally conductive fillers in the form of conventional dispersed filler particles or interconnected 3D networks. Although there are many reviews of thermally conductive polymer-based composites [8,16,17], systematic assessments of the effect of 3D networks on improving the k values of polymers and comparisons between the two aforementioned compounding strategies are rare. In view of this, it is essential to review the advances in 3D framework-strengthened polymer composites. Here, we provide an overview of the recent literature on enhancing thermal conduction via 3D framework-improved polymers and discuss the advantages of this strategy over the traditional mixed filling method. Additionally, the preparation methods and factors that influence the properties of polymer composites with different types of 3D structures are examined. A brief overview of the existing 3D heat-conducting frameworks is shown in Fig. 3.

2. Intrinsic thermally conductive polymers

In practice, the inferior k of polymers is one of the major technological barriers for advancements in electronic devices. Improving the heat transfer performance of polymers is crucial and has become a long-standing hot research topic. Generally, disordered polymer molecular

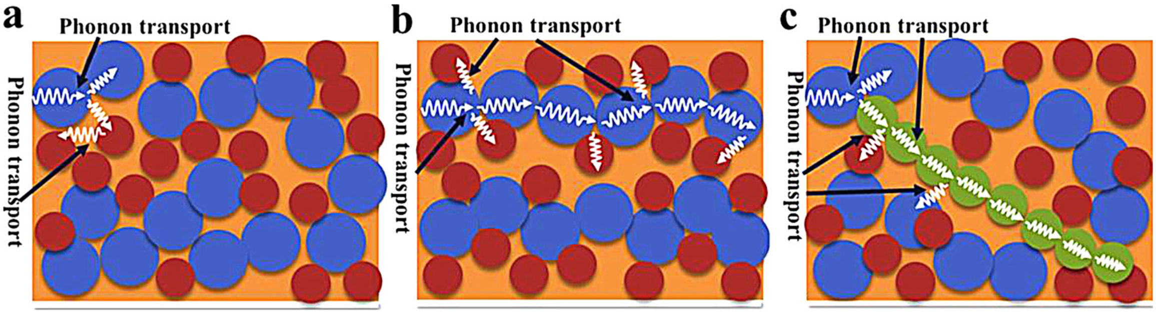

Fig. 1. Schematic diagrams of heat transfer in (a) a pure polymer, (b) a polymer with enhanced chain orientation, and (c) a polymer filled with a thermally conductive filler [11]. Copyright 2019, Elsevier Ltd.

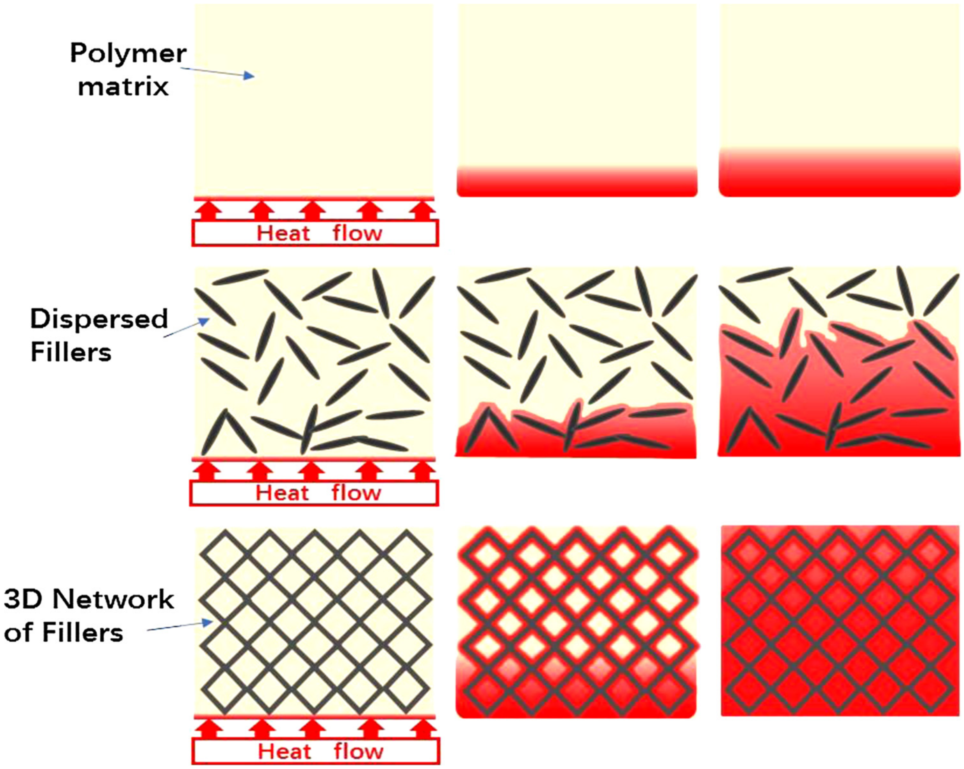

Fig. 2. Schematic diagrams of heat transport in a pure polymer, a polymer composite filled with a traditional dispersed filler, and a composite filled with a 3D interconnected network of fillers.

chains and weak molecular interactions are responsible for the poor *k* values of polymers, as shown in Fig. 4a, b. The amorphous structure and the vibrations of polymer chains can considerably reduce the mean free path of phonons and cause extensive phonon scattering. Therefore, the heat-conducting behavior of polymers can be greatly enhanced by engineering the morphology of polymer chains, for example, by improving the chain orientation, crystallinity, and molecular interactions (Fig. 4c). Common methods for engineering polymer chains include mechanical stretching, template-assisted growth, electrospinning, and surface grafting.

Many efforts have been devoted to engineering the orientation of polymer chains and improving polymer crystallinity, which are

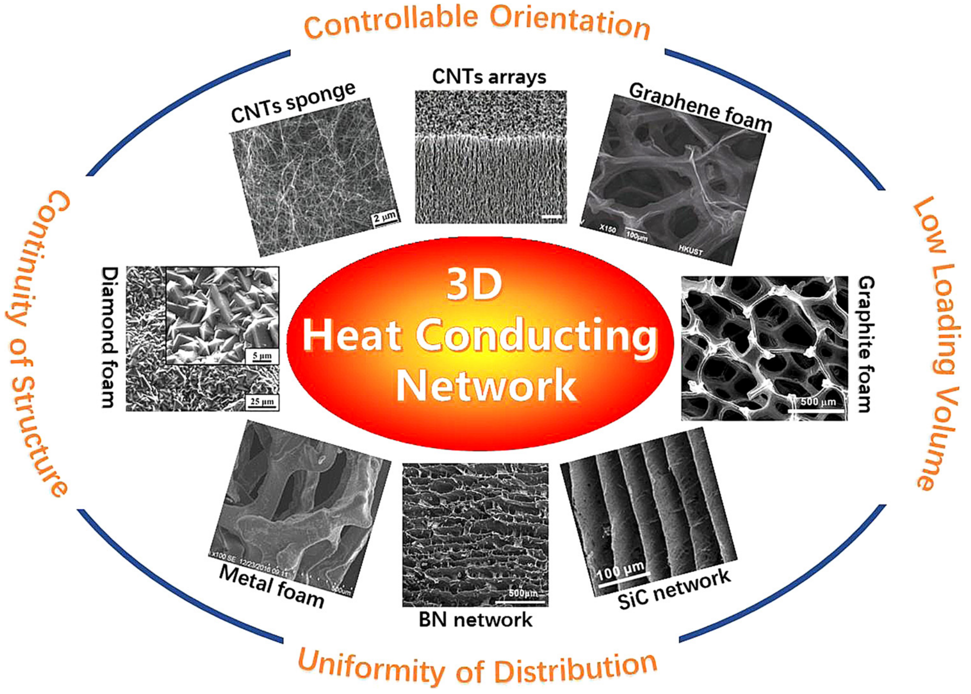

Fig. 3. Overview of existing 3D heat-conducting networks and their advantages as fillers [18–25]. Copyright, Wiley-VCH; Elsevier Ltd.; American Chemical Society; American Association for the Advancement of Science.

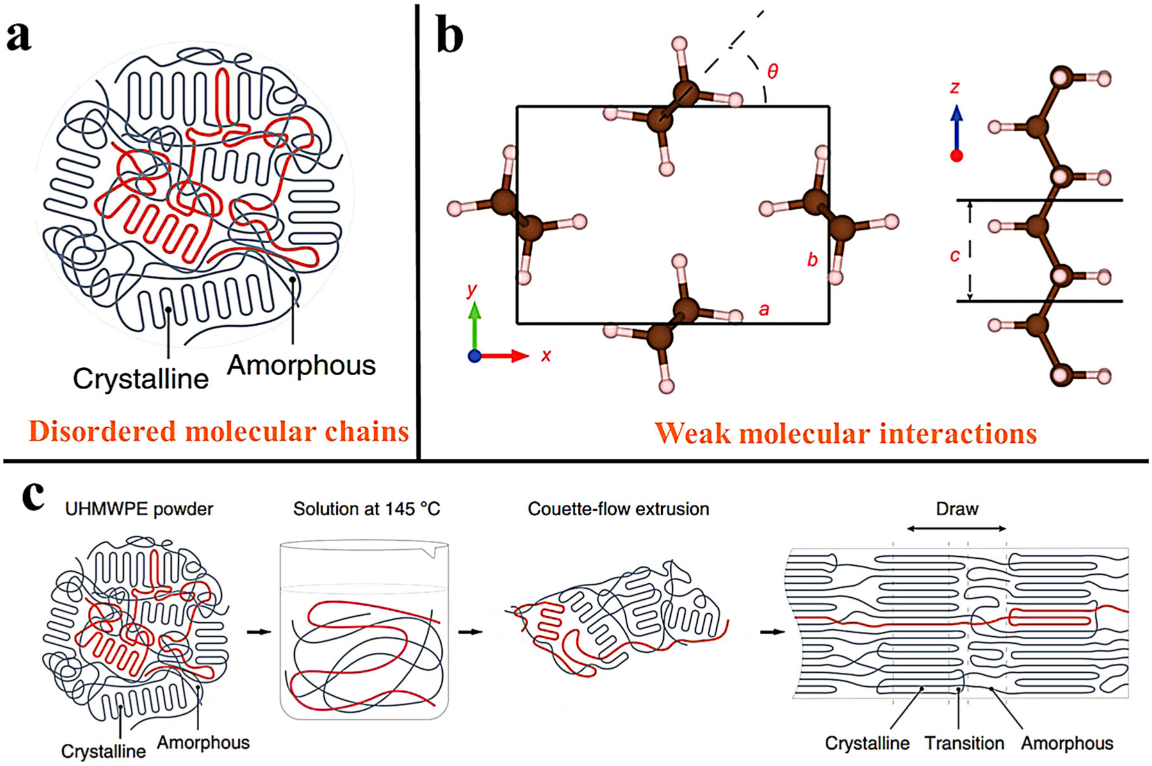

Fig. 4. (a) Illustration of the molecular chain of a polymer [28]. (b) Structure of a bulk plasma-enhanced (PE) crystal and a single-chain PE crystal [27]. Copyright 2017, Royal Society of Chemistry. (c) Illustration of the evolution of an oriented crystallite–interconnected film morphology during fabrication [28]. Copyright 2019, Nature Publishing Group.

considered essential for improving the *k*. Atomistic simulations have shown that an individual crystalline polymer chain always possesses a high *k* value [26,27]. Cahill et al. found that crystalline polyethylene fibers had a high *k* value of up to 20 W m^{-1} K^{-1}. Xu et al. [28] devised and synthesized nanostructured polyethylene films, which possessed an ultrahigh *k* value of 62 W m^{-1} K^{-1}, by minimizing the entanglement and maximizing the alignment of chains. Nanofibers with crystalline and amorphous regions along the fiber axis realized a remarkably high *k* value, which was responsible for the ultrahigh *k* value of the polyethylene film. Chen et al. [29] fabricated highly crystalline polyethylene nanofibers with diameters of 50–500 nm and lengths on the order of millimeters by stretching, and the *k* values of these nanofibers along the chain direction were as high as 104 W m^{-1} K^{-1}. Even amorphous polythiophene nanofibers achieved a high *k* value (~4.4 W m^{-1} K^{-1}) upon orientation of the molecular chains along the fiber axis using nanoscale templates [30].

Strengthening intramolecular interactions can also effectively improve the heat conduction of polymers. Inferior interchain phonon transport is caused by weak van der Waals interactions between individual chains. Thus, using intermolecular hydrogen bonding and conjugated bonds to displace van der Waals interactions is an effective method of increasing phonon transport across polymer chains. Kim et al. [5] exploited intermolecular hydrogen bonding to achieve a considerable improvement in the cross-plane *k* value (surpassing 1.5 W m^{-1} K^{-1}) in amorphous polymer films. Xu et al. [31] realized a high *k* value in a conjugated polymer film (up to 2.2 W m^{-1} K^{-1}) by means of strong C=C covalent bonding along the polymer chains and strong π–π stacking noncovalent interactions between the chains.

In summary, phonon transport along polymer chains can be effectively improved by increasing the crystallinity, maximizing chain orientation, and strengthening intramolecular and intermolecular interactions. At present, the most common method of increasing molecular chain alignment and crystallinity is to draw polymeric fibers or thin films [32] but this morphology severally limits thermal applications. It is still difficult to engineer the crystallinity and molecular chain orientation of bulk polymers over a wide range for use as thermal conductors [27]. Furthermore, not all polymers are amenable to the strategy of enhancing *k* by regulating morphology. In fact, this approach has narrow applicability, as it is only suitable for polymers that can crystallize easily and for those with linear molecular chains.

3. Polymer-based composites with dispersed fillers

Compared with improving the thermal conduction of polymers by engineering the morphology of their molecular chains, blending polymers with thermally conductive fillers is considered more efficient and convenient, and is applicable to almost all polymers. Owing to advances in nanotechnology, various new conductive fillers of different types, morphologies, sizes, and properties have been produced, which provides more options for the preparation of thermally conductive polymer composites. The heat-conducting mechanism in polymer composites is the formation of a highly heat-conductive transmission network of fillers [33]. Therefore, the formation of a filler percolation network plays key role in enhancing the *k* of polymer composites.

3.1. Blending with dispersed filler particles

Owing to their machinability and low cost, polymer composites with superior thermal conduction have been the primary choice for high-performance TIMs. Blending the filler particles with the polymer is a convenient and effective method for preparing polymer-based composites. Extensive research has been concentrated on the introduction of thermally conductive fillers, such as various carbon materials, metal particles, ceramic oxides (Al_2O_3, SiO_2), and nitrides (BN, aluminum nitride (AlN)), into a polymer matrix [21,34–37]. In particular, low-dimensional nanofillers with high *k* values (e.g., graphene sheets, CNTs, BN nanosheets, and metallic nanoparticles) are advantageous because of their excellent thermal conduction [38]. Balandin et al. [39] reported

Table 1
Thermal conductivity (k) values of various polymer composites with randomly dispersed filler particles.

Fillers	Polymer matrix	Solid loading	k (W m^{-1} K^{-1})	Enhancement in k (%)	Refs
BN/Diamond	Polyimide	40 wt%	0.98	420	2018 [42]
Graphene	PP	10 wt%	1.5	650	2017 [43]
Graphene	Polyimide	8 wt%	2.78	1440	2018 [44]
BN	Polyimide	60 vol%	7	3400	2010 [45]
Graphite/CNTs	Epoxy	10 wt%	1.75	775	2008 [46]
Graphene	PS	10 wt%	2.6	1344	2017 [47]
Graphene/CNTs	rubber	3 wt%	0.45	200	2017 [48]
BN/Al2O3	Epoxy	50 wt%	0.808	334	2014 [49]
Graphene/CNTs	Epoxy	20 wt%	2.41	1100	2013 [50]
BN	Polyimide	30 wt%	1.2	500	2010 [51]
SiC nanowire	PS	23.1 vol %	1.88	840	2013 [52]
ZnO	Polyimide	27.1 vol %	1.54	410	2011 [53]
CNTs/SiC	Epoxy	60 wt%	6.8	3300	2010 [54]
BN	PVA	30 wt%	4.41	2100	2013 [55]
Graphene	Epoxy	10 wt%	1.53	665	2013 [56]
BN	PMMA	24 wt%	3.16	2006	2009 [57]
SWCNTs	Epoxy	2.3 wt%	0.61	220	2006 [58]
BN	Epoxy	40 wt%	5.86	2510	2020 [59]

a hydrocarbon-based phase change material (PCM) filled with 20 wt% graphene nanosheets. The addition of graphene enhanced the k value by more than two orders of magnitude while simultaneously preserving its inherent ability to store latent heat. Shahil et al. [40] prepared a conductive composite by mixing monolayer/multilayer graphene sheets with an epoxy. A k value of 5.1 W m^{-1} K^{-1} was achieved at 10 vol% loading, corresponding to an improvement of approximately 2300 % in k. Shtein et al. [41] reported that the use of graphene nanosheets as fillers could increase the heat conduction of epoxy, and the composite possessed an ultrahigh k value of 12.4 W m^{-1} K^{-1} at 25 vol% loading. Table 1 summarizes the k values of previously reported polymer-based composites with various dispersed fillers.

The general preparation process for polymer composites with blended fillers is shown in Fig. 5a. Briefly, a certain amount of filler nanoparticles is mixed with the polymer in a solvent to form a homogeneous precursor with the assistance of ultrasonic vibration or strong stirring. As a result, the filler is uniformly dispersed in the matrix. Then, a thermally conductive composite is obtained through in situ polymerization, followed by curing in a mold under suitable conditions, such as high temperature or light. A percolation network of fillers can usually be formed when the packing amount of the filler is sufficient (Fig. 5b). This facile method is not only convenient but also low cost without any requirements for complex equipment. Therefore, it has become the most commonly used method for preparing polymer-based composites.

3.2. Factors affecting thermal conduction

The thermal conduction of polymers with dispersed filler particles is affected by several factors, including the filler type and size, the filling ratio, the dispersion of filler particles, and interfacial thermal resistance.

3.2.1. Filler type and size

Highly thermally conductive fillers can be classified into three categories: carbon-based fillers (carbon fibers, CNTs, graphene, graphite, diamond, etc.), metallic fillers (copper, aluminum, sliver, etc.), and ceramic fillers (Al_2O_3, AlN, BN, SiC, etc.) [21,35,36]. Different types of fillers can be selected according to the application requirements. Generally, polymers filled with carbon-based fillers (except diamond) and metallic fillers exhibit simultaneous improvements in thermal and electrical conduction. The excellent electrical insulation properties of ceramic fillers allow polymer composites to maintain their electrical insulation performance while increasing their thermal conduction. This behavior makes polymers with ceramic-based fillers suitable for applications in electronic packaging.

Furthermore, filler shape and size also have considerable influence on the k of polymer-based composites. For example, it has been reported that long CNTs have a better upgrading effect than short CNTs do in polymer composites [60], and that graphene sheets of different sizes and thicknesses have different effects on enhancing the k of polymers. Some reports have suggested that the greater the thickness and the horizontal size of graphene sheets, the higher the k values of the resultant graphene/polycarbonate composites [61]. Some studies have also indicated that despite the higher intrinsic k values of nanofillers, composites with micro-sized fillers exhibit higher efficiency improvements than those with nanosized fillers. The high surface energy resulting from the enormous specific surface area of nanofillers renders their uniform dispersion in a polymer matrix difficult, which may create a large interfacial resistance in composites. In contrast, the small surface area of micro-sized fillers can decrease the interfacial area and the thermal resistance at filler–polymer interfaces.

In addition, some studies have suggested that heat conduction can

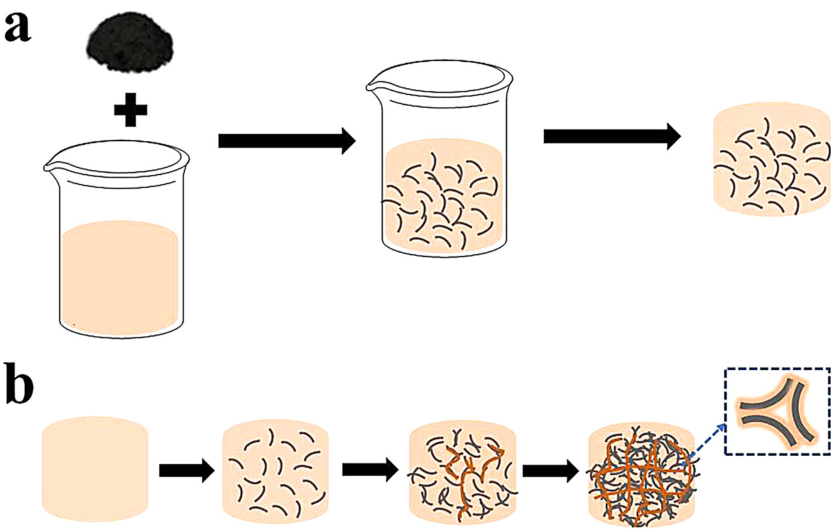

Fig. 5. (a) General preparation process for polymer composites by facile solution blending. (b) Distribution of different filler contents in the polymer matrix.

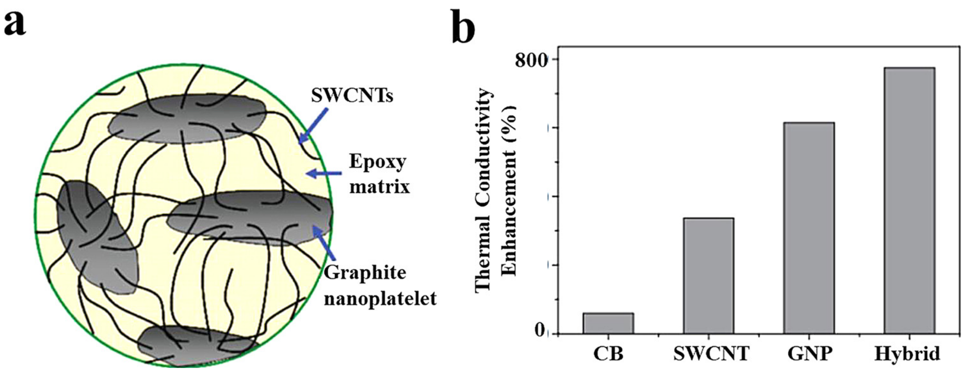

Fig. 6. (a) Schematic diagram of a thermally conductive network of graphite–CNTs in polymer composites. (b) Enhanced values for the thermal conduction of epoxy composites with carbon black, CNTs, graphite sheets, and a graphite–CNTs hybrid filler at 10 % loading [46]. Copyright 2008, Wiley-VCH.

be effectively enhanced by incorporating a combination of different types of fillers, e.g., microsized and nanosized fillers. Compared with fillers with a single morphology and size, the synergistic effect of multiple structures makes it easier to construct a heat-conductive network in a polymer matrix [62]. This behavior can be observed in Fig. 6, wherein CNTs and graphite sheets as hybrid fillers easily form a continuous network, with the one-dimensional (1D) CNTs bridging the adjacent two-dimensional (2D) platelets to create additional pathways for heat flow [46]. Steve and co-workers [51] prepared a thermally conductive polyimide composite film using hybrid micro-/nanosized BN particles as fillers, and the k value of this composite was up to 1.2 W m^{-1} K^{-1} with 30 wt% BN. Xie [63] prepared a thermal grease filled with 1 wt% graphene sheets and 63 vol% Al_2O_3 particles, and this combination of hybrid fillers improved the k value of the grease from 2.7 to 3.45 W m^{-1} K^{-1}.

3.2.2. Filling ratio

Generally, thermally conductive polymer nanocomposites are fabricated via mechanical mixing or chemical bonding methods to achieve synergistic interactions between the polymer and the fillers. However, even though the individual filler particles possess ultrahigh k values, it is difficult to completely transfer their excellent thermal conduction properties to the polymer. As a result, until now, the k values of polymer-based composites have been low (generally ≤ 10 W m^{-1} K^{-1}). This is because effective heat conduction improvement often requires a large filling ratio to create a continuous filler network, which in turn, reduces the interfacial thermal resistance.

The effective medium theory (EMT) can be used to understand the heat transfer performance of a polymer-based composite with dispersed fillers. As shown in Fig. 5b, with a small filler concentration, heat cannot be transferred from one particle to a neighboring particle, because the space between adjacent particles is considerably larger than the particles themselves. When the filler concentration is increased, clusters are formed via aggregation of filler particles. This close contact between thermally conductive filler particles is beneficial for the formation of efficient heat transport pathways. The greater the filling ratio, the larger the number of heat transfer routes formed in the polymer composite and the higher the k value of the material. Therefore, based on this theory, a high k value can only be achieved in polymer-based composites with large filler loadings [7,34].

In the case of polymer composites, a thermal conduction mechanism based on percolation theory, which is similar to the mechanism of electrical conduction, has been widely accepted. As shown in Fig. 7, polymer composites prepared by the blending method often require filling with a large volume fraction of thermally conductive particles (generally, $>$ 30 vol%) to achieve a significant enhancement in thermal conduction. This thermal percolation threshold is much larger than the electrical percolation threshold (≤ 5 vol%) [64]. When the filler concentration is low, the particles are independent of each other, and no filler network can be formed. In this case, the heat conduction is determined by the filler–matrix coupling, the interfacial thermal resistance between the matrix and the fillers, and the geometry and concentration of the filler particles [41]. With a sufficiently high filler concentration, contact occurs between the filler and thermal conduction pathways are formed because there is insufficient volumetric space.

Although large concentrations of fillers significantly improve the k of polymer composites, other critical properties of the polymers, such as insulating properties, optical properties, machinability, and mechanical properties, will be severely weakened. In addition, a large volume fraction of fillers in a polymer matrix may result in uneven surfaces, low flexibility, fragility, high weights, and poor mechanical performance. These limitations are attributed to weak polymer–particle interfacial adhesion and the agglomeration of filler particles.

3.2.3. Dispersion and interfacial compatibility

With nanofillers uniformly dispersed in a polymer matrix, significant phonon scattering is inevitable at the nanofiller–polymer and nanofiller–nanofiller interfaces. The large thermal resistance at these interfaces is the primary reason for the poor k of polymer composites with dispersed filler particles [65]. In polymer-based composites, the thermal resistance mainly consists of (i) the intrinsic thermal resistance of the polymer and the fillers, (ii) the interfacial resistance at the filler–polymer interface, and (iii) the thermal resistance among filler particles. Among these, the interfacial thermal resistance at the filler–polymer and filler–filler interfaces determines the k of the composite material.

Although the k values of polymers with filler networks may be superior to those of polymers without a network, they are still poor owing to the ultrahigh contact thermal resistance among filler particles. During the mixing and dispersing process, the surfaces of the filler particles will mostly be coated with a layer of the polymer, which inhibits real contact among the filler particles in the polymer matrix. As a result, the contact thermal resistance among adjacent particles increases, which affects the formation of a heat-conducting network. In polymer composites, the thermal conductance across filler–filler particle contacts dominates the thermal transport rather than the heat conductance inside the filler particles [66]. Thus, the existence of interfacial contact resistance has a detrimental impact on hotspot remediation, even if the lateral thermal conductivity is very high. Consequently, controlling the thermal boundary resistance and improving the contacts at the interfaces among the thermally conductive filler particles are equally important for both fundamental research and practical applications [67].

In most cases, the fillers, especially nanoparticles such as graphene nanosheets, CNTs, and BN nanosheets, aggregate during processing in solution because of their high surface energy, which is attributed to π–π interactions and van der Waals forces. As a result, the dispersion of

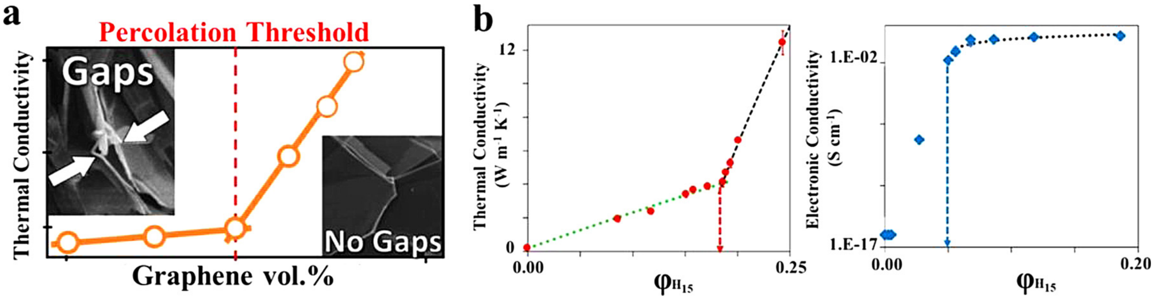

Fig. 7. (a) Percolation threshold for thermal conduction in graphene–polymer composites. (b) Comparison of the thermal and electrical percolation thresholds of graphene–polymer composites [41]. Copyright 2015, American Chemical Society.

these fillers is difficult, and their agglomeration occurs easily [68,69]. The agglomeration of nanostructured fillers can hinder phonon transport and hence adversely influence the heat transport characteristics of polymer-based composites. To obtain polymer composites containing homogeneously dispersed filler particles, it is often necessary to modify the filler particle surfaces, which can improve their dispersion as well as the compatibility between the matrix and the filler [70,71]. Furthermore, the formation of strong covalent interface between the modified fillers and the polymer can minimize phonon scattering at the filler–polymer interface. Hubmann et al. [72] modified multiwalled CNTs (MWCNTs) via oxidative functionalization by soaking them in an acid mixture, which improved the thermal conduction of the polymer composite. This work indicated that the surface functionalization of filler particles is an efficient way to lower the thermal interface resistance and prepare a polymer-based composite with excellent heat transfer performance. Jiang et al. [49] functionalized BN and Al_2O_3 with a hyperbranched aromatic polyamide, which was suggested to enhance the compatibility of the fillers with the polymer matrix and improved their dispersibility.

Surface modification with various chemical groups is an effective strategy for optimizing the dispersion and compatibility of the filler particles in a polymer matrix. However, although surface functionalization of the filler particles results in uniform dispersion and stronger connections with the polymers, it can weaken the mechanical robustness and intrinsic superior heat conductivity of the fillers by destroying their surface structures. Some researchers have verified that the heat conductivities of fillers are extraordinarily sensitive to the presence of defects and functionalization, with the addition of surface chemical groups inducing a thermal barrier that decreases the effects of fillers on k enhancement [12,22,73,74]. This is because the existence of extra chemical bonds on the surfaces of the fillers destroys the integrity of their crystal structures [75–77]. Molecular and lattice dynamics simulations revealed that chemical functionalization of a pristine graphene monolayer could reduce the k value by more than 40-fold (Fig. 8a) [77], and a defect concentration of only 0.25 % in graphene could reduce the thermal conductivity by more than 50 % (Fig. 8b) [78]. The intrinsic k of a filler is one of the primary factors governing the k of a polymer-based composite. The higher the k value of a filler, the greater the enhancement of the thermal conduction of the composite. The presence of structural defects and chemical functional groups on the filler surface dramatically restricts phonon migration and leads to substantial phonon scattering, which will reduce the intrinsic k of the filler and eventually impact heat transfer in the polymer matrix detrimentally. Kim et al. [79] reported that phenolic resin composites with highly crystalline CNTs had better k values than defective CNTs (Fig. 8c).

In addition, the thermal resistance at filler-polymer interface mainly originates from a large mismatch between the inherent phonon spectra [80,81]. Therefore, irrespective of the type of surface functionalization, the lattice vibration energy will be severely weakened and scattered at the filler–polymer interface. Hence, it is reasonable to believe that the surface modification of fillers is not an advisable method for improving the dispersion of fillers in polymers, as it impairs their intrinsic thermal conduction properties.

3.3. Theoretical calculations of dispersed filler systems

In previous reports, the k values of polymer-based composites were predicted using various theoretical models, such as the Bruggeman model, the Maxwell model, the Cheng–Vachon model, and the two-phase Lewis–Nielsen model. However, all these theoretical models are limited by the assumption that the fillers are randomly distributed spherical or cylindrical particles. This assumption cannot reflect the actual microscopic irregularities in the filler shape and distribution, especially when a continuous filler network is formed at a large filler ratio. For example, as the most representative model, the Maxwell model can be expressed as

$$k = \frac{2k_1 + k_2 + 2V_2(k_2 - k_1)}{2k_1 + k_2 - V_2(k_2 - k_1)}k_1 \tag{1}$$

where k represents the effective thermal conductivity of the composite;

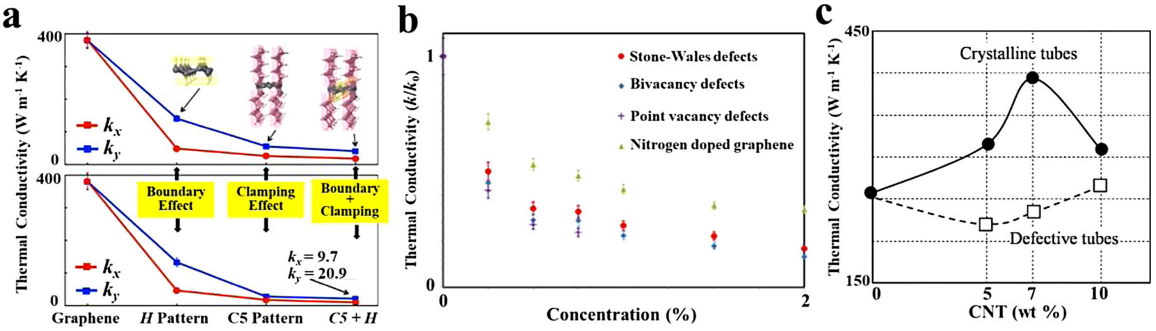

Fig. 8. (a) Influences of chemical groups on the k values of monolayer graphene [77]. Copyright 2012, American Chemical Society. (b) Normalized k values of graphene as a function of defect concentration [78]. Copyright 2013, Elsevier Ltd. (c) k values of CNT–phenolic composites with highly crystalline CNTs and defective CNTs [79]. Copyright 2007, American Institute of Physics.

V_2 represents the volume fraction of the filler; and k_1 and k_2 are the thermal conductivity values of the polymer matrix and the filler, respectively. In addition, this model assumes that all the filler particles are spherical and are sufficiently separated from each other, which means that each isolated sphere is randomly embedded in a polymer matrix and is not affected by the presence of other particles. Considering this assumption, it can be inferred that the Maxwell model is only suitable for composites with dilute filler concentrations.

Subsequently, other theoretical models based on EMT and percolation theory have been proposed, which have proved useful for understanding the heat transfer mechanism in nanocomposites. EMT is usually used to model the k values of polymer composites with randomly dispersed fillers [82], where the k value of the composite obeys the following equation:

$$k = k_m \frac{3 + 2V_f\left(\frac{k_p - k_m}{k_m}\right)}{3 - V_f\left[(1-\alpha) - \frac{k_m}{k_p}\right]} \tag{2}$$

$$\alpha = \frac{R_{BD}K_m}{d} \tag{3}$$

where k_p and k_m are the thermal conductivity values of the filler and the polymer, respectively; V_f is the volume fraction of the filler; R_{BD} is the thermal resistance between the filler nanoparticles and the polymer; and d is the size of the filler particles. The EMT model assumes that the filler particles are completely surrounded by the polymer matrix and can provide a reasonable R_{BD} value for the polymer composite.

In percolation theory, the relationship between the effective k value of a polymer composite and the filler volume fraction can be expressed as

$$k \propto k_2(V_2 - V_c)^n \tag{4}$$

where k is the thermal conductivity value of the composite; k_2 is the thermal conductivity value of the filler; V_2 is the volume fraction of the filler; V_{c} is the percolation threshold; and n is a percolation exponent. According to percolation theory, the k value will increase rapidly when the filler ratio exceeds the percolation threshold value. When the ratio is below the threshold value, the enhancement effect of the filler is negligible and the threshold conduction of the composite is the same or slightly higher than that of the polymer [83,84].

In summary, the heat conduction of polymers can be enhanced by compounding polymers with thermally conductive fillers. However, the resulting polymer composite displays only a moderate enhancement in thermal conduction. Sufficient improvements in thermal conduction often require that the filler satisfy several fundamental requirements, such as high quality, uniform dispersion, and a high-volume fraction, which are often difficult to fulfill simultaneously. In composites with dispersed filler particles, random dispersion in the polymer almost always causes transverse contact between filler particles over a relatively small contact area, which leads to a very high thermal resistance that dominates the overall thermal resistance [70]. As a consequence, the composites with a low filler content will lead to the inferior improvement in k values, but the high filling ratio of fillers will weaken the processability and mechanical properties of the polymers. In this condition, it is possible to overcome these thermal barriers by creating new interfacial architectures with inherently low thermal interface resistance.

4. Polymer-based composites with preconstructed 3D frameworks

According to Maxwell's mixing theory, single-walled CNTs (SWCNTs) should improve the k value of a polymer by 50-fold at a volume fraction of 1%. However, such improvements cannot be achieved in practice, as the experimentally observed improvement is at least an order of magnitude less than expected [85]. This contrast results from the huge thermal resistance inside the composite, which mainly consists of the thermal resistance at the filler–polymer interface and the interfacial resistance between individual filler particles. Based on the concept of Kapitza resistance, interfacial resistance occurs because of a modulus mismatch between the matrix and the filler, and the greater the mismatch, the greater the resistance [85,86]. Therefore, interfacial resistance at the matrix–filler interface is unavoidable in polymer-based composites. Fortunately, the interfacial contact thermal resistance among individual filler particles can be significantly reduced through structural design. The construction of a 3D-connected conduction network is an efficient and feasible strategy for reducing the interfacial resistance among the filler particles.

All highly thermally conductive fillers can be constructed into 3D interconnected thermal conductivity networks using various methods. As CNTs and graphene present the best k values among known conductors, there have been many reports on the construction of their 3D conductive networks. Recently, BN-based 2D fillers have also attracted extensive attention because of their unique electrical insulation properties, which are significant for thermal management systems in microelectronic devices.

4.1. 3D conductive architectures

Using nonequilibrium molecular dynamics simulations, novel interfacial carbon-based architectures have been engineered to create 3D thermal transport networks, including a 3D pillared-graphene framework consisting of graphene and CNTs, and CNT-based 3D porous network structures (Fig. 9a, b). By investigating the phonon thermal transport behavior in these new network structures with covalent bond connections, Varshney et al. [70,87] found that these architectures exhibited inherently low interface thermal resistance owing to the presence of perfect junctions. As shown in Fig. 9c, the high axial thermal conductivity of a unique graphene–CNT structure results from the replacement of noncovalent interactions with covalent bonding. Additionally, the CNT-dense regions in the graphene–CNT structure also influence the axial heat transfer because a larger inter-CNT interaction (χ) in such regions enhance phonon scattering [88]. The graphene and CNT network nanostructures play important roles in improving the overall k of materials, as the junctions between these fillers have a remarkably low resistance, which enables heat to be transferred in an efficient manner. These studies confirm that the construction of a 3D network can provide a larger contact area for efficient heat removal, and the thermal transport performance of such systems exceeds that of state-of-the-art TIMs by two to three orders of magnitude [87].

Thus, a 3D continuous framework can effectively enhance the k of polymers. Recent research suggests that the buildup of a graphene framework is conducive to overcoming the dispersion inhomogeneity while simultaneously endowing materials with highly favorable comprehensive properties [90,91]. Furthermore, a 3D continuous filler framework helps avoid redundancies in the thermal resistance by reducing the number of interfaces between the matrix and the filler, thus ensuring that sufficient phonons can be transported through the 3D network. In addition, this method can realize the formation of a 3D transport network in the polymer matrix at extremely low filler concentrations.

Percolating composites with ultralow filler ratios can be prepared by utilizing the 3D filler framework as a conductive network; the general preparation process is shown in Fig. 10 [92]. 3D continuous frameworks are usually prepared by two strategies. The first strategy is to prepare the 3D framework directly through in situ growth by CVD. For example, Cheng [93] built a 3D GF through CVD on a nickel foam template, and Xu [94] and Gui [25] prepared 3D CNT frameworks by CVD. The second strategy is to assemble nanoparticles or nanosheets of the fillers into a 3D network architecture. By backfilling the polymer into the filler framework, the 3D network structure can be impregnated with or embedded in the polymer without disrupting the monolithic structure of the filler, with the final composite obtained after a curing

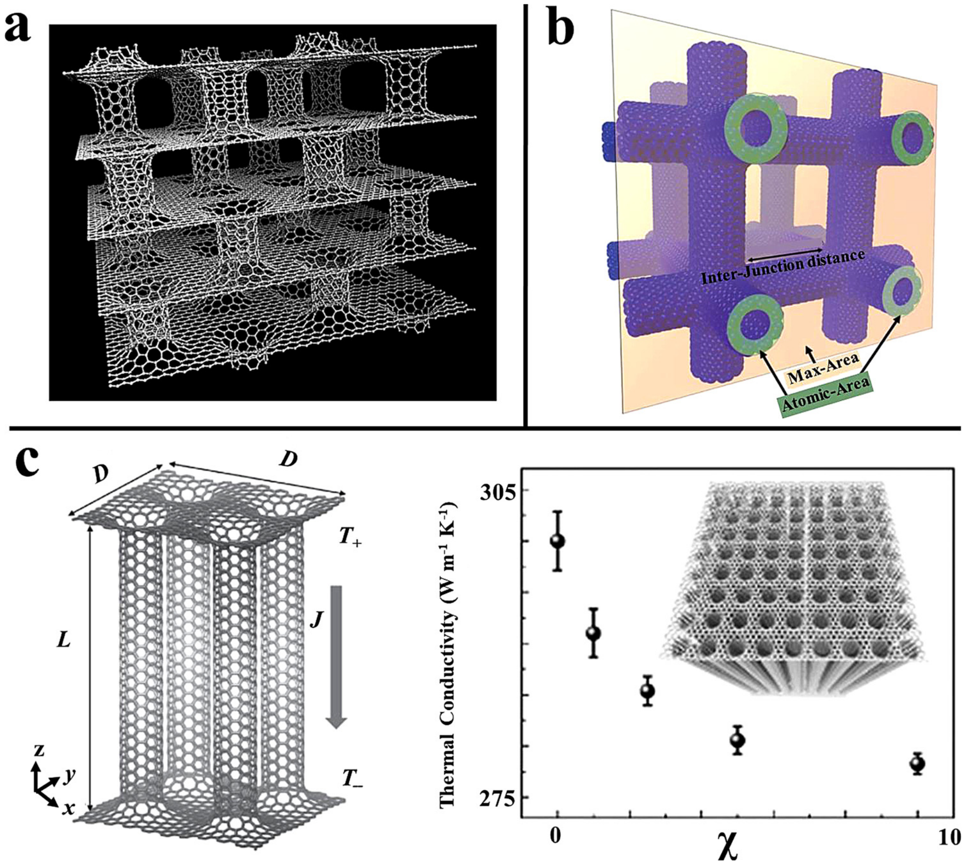

Fig. 9. (a) Simulation of a novel 3D graphene–CNT network nanostructure [89]. Copyright 2012, American Chemical Society. (b) Simulation of porous nanotube 3D network structures [87]. Copyright 2011, Royal Society of Chemistry. (c) Molecular dynamics simulation of the cross-plane k of a graphene–CNT hybrid structure at ambient temperature [88]. Copyright 2015, Wiley-VCH.

process. As the 3D connective framework is completely preserved during the compounding process, the interconnected structures are not destroyed. This interconnected framework not only has a significant mechanical enhancement effect on the composite but also provides a fast transmission channel and a large number of transmission pathways for phonons, which can significantly enhance the k of the composite.

4.1.1. Heat transfer improvement efficiency

The continuous framework of a thermally conductive filler has excellent heat transfer performance because the interconnected structure has lower thermal interfacial resistance. Zhang's group [19] reported that the interfacial thermal resistance of an interconnected GF was low at the Si–Al interface (0.04 cm^2 K W^{-1}), which is more than 12 times lower than those of conventional thermal greases and thermal pastes. Other researchers have found that the interfacial thermal resistance of freestanding vertically aligned CNTs (VACNTs) was as low as 0.07 cm^2 K W^{-1} [95,96]. Liang and co-workers [97] proposed high-performance TIMs using a freestanding multilayer reduced graphene oxide (rGO) skeleton with a thermal interfacial resistance of approximately 0.07 cm^2 K W^{-1}.

From the abundant literature on the development of thermally conductive polymer-based composites, we have collated data on the two preparation methods, namely, using a dispersed filler and using a 3D interconnected framework, as listed in Tables 1 and 2, respectively. To compare the influence of the filling method on the properties of the thermally conductive composites, we have summarized the thermal performance of the polymer composites in terms of the k values of the composites against the filler mass fractions, as shown in Fig. 11a. The composites with 3D interconnected networks achieve high k values more easily at relatively low filling fractions, whereas for composites with dispersed fillers, it is difficult to obtain satisfactory k values. For a better comparison of the contributions of the two methods to the improvement of the k of composites, we quantified the filler load to compare the k values of composites under unit filling. This evaluation obviously reveals that interconnected 3D structures have a greater advantage in enhancing the k of composites.

For thermally conductive composites, it is important to realize high enhancements in k at low filler loadings. To accurately reflect the superiority of 3D architectures in improving the heat conduction of the polymers, the enhancement efficiencies (η) of 3D filler frameworks and dispersed fillers in polymer composites were characterized using the enhancement achieved with respect to the wt% loading, which can be defined as:

$$\eta = \frac{k - k_p}{100 \times M_f \times k_p} \times 100\% \tag{5}$$

where k and k_p are the thermal conductivity values of the polymer composite and the pristine polymer, respectively; and M_f is the loading

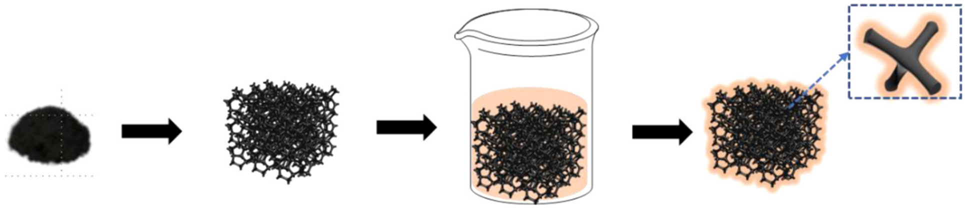

Fig. 10. General preparation process for polymer composites by compounding with a 3D continuous framework.

Table 2
Thermal conductivity (k) values of various polymer-based composites with interconnected 3D continuous frameworks.

Fillers	Polymer matrix	Solid loading	k (W m^{-1} K^{-1})	Enhancement in k (%)	Refs
3D graphite/CNTs	Polyimide	2.6 wt%	4.09	424	2015 [98]
3D graphene	Polyimide	0.35 wt%	1.7	1033	2015 [99]
3D graphene	PDMS	0.7 wt%	0.56	195	2015 [100]
3D graphene	PCM	5 wt%	4.28	1761	2018 [101]
3D graphene	Epoxy	35 wt%	35.5	16,805	2018 [102]
3D graphene	PMMA	2.5 vol%	0.7	250	2015 [103]
3D graphene	Epoxy	0.92 vol%	2.13	1231	2016 [104]
3D graphene	PCM	12 wt%	5.92	2474	2016 [105]
3D graphene	Epoxy	5.5 wt%	10	5560	2018 [106]
3D graphene	Epoxy	5 wt%	1.52	744	2016 [107]
3D graphene/BN	Epoxy	13.16 vol%	5.05	2700	2018 [81]
3D graphite foam	PCM	1.2 vol%	3.4	1800	2014 [108]
3D Cellulose/graphene	PCM	5.3 wt%	1.35	463	2016 [109]
SiC/graphene	Polyimide	11 wt%	2.63	996	2015 [110]
Graphene/BN	Epoxy	44 wt%	11.01	7240	2018 [111]
Graphene	PEG	2.25 wt%	1.43	361	2016 [112]
3D graphene	PA6	0.25 wt%	0.69	288	2018 [113]
3D graphene	Epoxy	8.3 wt%	8.8	4300	2018 [114]
3D diamond	Epoxy	1.2 wt%	2.28	891	2018 [24]
3D BN	Epoxy	24.4 wt%	5.19	2780	2018 [115]
3D Cu-CFelt	Epoxy	29.34 vol%	30.69	13,850	2020 [116]

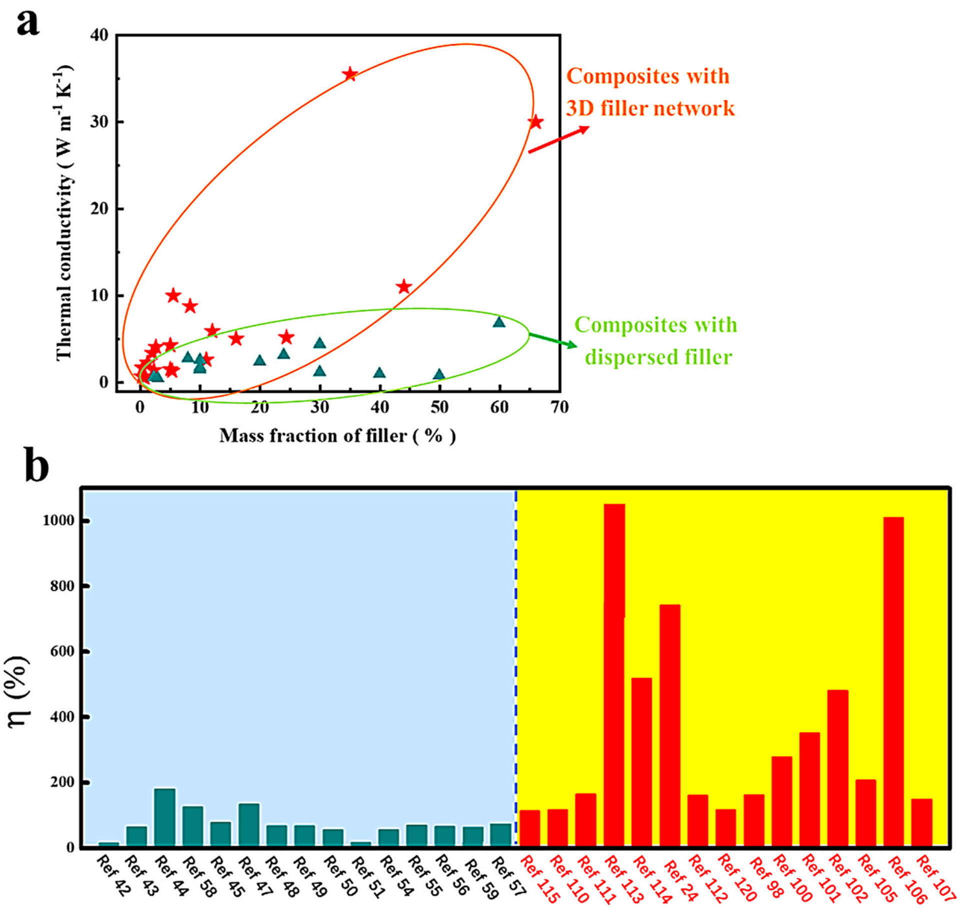

Fig. 11. (a) Comparison of the thermal performance of polymer composites with dispersed and 3D interconnected fillers in terms of thermal conductivity vs mass fraction. (b) Comparison of the η values of composites with dispersed filler particles and interconnected 3D filler networks.

mass fraction of the filler in the composite. Fig. 11b clearly reveals that the η values of 3D network fillers are far higher than those of dispersed fillers. Thus, 3D architectures outperform the random dispersion approach in improving the k of polymers because the 3D framework embedded in the matrix offers more effective continuous pathways for phonon transfer. Therefore, interconnected architectures are conducive to forming efficient 3D heat-dissipative networks in polymer matrices.

In composites with dispersed fillers, the filler particles are coated by the polymer; thus, there are no real effective connections between the particles. This discontinuity causes a large contact thermal resistance in composites, which hinders phonon transmission and limits the improvement in the k of composites. In contrast, interconnected free-standing 3D networks can reduce the internal contact thermal resistance drastically, as individual particles in the 3D architecture

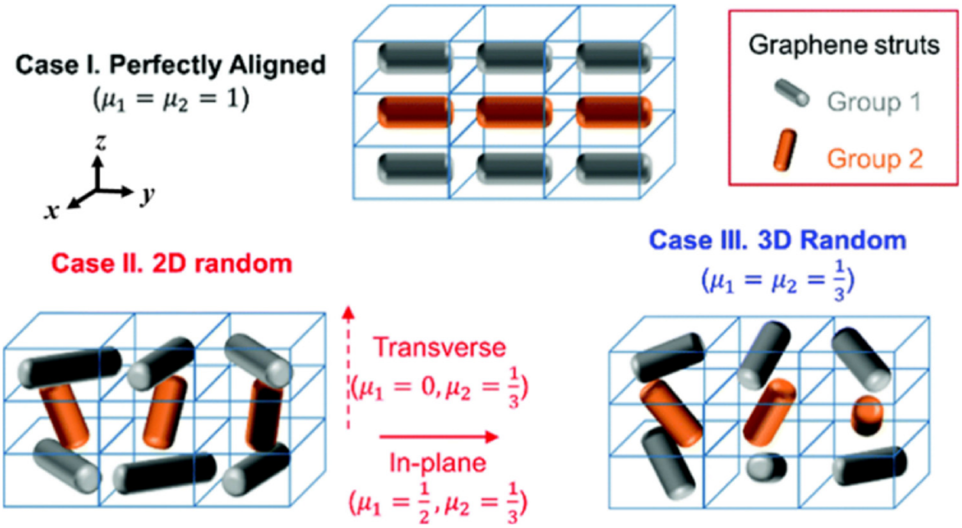

Fig. 12. Analytical models with different orientation parameters for graphene struts [114]. Copyright 2018, Royal Society of Chemistry.

strongly bond with one another in a continuous network [3,117]. Zhang et al. [19] reported that a 3D structure had better thermal interfacial characteristics than other surfaces because of a significant increase in contact sites. It is believed that the overall thermal extraction performance of composites can be further enhanced by improving the compactness of the 3D framework. Ji et al. [108] found that the *k* value of a PCM could be enhanced 18-fold by integrating a 3D graphite framework at volume fractions of 0.8–1.2 %.

4.1.2. Control of heat transfer orientation

Composites with isotropic and anisotropic thermal conductivities can satisfy different application requirements. The most effective and convenient way to control the conductive performance in different directions is to control the orientation of the enhancers. In general, with a homogenous dispersion in a polymer matrix, it is difficult to adjust the orientation of the filler. In contrast, the orientation of a filler network can be controlled using the preconstructed 3D structure. Methods for constructing ordered 3D structures include directional freeze-drying, the application of magnetic or electric fields, and the use of directional templates [118–120].

Among the various types of thermally conductive fillers, individual 1D and 2D fillers, such as CNTs, graphene sheets, and BN sheets, can easily form 3D multilevel ordered structures [121]. Highly oriented 3D structures of CNT arrays, which can be obtained via direct CVD growth, are widely used for preparing highly anisotropic thermally conductive materials. Anisotropic graphene and BN networks can be constructed easily using directional freeze-drying technology. By controlling the orientation of the structure, the heat conduction of a material can be greatly improved in a specific direction, even at low filler contents. Therefore, through the design of the preconstructed structure, the orientation of the heat conduction network can be easily controlled to obtain composite materials with anisotropic properties.

4.1.3. Theoretical calculations of 3D thermal conduction systems

Most theoretical models of thermal conduction are based on EMT and percolation theory, which are reliable for nanocomposites with randomly dispersed fillers; however, these theories are not appropriate for 3D network composites. Because the EMT model assumes that the filler particles are completely surrounded by the polymer, it mainly considers the thermal resistance at filler–polymer interfaces. In contrast, in a 3D-connected structure, it has been reported that the interfacial thermal resistance mainly originates from the filler–filler interfaces rather than the filler–polymer interfaces [12,22]. Owing to the inherently interconnected network of the 3D filler framework, heat conduction channels can be constructed in the polymer matrix, and therefore, it is not affected by the percolation threshold.

Some useful models have been proposed to understand the thermal transfer performance of 3D filler frameworks. Foygel et al. [22,81,122] proposed a nonlinear model that analyzes the intrinsic heat transport performance of a 3D framework and the thermal resistance between the fillers, as follows:

$$\mathrm{K}(V_f, p) = K_0(V_f - V_c)^{t(p)} \tag{6}$$

where K is the pre-exponential factor ratio, which is the expected contribution from the 3D framework alone; Vc is the critical volume ratio of the 3D filler, which has a conductive exponent depending on the aspect ratio of the 3D structure; and V_f is the loading volume of the 3D filler in the composite.

Based on metal foam theory [123], another model was proposed in which the thermal conductivity of a sample containing an isotropic connected 3D filler framework can be predicted based on the rule of mixtures [108,114]:

$$k_{foam} = \frac{1}{3} f k_s \tag{7}$$

$$k_c = k_{foam} + (1 - f)k_p = \frac{1}{3} f k_s + (1 - f)k_p \tag{8}$$

where k_{foam} represents the thermal conductivity of the isotropic filler network; k_s represents the inherent thermal conductivity of the filler struts; f represents the volume fraction of the filler; k_p represents the thermal conductivity of the polymer; and the coefficient 1/3 denotes the completely random orientation of the filler struts.

However, Eq. (8) cannot correctly reflect the *k* values of anisotropic 3D filler networks such as CNT arrays and oriented GF. Kim [114] proposed an improved model, based on Eq.s (9) and (10), by introducing two orientation parameters, μ_i and ξ, which are used to calculate the *k* values of anisotropic 3D multilayer graphene/epoxy composites. These authors divided the composites into two groups according to the orientation of the graphene struts (Fig. 12). Group 1 represented in-plane oriented graphene struts and group 2 represented 3D randomly oriented graphene struts. The exact values of μ_i $(i = 1, 2)$ represented directional average coefficients corresponding to each orientation state, and ξ represented the relative concentration of in-plane oriented graphene struts:

$$\mu_i = \langle \cos^2\theta_i \rangle, \ (i = 1,\ 2;\ 0 \le \mu_i \le 1) \tag{9}$$

$$\xi = \frac{f_{in-plane}}{f},\ (0 \leq \xi \leq 1) \tag{10}$$

where θ is the angle between the thermal transfer direction and the graphene strut; $\mu = 0$ indicates that all graphene struts are perpendicular to the direction of thermal transfer; and $\mu = 1$ suggests that all graphene struts are arranged in the direction of thermal transfer. In addition, a higher ξ value implies that more graphene struts are confined to the 2D plane rather than being randomly arranged in 3D space. When μ_i and ξ are considered, the k values of anisotropic polymer composites can be calculated using the weighted average of these two groups:

$$k_c = \mu_1 \xi f k_G + \mu_2 (1 - \xi) f k_G + (1 - f) k_{ep} \tag{11}$$

Different μ_1 and μ_2 values are calculated depending on the orientation. For example, for the perfectly aligned case, the orientation parameters are the same for groups 1 and 2 ($\mu_1 = \mu_2 = 1$); therefore, the k values of materials with aligned graphene struts can be written as:

$$k_c = \xi f k_G + (1 - \xi) f k_G + (1 - f) k_{ep} = f k_G + (1 - f) k_{ep} \tag{12}$$

For a completely randomly oriented framework, $\mu_1 = \mu_2 = 1/3$; therefore, the k values of materials with randomly oriented graphene struts can be written as:

$$k_c = \frac{1}{3} \xi f k_G + \frac{1}{3}(1 - \xi) f k_G + (1 - f) k_{ep} = \frac{1}{3} f k_G + (1 - f) k_{ep} \tag{13}$$

In addition, the series and parallel models can also be used to predict realistic k values for composites with 3D filler networks [124,125]. The formulae for the series and parallel models of composites with traditional filler particles can be written as

$$\text{Series model: } \frac{1}{k} = \frac{(1 - f)}{k_p} + \frac{f}{k_f} \tag{14}$$

$$\text{Parallel model:} k = (1 - f) k_p + f k_f \tag{15}$$

where k, k_p, and k_f represent the thermal conductivity values of the composite, polymer matrix, and filler particles, respectively; and f represents the volume fraction of the filler particles.

Qin et al. formulated a thermal conduction equation for 3D thermally conductive networks according to the series and parallel theory [124]. As shown in Fig. 13, rGO@MF/polydimethylsiloxane (PDMS) composites can be depicted using a simplified thermal conduction element model, enabling the calculation and predication of the total in-plane thermal conductivity (k_{II}) and resistance (R) of such materials. Similar to the series–parallel connection for the resistance, thermal resistance R can also be calculated using Eq. (16):

$$\frac{1}{R} = \frac{1}{R_a} + \frac{1}{R_{b2} + R_{c2}} + \frac{1}{R_{b1} + R_{c1}} + \frac{1}{R_{c3}} \tag{16}$$

Furthermore, k_{II} can be written as Eq. (17):

$$k_{\parallel} = \frac{L_3}{(L_3 + L_4)} \left(\frac{k_a \bullet L}{L + L_4} + \frac{L_4 \bullet k_{b2} \bullet k_{c2}}{L \bullet k_{c2} + L_4 \bullet k_{b2}} \right) + \frac{L_4}{(L_3 + L_4)} \left(\frac{k_{c3} \bullet L_4}{L + L_4} + \frac{L \bullet k_{b1} \bullet k_{c1}}{L \bullet k_{c1} + L_4 \bullet k_{b1}} \right) \tag{17}$$

In contrast to randomly dispersed filler particles, interconnected architectures have proven to be better candidates for preparing high-performance polymer composites. First, a preconstructed 3D continuous filler network can overcome the disadvantages of aggregation during the preparation process and ensure a uniform dispersion of fillers in the polymer matrix. Second, an interconnected filler network provides more heat transfer channels in the polymer and increases the k by minimizing the negative impact of interfacial thermal resistance. Third, the preconstruction approach makes it easier to regulate the orientation of the 3D network. Hence, prefabricated 3D conductive networks can further improve the heat dissipation capabilities of polymer-based composites at low filling ratios.

4.2. 3D graphene continuous frameworks

As a unique 2D structural material, graphene exhibits excellent electrical conductivity, mechanical robustness, flexibility, thermal conductivity, and optical transparency. It has been considered the perfect reinforcing element for improving the electrical, thermal, and mechanical properties of polymer matrices [14,126–128]. Graphene is widely used as a filler in the preparation of functional composites, which are used in thermal interfaces, supercapacitors, sensors, antistatic films, electromagnetic shielding, and energy storage [129]. The k value of suspended single-layer graphene has been measured as 5000 W m^{-1} K^{-1} at ambient temperature, which makes graphene one of the best thermally conductive materials known at present [130]. Thus, graphene and its derivative materials have widely served as thermally conductive fillers in the preparation of thermal management composites. Graphene is mainly used in the form of nanosheets [67]. Although individual graphene sheets have excellent k values and many great improvements in the properties of polymer composites have been achieved, several factors, including agglomeration and high thermal contact resistance with both the medium and adjacent nanosheets, prevent graphene-based fillers from reaching their full potential in thermally conductive composites [3,131]. Owing to these inherent drawbacks and the discontinuous structure of graphene nanosheets, the reported practical performance is always inferior to the theoretical prediction.

In recent years, the construction of 2D lamellar graphene into freestanding 3D structures has attracted significant attention, as such structures provide better electron, phonon, and ion transfer abilities than graphene sheets [90,107,132,133]. In particular, 3D GFs are of considerable interest owing to their unique interconnected 3D microstructures [93,134]. 3D graphene monoliths can be constructed via the CVD method and self-assembly. In 2011, Cheng et al. first prepared a 3D GF through the CVD method on a nickel foam template [93]. The freestanding GF successfully integrated 2D graphene sheets into a macroscopic structure, while preserving most of the excellent physical/chemical properties of graphene, including thermal conductivity,

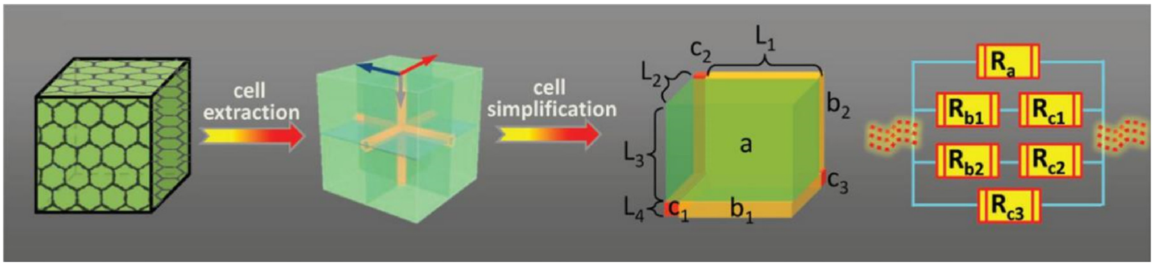

Fig. 13. Calculation of the thermal conductivity of 3D network composites using series–parallel connection theory [124]. Copyright 2018, Wiley-VCH.

electrical conductivity, thermal stability, chemical/radiation resistance, and electromagnetic shielding properties [3,99,135,136]. The *k* values of 3D graphene networks have been reported to be 0.26–1.7 W m^{-1} K^{-1} with a thermal interfacial resistance as low as 0.04 cm^2 K W^{-1} at the Si–Al interface, which is of great significance for developing materials to effectively manage heat dissipation [66]. In addition, the mechanical properties of 3D graphene are favorable owing to the cross-linked structure between the inner nanosheets. The good mechanical and structural stability of 3D monoliths can hamper the agglomeration of graphene nanosheets [137–139]. Owing to the excellent thermal conduction properties, large surface area, and mechanical strength of 3D graphene networks, a series of advanced polymer composite materials can be prepared.

4.2.1. *Construction of graphene architectures*

The construction of an interconnected 3D graphene network in a polymer matrix has been a widely used approach for preparing high-performance composites. To construct graphene networks, several methods can be used, such as CVD, electrochemistry, the reduction of graphene oxide (GO)-based materials, self-assembly, lithographic patterning, vacuum filtration, and nucleate boiling [3,93,97,140–144]. Among these technologies, CVD and the chemical/thermal reduction of GO foams are considered the most efficient for preparing high-quality and large-scale graphene networks [145].

As the main strategy for preparing interconnected 3D graphene monoliths, in situ CVD involves growing graphene on a metal catalyst foam. In this typical bottom-up approach, a carbon source provides carbon atoms for constructing graphene in a 3D catalyst skeleton. This method produces 3D graphene with a perfect lattice and a connected structure. Another strategy is to build the 3D structure based on GO and then reduce it to 3D graphene, which has been achieved using various methods, including in situ self-assembly strategies (hydrothermal method) [141,146–148]. cross-linking methods [149–151], template methods [152,153], wet spinning [154], and 3D-printing techniques [155–158].

4.2.1.1. Self-assembly of GO. GO, an inexpensive graphene-derived material, is prepared using graphite powder as a raw material through the processes of graphite oxidation and graphite oxide exfoliation. The emergence of GO has made the mass production of graphene possible. Importantly, uniform dispersions of GO can achieve in water and many other organic solvents owing to the abundant oxygen-containing groups on its basal planes and edges. A GO-based network can be reduced to a graphene network using chemical reductants or a high temperature [159].

The most common strategy for constructing 3D graphene frameworks using GO as a raw material is self-assembly (Fig. 14a, b). Based on this strategy, several methods have been developed. In a typical method, a GO dispersion in an aqueous solvent is first gelled and then reduced to convert GO to rGO, eventually producing a 3D graphene network (Fig. 14a). The equilibrium between the van der Waals forces and electrostatic repulsion facilitates the dispersion of GO in the aqueous solvent to form a stable dispersion [134]. During the gelation process, the balance between these forces is broken and the GO sheets become partially overlapped, resulting in a gel with a self-supporting architecture. The 3D graphene network is obtained after subsequent solvent removal and the reduction process. For the gelation of GO dispersions, a cross-linker is usually needed to strengthen the connections between GO sheets and efficiently accelerate gel formation. Many cross-linkers have been reported, such as polyvinyl alcohol (PVA) [160], 2-ureido-4[1H]-pyrimidinone (UPy) [161], DNA [162], metal ions [163,164], polymers [165], and organic molecules [166].

Besides gelation, various other methods are available to assemble GO sheets into 3D macrostructures, including freeze-drying [101,169–171], tape casting, and electrochemical deposition. These methods involve first preparing a 3D GO structure followed by reduction to produce the graphene network. 3D graphene networks can also be obtained using one-step processes, such as the hydrothermal treatment [102,141,172–174] or chemical reduction [147,175–177] of GO sheets.

Although the construction of 3D graphene networks by assembling GO or rGO is flexible, simple, inexpensive, and yields a high output, there are some deficiencies that should be addressed in future research. In addition to the abundant oxygen-containing groups (epoxides, hydroxides, phenols, and carboxylic acids), the structural defects in the graphene macrostructures obtained from GO also have a considerable influence on the *k* value [178]. Graphene prepared by reducing GO usually contains numerous lattice defects, which cause significant phonon scattering and affect the inherent *k* of graphene. Acquiring high-quality graphene with fewer structural defects is an urgent issue that warrants immediate attention.

4.2.1.2. CVD method. Similar to self-assembly methods, the growth of 3D graphene networks directly on a 3D catalyst template by CVD is also a very popular method for producing high-purity and large-scale graphene [93,179]. The CVD method is a popular microfabrication technology widely used in the semiconductor industry. A metal catalyst (Cu, Au, or Ni foam), which also serves as a 3D template, is needed to prepare graphene architectures via CVD [93,180]. The formation mechanism of graphene involves carbothermic reduction at the template surface, which initializes the nucleation and growth of graphene. To obtain a high-purity graphene network, the catalyst framework needs to be removed. To preserve the integrity of the graphene architecture and prevent the 3D structure from collapsing during the catalyst etching process, thin layers of PDMS are often deposited as a support structure (Fig. 14c). In addition to metal templates, other 3D structural materials can be used to grow 3D graphene networks [181–185]. Lin et al. [181] grew a 3D graphene architecture on a porous Al_2O_3 ceramic template using the ambient-pressure CVD method. Ning et al. [182] synthesized 3D graphene nanomeshes, which have only one or two graphene layers, via template growth on porous MgO layers. Huang et al. [183] obtained a macroscopic 3D graphene network by growing multilayer graphene on interconnected porous silica substrates using the CVD method.

Compared with the 3D graphene structures obtained by self-assembly techniques, such as hydrothermal and sol–gel methods, those prepared by the CVD technique are considered more efficient in optimizing the *k* of polymers [19,186]. The is because the weak van der Waals, hydrogen-bonding, and π–π-stacking interactions at the interfaces in the graphene aerogel cause abundant phonon scattering between different graphene sheets [168,170,187,188]. By contrast, covalently bonded GFs can provide continuous fast channels for phonon transfer [3,108]. In addition, graphene prepared by CVD has a better crystal structure with fewer oxygen-containing groups and structural defects than rGO. Hence, the high-quality graphene structures produced by CVD are more effective in improving *k*. Although the CVD method can grow high-quality graphene networks, this high-cost process is complex and time consuming, which are serious shortcomings. Thus, future studies need to address reducing the manufacturing costs, optimizing the growth conditions, and quickly removing the catalysts.

4.2.1.3. Other methods. In addition to the main strategies of self-assembly and CVD, some researchers have prepared 3D graphene networks using other methods, such as pyrolytic polymer templates [189,190], 3D printing technology [157,158,191], laser-induced technology [192–196], and 3D template assembly techniques [190,197–200]. Tour et al. [192–196] synthesized 3D GFs based on laser-induced technology, as shown in Fig. 15a–d. A commercial polyimide film was irradiated by a CO_2 infrared laser, resulting in the conversion of the polyimide film into porous graphene. The graphene layers were then adhered to each other and stacked, and the laser irradiation was repeated on subsequent polyimide layers (Fig. 15a).

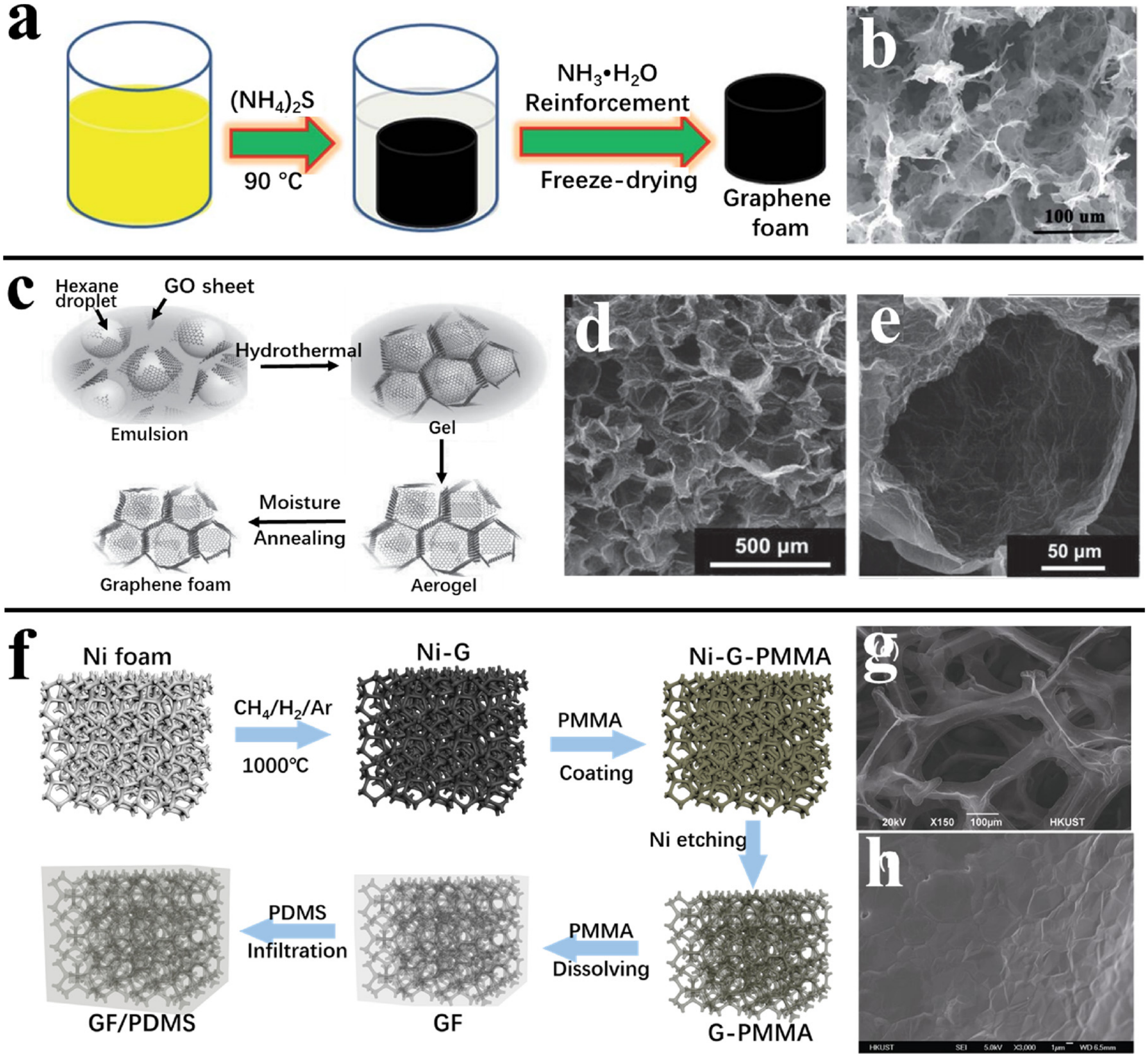

Fig. 14. (a) Schematic diagram of the construction of graphene aerogels via self-assembly. (b) Scanning electron microscopy (SEM) images of the aerogel cellular structure [167]. Copyright 2015, Royal Society of Chemistry. (c) Schematic diagram of the microporous graphene framework obtained by a hydrothermal method. (d, e) The SEM images of graphene foam prepared by hydrothermal assembly [168]. Copyright 2014, Wiley-VCH. (f) Schematic diagram of the CVD method for building GFs via a nickel framework template and the micromorphology of the GF. (g, h) The micromorphology of graphene foam grown by CVD [93]. Copyright 2014, Elsevier Ltd.

Worsley et al. [191] applied a 3D printing technique to fabricate engineered 3D graphene architectures by depositing GO ink filaments precisely on predesigned paths (Fig. 15e–h). Polsky et al. [197] reported that prestructured pyrolyzed photoresist films could be used to synthesize 3D interconnected graphene networks via a chemical conversion. Yu et al. [109] prepared a cellulose/graphene aerogel by incorporating defect-free graphene nanoplatelets into 3D cellulose aerogels. Liao’s group [190] prepared a GF using a polyurethane (PU) foam as a template (Fig. 16a–c). Under high-temperature treatment, GO was reduced to graphene, and PU was decomposed completely. Qin et al. [124] built a 3D graphene network structure by impregnating a GO solution into a commercial PU foam (Fig. 16d).

In summary, there are two main methods for preparing the 3D graphene networks: in situ CVD growth and GO self-assembly. The GO self-assembly method, which is convenient, inexpensive, and density controllable, can produce large samples and is conducive to mass production. However, the 3D graphene structures prepared using this method have several defects, and subsequent improvements are needed to address these. In addition, as the assembly of the graphene sheets in the 3D structure depends on weak interactions, the structure is unstable and the continuity is poor; thus, phonon transmission between different graphene sheets is hindered. In comparison, the 3D graphene networks prepared by CVD are of high quality with good continuity because the constituent covalent bonds are beneficial for electron and phonon transfer. However, this method generally requires a 3D growth template, and subsequent template removal is complicated and can cause structural damage. Furthermore, the high growth temperature and the elevated costs entailed by this method are not conducive to large-scale production and thus limit its application. Thus, for the CVD method, it is necessary to improve the reaction conditions, reduce the growth temperature, and realize rapid template removal.

4.2.2. *3D graphene/polymer composites*

Compared with traditional graphene powder, a 3D graphene architecture is advantageous for improving the *k* of polymers owing to its intrinsic interconnected structure. In addition, unlike powders, preconstructed 3D networks can achieve a fine dispersion of fillers in the polymer without agglomeration, thus providing a stable structure and strengthening the mechanical properties.

Numerous papers have reported the evident advantages of 3D graphene frameworks over 2D graphene sheets for preparing thermally conductive composites [3,143]. Bai et al. [100] prepared thermally

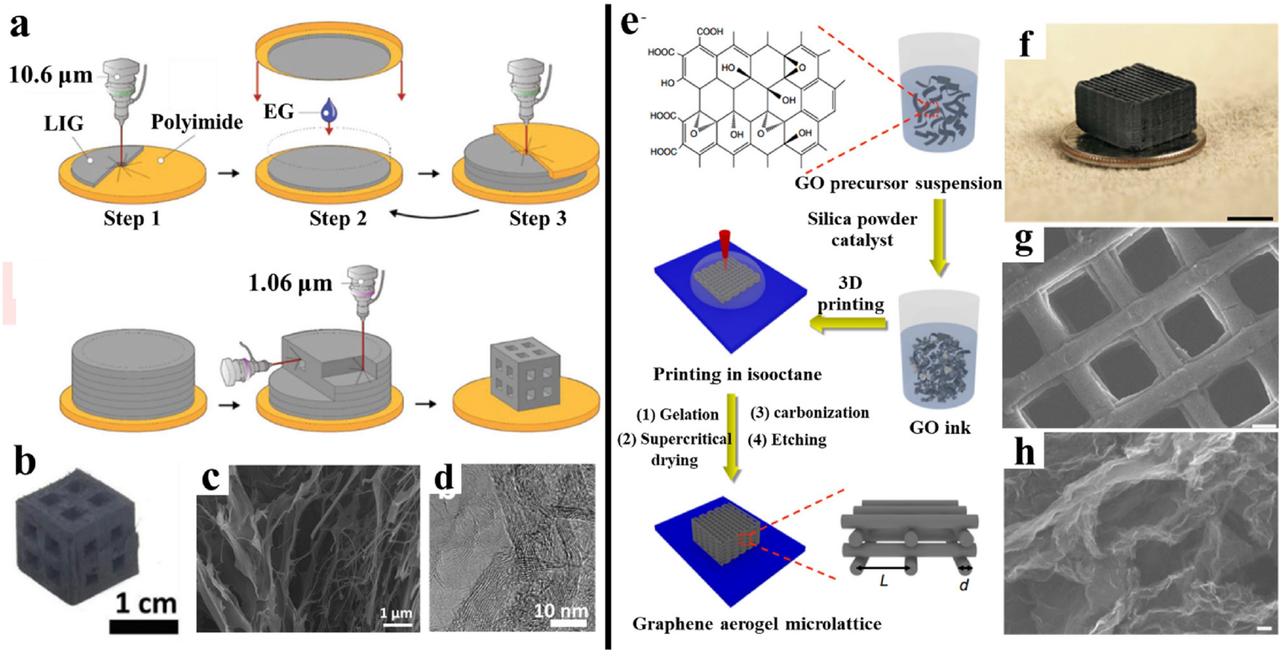

Fig. 15. (a) Preparation process for 3D GFs based on laser-induced technology and a laser milling process. (b) Optical photograph, (c) SEM image, and (d) transmission electron microscopy (TEM) image of the GF prepared by laser-induced technology [192]. Copyright 2018, Wiley-VCH. (e) Engineered graphene aerogel prepared by direct ink writing via a 3D printing technique. (f) Optical image and (g, h) SEM images of the GF fabricated by 3D printing [191]. Copyright 2015, Nature Publishing Group.

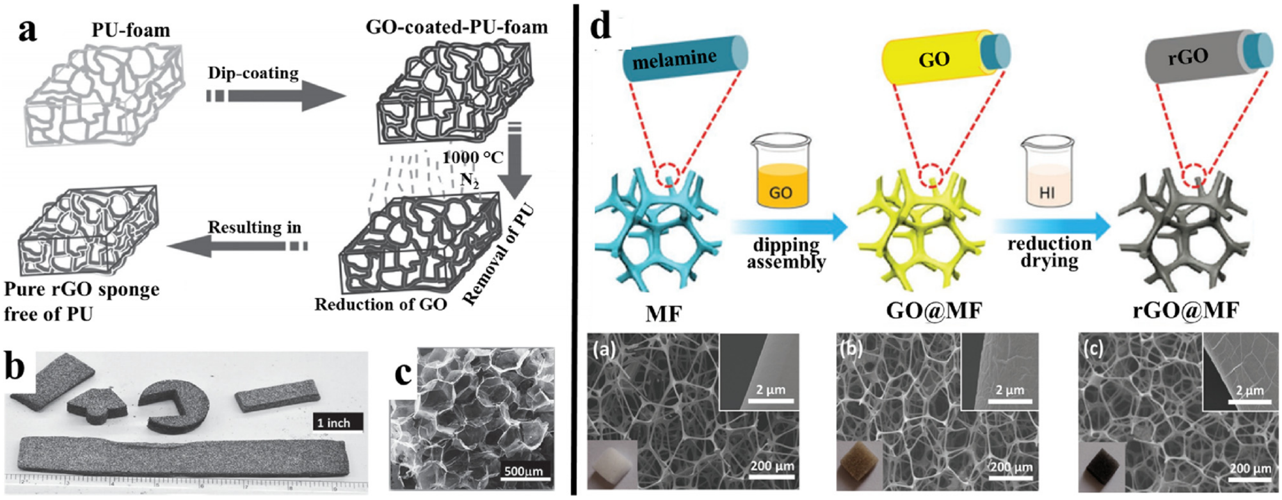

Fig. 16. (a) Formation of a GF via GO coating of a PU foam template and subsequent removal of the PU foam by heating. (b) Photograph and (c) SEM image of the GF prepared using the PU foam template [190]. Copyright 2015, Wiley-VCH. (d) Preparation of a continuous graphene network using a melamine–formaldehyde foam template immersed in a GO solution [124]. Copyright 2018, Wiley-VCH.

conductive PDMS composites by filling a 3D GF, and the *k* value of the composite increased to 0.56 W m^{-1} K^{-1} with 0.7 wt% graphene, which corresponds to a 20 % increase compared with that of a composite with dispersed graphene sheets at the same loading. Zhang and co-workers [201] prepared a 3D graphene structure by chemically reducing GO, which was used as a thermally conductive network to enhance the *k* of PU. The *k* value of the resultant GA/PU composite reached 3.36 W m^{-1} K^{-1} at ambient temperature with 2.5 wt% graphene, confirming that graphene networks are favorable for internal thermal transfer, thermal dissipation, and other thermal applications. Thus, devising and constructing a graphene macrostructure as a conductive network has been demonstrated as an efficient method for improving the *k* of polymers.

The typical process for preparing thermally conductive polymer composites involves first constructing a 3D graphene structure and then infiltrating the polymer into the interconnected 3D graphene framework by capillary adsorption or vacuum-assisted methods. This facile compounding method ensures that the 3D interconnected structure is not destroyed during composite preparation, and the embedding of graphene improves the polymer stability and reduces composite shrinkage. Yang et al. [112] prepared a hybrid carbon network consisting of GO and graphene nanoplatelets, which was then mixed with polyethylene glycol to obtain a composite with good heat conduction ($k = 1.43$ W m^{-1} K^{-1} at 2.25 wt% loading), excellent structural stability, reliable thermal cyclicity, and the capability for light-to-heat energy storage. In this hybrid freestanding framework, the GO nanosheets formed a 3D support network to stabilize the shape, and the graphene nanoplatelets uniformly covered the GO network to construct heat transport pathways. In another effort, these authors [186] constructed a

3D hybrid graphene network by self-assembly and CVD methods to improve the heat conduction (k = 1.82 W m^{-1} K^{-1}) and shape-stability of PCMs. To construct this hybrid graphene network, GO was first introduced into a Ni template, followed by the growth of graphene by CVD.

In the preparation of polymer-based composites, graphene crystal quality and network compactness are two key factors that influence the k values of materials. A network of graphene with fewer defects has a smaller intrinsic thermal resistance and better thermal conduction. In contrast, the k of composites is proportional to the density of the filler network in the composites. A higher network density increases the number of thermally conductive paths formed, resulting in a higher k value.

4.2.2.1. Crystal quality of graphene networks. Compared with the GFs prepared by GO self-assembly, the 3D graphene structures prepared by CVD have excellent intrinsic k values owing to their high purity and high quality [3,202]. Teo et al. [99] prepared a composite by constructing a 3D graphene network and infiltrating it with polyimide. This continuous graphene network significantly increased the k value of the polymer from 0.15 to 1.7 W m^{-1} K^{-1} with only 0.3 vol% graphene. Bai et al. [100,203] used a 3D GF prepared by CVD to increase the k of PDMS. A high-quality GF consisting of defect-free graphene nanosheets is essential for enhancing the k of the polymers. In the networks grown in situ via CVD, the graphene sheets are covalently bonded to each other, and there are no other weak bonding interactions. Thus, this intrinsically continuous structure can overcome the high interfacial thermal resistance that is problematic in van der Waals bonded rGO networks.

The preparation of graphene frameworks via GO self-assembly is a convenient and effective method. However, many reports have shown that rGO networks cannot significantly improve the k of polymers. This unsatisfactory performance mainly results from the inferior k of the rGO network, which has been attributed to large amounts of defects and oxygen-containing groups [14,204,205]. These imperfect structures cause excessive phonon scattering, which adversely affects the efficiency of heat transfer, resulting in the polymer composites exhibiting only moderate improvements in k.

High-temperature annealing is quite effective for improving the quality of graphene sheets and realizing large improvements in the inherent k of graphene [101,204,206–210]. High-temperature annealing removes the organic functional groups on rGO and aids in the formation of defect-free graphene structures by repairing lattice defects, which, in turn, can enhance the k of graphene. For example, Yu et al. [101] constructed a somewhat defect-free graphene architecture by annealing a GO aerogel at 2800 °C. This treatment effectively removed the oxygen-containing groups on the GO sheets and healed the lattice structure, imparting the graphene aerogel with a high thermal conduction capacity. Impregnating this graphene aerogel with octadecanol gave a composite that exhibited an exceptional k value of approximately 4.28 W m^{-1} K^{-1} at a low graphene loading of 5.0 wt%. This beneficial effect was a direct consequence of the defect-free graphene and the interconnected thermally conductive network. Li et al. [211] fabricated a vertically aligned graphene conductive network by the directional freezing of a GO hydrogel with subsequent graphitization at 2800 °C. With only 0.75 vol% of this graphene network, an epoxy composite exhibited a k value of 6.75 W m^{-1} K^{-1} in the vertical direction. These significant improvements in thermal conduction verify the importance of high-temperature heat treatments for graphene networks.

4.2.2.2. Density of graphene networks. The density of the transmission network is another key factor that remarkably affects the heat transfer properties of composites. Although GFs grown in situ by CVD have favorable thermal and mechanical properties, they also have low densities and the graphene content in polymer composites is generally lower than 1 vol%. This is because the CVD method is restricted by the pore structure of the metal catalyst skeleton, which causes difficulties in growing dense structures using this method. The low graphene content prevents the GF from forming sufficient heat conduction channels and hinders further improvement in the k of composites [212]. Similarly, if the density of the graphene structure is too low, it cannot supply adequate heat transfer pathways. Therefore, constructing high-quality and dense graphene architectures is important for realizing efficient and high-speed heat transfer.

In comparison, the densities of architectures constructed by GO self-assembly can be easily controlled and dense network structures can be achieved. Yu and co-workers [105] prepared a dense graphene hybrid aerogel by hydrothermally assembling aqueous mixtures of GO and graphene nanosheets. As a heat-conducing filler, this graphene aerogel increased the k of octadecanoyl. The obtained octadecanoyl/graphene composite showed a k value of approximately 5.92 W m^{-1} K^{-1}, which was 26 times larger than that of neat octadecanoyl. An et al. [102] constructed a high-density thermally conductive network via the hydrothermal reduction of GO and graphene nanoplatelets, followed by graphitization at 2800 °C. This dense network efficiently increased the heat conduction of an epoxy composite, achieving an exceptionally high k of 35.5 W m^{-1} K^{-1}, which is far greater than those of composites filled with low-density networks (Fig. 17).

In summary, to enhance the heat transfer performance of a polymer composite, the construction of a high-quality and dense 3D continuous graphene network is critical. It is essential that the contents of oxygen-containing groups and lattice defects in the 3D-connected graphene network structure be reduced to improve the intrinsic thermal conduction properties. Simultaneously, it is necessary to increase the density of the graphene network structure as much as possible to provide more transmission channels for phonons.

4.3. 3D CNT conductive networks

Because their crystal structure is similar to that of graphene, CNTs also exhibit favorable mechanical properties and high electrical and thermal conductivities. It has been reported that the k values of MWCNTs are more than 3000 W m^{-1} K^{-1} [213]. Furthermore, the experimentally measured k values of isolated MWCNTs are in the range of 200–3000 W m^{-1} K^{-1} at ambient temperature. Using a molecular dynamics model, Kim et al. predicted that the k values of SWCNTs could reach 6600 W m^{-1} K^{-1} [214]. The ultrahigh heat transfer properties of CNTs allow them to play a critical role as fillers in thermally conductive polymer composites.

According to Maxwell's equation, the incorporation of 1 vol% of CNTs is expected to cause a 10-fold increase in the k of a polymer. However, until now, the actual results have not been encouraging in most cases [17]. For instance, Biercuk et al. [215] reported that a 2 wt% (approximately 1 vol%) loading of CNTs powder in an epoxy resin only improved the k value by up to 12.5 %. This unsatisfactory improvement in the k of the polymer was mainly due to excessive interfacial thermal resistance, which was mainly caused by the large tube–tube contact resistance, structural defects in the CNTs, and an inadequate number of contact areas between the tubes. Compared with traditional CNTs powders, an interconnected 3D CNT framework is more advantageous for preparing polymer composites.

To utilize the outstanding heat conduction properties of CNTs effectively, a feasible strategy is to construct a macroscopic CNT thermal conductivity network. As the 1D nanotube structure is strong, conductive, and flexible, it can be used as a basic unit for the macroscopic framework. CNT arrays and randomly oriented CNT aerogels are the main components of macroscopic CNT frameworks. In particular, aligned CNT arrays have been widely used to prepare oriented thermally conductive polymer composites [4,216–218]. The parallel arrangement of the CNTs provides excellent heat transfer from two points into the parallel planes, and this highly orientated structure makes CNT

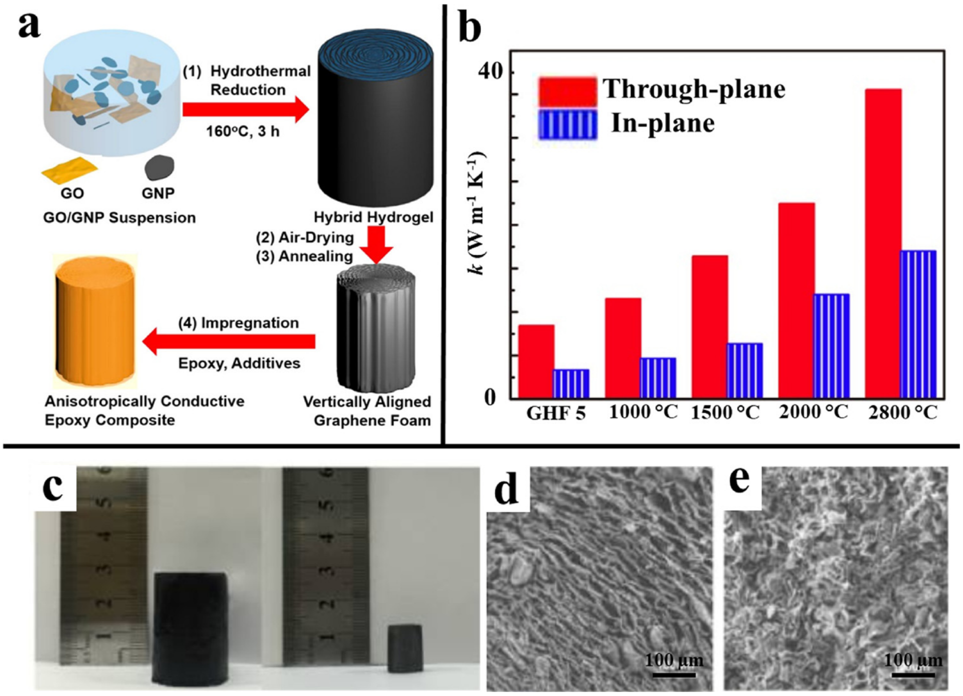

Fig. 17. (a) Schematic illustration of the construction of dense 3D graphene hydrogels used to fabricate thermally conductive epoxy composites. (b) k values of the composites after treating at different annealing temperatures. (c) Digital image and (d, e) SEM images of the dense GF [102]. Copyright 2018, American Chemical Society.

arrays applicable as efficient heat management materials. In contrast, randomly oriented CNT aerogels have isotropic properties and can be used to prepare polymer composites with isotropic properties. However, compared with CNT arrays, CNT aerogels have lower k values owing to their lower densities, random permutations, and poor connections between the tubes [219]. Theoretical calculations for randomly oriented pure CNTs performed using Green's function have revealed the upper bound of the overall k value to be very small [220]. Therefore, there have not been many reports on the preparation of thermally conductive composites with CNT aerogels as fillers.

4.3.1. *CNT arrays*

4.3.1.1. Preparation methods. CNT arrays can be synthesized from ready-made CNTs using a physical method that involves magnetically or electrically induced assembly [4,221]. Although this method is simple and feasible, the obtained CNT arrays exhibit low densities and imperfect orientations and arrangements. CVD, plasma-enhanced CVD, laser ablation, and template-assisted methods can also be used to prepare aligned CNTs [222–224]. Among these methods, CVD is considered the most suitable for producing high-quality CNT arrays as it provides a high yield, high purity, and excellent orientation. CNT arrays can be grown on various substrates, such as quartz chips, planar silicon substrates, mesoporous silica, carbon fibers, carbon paper, graphite sheets, and metallic substrates [225,226]. This method also requires a metal catalyst, such as Fe, Co, Ni, Al, or any hydride-forming metal [225]. The mechanism for synthesizing CNT arrays using the CVD method, as shown in Fig. 18, involves a growth process, in which the tubes are arranged in an orderly manner owing to the "crowding effect". Owing to van der Waals forces and the high-density catalyst particles, there is a limited space for the growth of CNTs [222,227].

The synthesis of CNT arrays is affected by several factors, such as catalyst type, particle size, substrate, carbon source, growth temperature, and gas flow rate. By adjusting the growth parameters, CNT arrays with different lengths, diameters, sizes, and qualities can be prepared. For example, Hata et al. [20,228] synthesized high-quality SWCNT and MWCNT arrays via water-assisted CVD. In this growth process, ethylene was used as the carbon source, and Ar or He with H_2 was used as the shielding gas. In addition, sputtered metal nanofilms (Fe, Al/Fe, Al_2O_3/Fe, or Al_2O_3/Co) on Si wafers, quartz, and metal foils were used as the catalyst and substrate, and trace water vapor was used to promote and preserve the catalytic activity. Using this method, a VACNT array can be grown to a millimeter length in 10 min. Floating-catalyst CVD has also been proven to be highly effective for the synthesis of MWCNT arrays. Ferrocene, $Fe(CO)_5$, iron(II) phthalocyanine, and $FeCl_3$ can be used as floating-catalyst precursors [229] with xylene [230] or toluene [229] as the carbon source. Using the floating-catalyst process, aligned CNT arrays can be prepared rapidly under continuous operation.

4.3.1.2. CNT arrays for thermal management. Owing to their high anisotropy, aligned CNT arrays have volume-averaged axial k values of up to 265 W m^{-1} K^{-1} [231] and are therefore considered promising for preparing composites with superior out-of-plane thermal conduction. Aligned CNT arrays show excellent heat conduction but fragile mechanical properties. In contrast, polymers exhibit outstanding machinability and poor thermal conduction. Therefore, it is practical to prepare high-performance TIMs by compositing CNT arrays with polymers. Various aligned CNT/polymer composites have been prepared [232–235], in which the highly thermally conductive CNT arrays are responsible for the majority of heat transport. Goodson et al. [232], who reported k values for polymer composites with various CNTs volume fractions, found that 1 vol% CNTs can realize a more than 2-fold improvement in the k value of the polymer. Furthermore, the k values of the composites in the axial direction could reach 4.87 W m^{-1} K^{-1} when the CNTs content was 16.7 vol%. These results confirmed that densified and aligned CNT arrays are crucial for improving the heat conduction of polymers. Ivanov et al. [233] reported that millimeter-tall VACNT arrays prepared via CVD on Si substrates could achieve fast and highly anisotropic thermal transport. The out-of-plane k value of the CNT array (8 ± 1 vol%) in air was 15.3 ± 1.8 W m^{-1} K^{-1}, and that of the epoxy-infiltrated CNT array was 5.5 ± 0.7 W m^{-1} K^{-1}. These authors suggested that k could be further enhanced by optimizing the density and reducing the defects of the CNT arrays. Tasciuc's group [234] prepared a high k composite by infiltrating PDMS into MWCNT arrays at ambient temperature. The thermal diffusivity of the composite along the CNT alignment direction was over six times larger than that of neat PDMS.

The heat conductivity of CNT frameworks is affected by many parameters, such as the axial dimensions and diameters of the

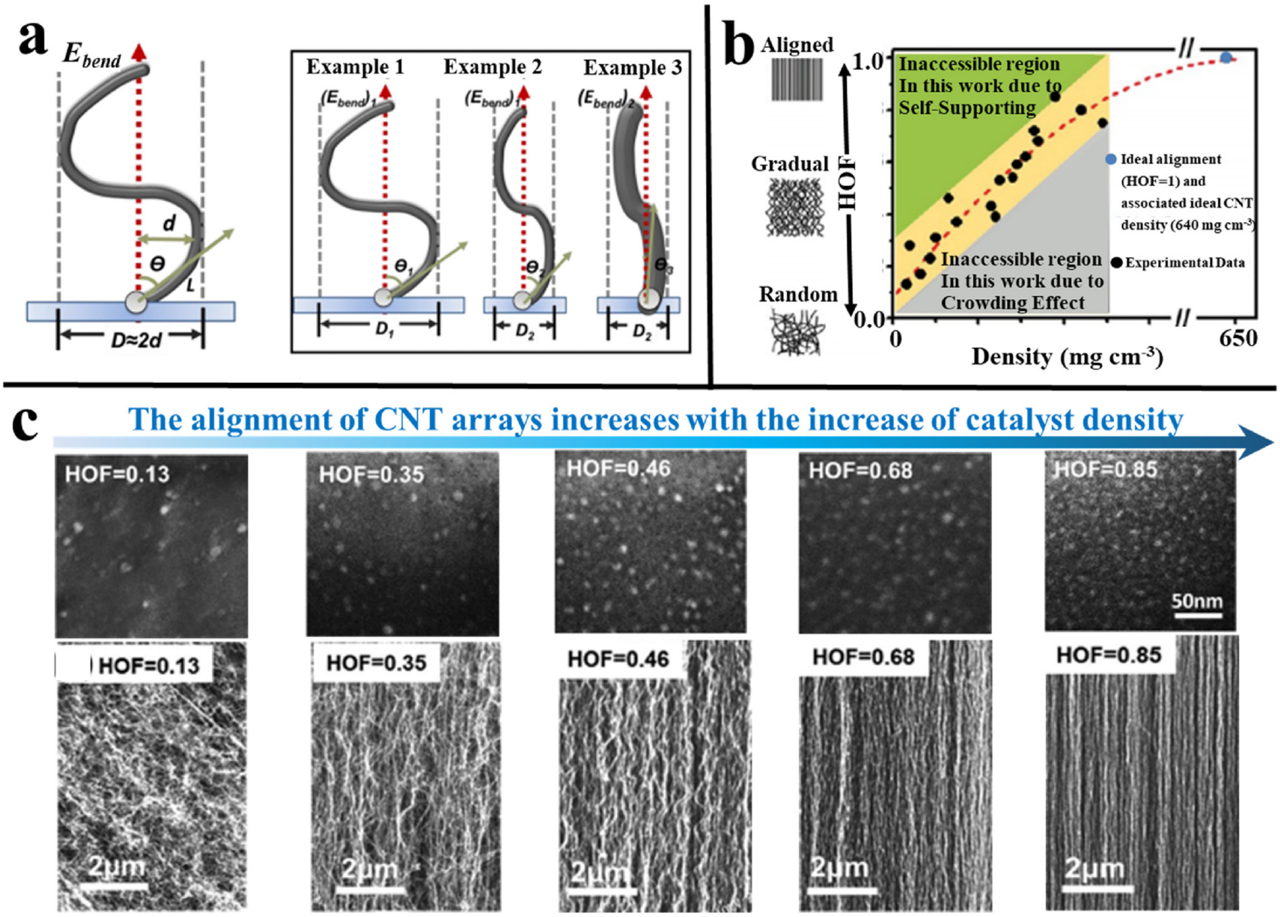

Fig. 18. (a) Schematic of the preparation of CNT arrays by the "crowding effect." (b) Relationship between CNT alignment and catalyst density. (c) SEM images of CNT arrays with different catalyst densities [227]. Copyright 2012, American Chemical Society.

individual CNTs, the defect level, and the density and orientation of the CNT framework [235–238]. An increased CNT framework density benefits heat dissipation by providing more effective pathways for heat flow and minimizing the phonon scattering induced by air. Zhu et al. [235] fabricated MWCNTs/bismaleimide composites using MWCNT arrays with lengths of 0.65–1.3 mm. They found longer CNT arrays were more conducive to thermal conduction. For example, the composite prepared with a CNT array of 0.65 mm in length and 37 nm in diameter exhibited a k value of 33 W m^{-1} K^{-1}, whereas that filled with a CNT array of 1.1 mm in length and 59 nm in diameter exhibited the highest k value of 70 W m^{-1} K^{-1}. This behavior could be attributed to heat dissipation in the CNTs/polymer composite via phonon transport [238]. In the composites, the CNTs lengths were much larger than the mean free path of the phonons. Therefore, while the effect of phonons with short wavelengths could reach a constant level, the phonons with long wavelength continued to contribute to the thermal dissipation process. Similarly, longer CNTs could provide more efficient phonon transfer pathways, which would allow the transfer of phonons with long wavelengths.

4.3.2. CNT aerogels

4.3.2.1. Preparation of CNT aerogels

4.3.2.1.1. CVD method. In 2010, Gui et al. [25] and Xu et al. [94] developed isotropic CNT frameworks using floating-catalyst CVD and fixed-catalyst CVD, respectively. Gui et al. [25,239]created a macroscopic porous CNT sponge with a unique isotropic structure by changing the carbon source for the CVD process from xylene to dichlorobenzene, which could disturb the aligned growth and create a random stacking structure (Fig. 19a). These CNT sponges had stable 3D porous networks with great versatility in structural deformation and shape recovery. The CNT sponges consisted of randomly overlapped individual CNTs and exhibited low densities, ultrahigh porosities, flexibility, and resilience (Fig. 19b, c). Xu et al. [94] fabricated a rubber-like resilient CNT macroscopic monolith with outstanding thermal stability over a wide temperature range (–196 to 1000 °C). During the CVD process, a gas flow consisting of ethylene as the carbon source with a small amount of water vapor was introduced into the substrate, which was sputtered with thin Al_2O_3/Fe catalytic layers. Few-walled CNTs were continuously generated on the substrate and subsequently intertwined with each other to construct an isotropic scaffold (Fig. 19d, e). In this system, the density, structural orientation, and mechanical behavior of the CNT framework could be adjusted by controlling the distribution and density of the catalyst [240,241]. Furthermore, by controlling the concentration and distribution morphology of the catalyst, a CNT framework was converted from a random distribution network (isotropic) to a CNT array (anisotropic) [227]. Yu et al. [242] also synthesized a cylindrical sponge-like CNT structure (Fig. 19f) using the CVD method. As illustrated by the growth reaction in Fig. 19g, ferrocene was decomposed at 400 °C, and the volatilized products were continuously delivered to the reaction zone. The added iron nanoparticles attached to the walls of the existing CNTs during the synthesis process, resulting in the formation of a 3D sponge-like porous structure.

The preparation of CNT frameworks by other strategies, such as covalent junctions and elemental doping, have also been reported. Ajayan et al. [243] generated a boron-doped MWCNT monolith using an aerosol-assisted CVD process. The boron doping created a kinked morphology of atomic-scale "elbow" junctions. Shan et al. [244]

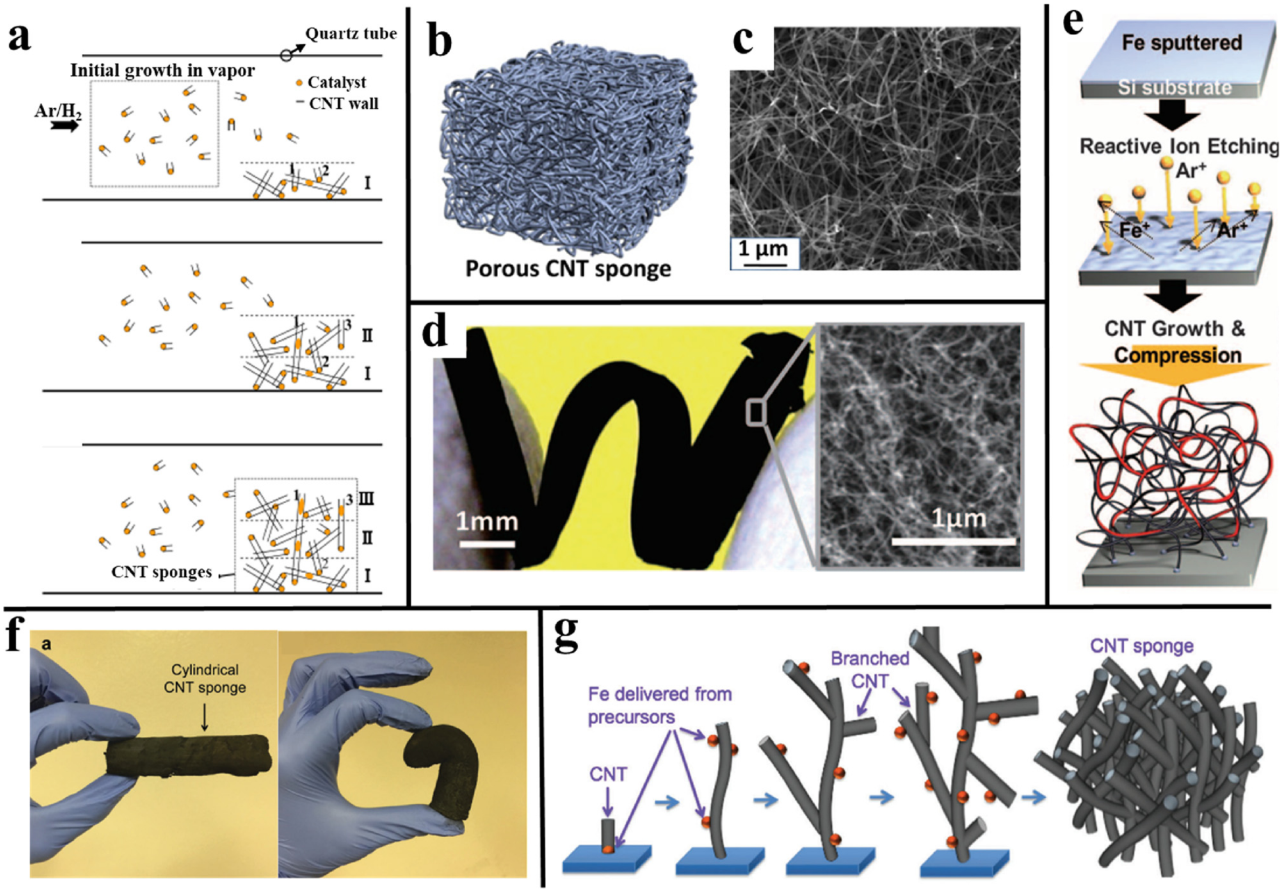

Fig. 19. (a) Schematic of the growth process for CNT sponges in the floating-catalyst CVD method. (b) Schematic diagram of porous CNT sponges. (c) SEM image of the CNT sponges [239]. Copyright 2013, IOP Publishing Ltd. (d) Optical photographs and SEM images of the rubber-like CNT monolith. (e) Schematic of the growth process for the rubber-like CNT monolith via the fixed-catalyst CVD method [94]. Copyright 2010, American Association for the Advancement of Science. (f) Digital images of the sponge-like CNT structure. (g) Time evolution of the proposed growth process for the sponge-like CNT structure [242]. Copyright 2015, Royal Society of Chemistry.

prepared nitrogen-doped CNT sponges in a similar manner. Moreover, it was reported that a 3D catalyst template could also be used to grow CNT macroscopic structures [245].

4.3.2.1.2. Cross-linking method. Dispersed CNTs can also be constructed into macroscopic monoliths with interconnected 3D scaffold structures using a sol–gel, cross-linking, and ice template method [246–249]. Islam’s group [246,247] constructed a freestanding SWCNT aerogel by introducing sodium dodecylbenzene sulfonate as a cross-linker. As shown in Fig. 20a, c, the fabrication process usually involves three stages [250]. First, the CNT powder and the chemical cross-linker are evenly dispersed in a liquid solvent to form a colloidal solution. Then, the colloidal solution is hydrolyzed to obtain an integrated network (gel) with homogeneous cells. Finally, a 3D CNT framework is built via freeze-drying or supercritical drying of the gel (Fig. 20d, e) [251]. The cross-coupled CNTs could be assembled into macroscopic architectures with different junction structures (Fig. 20b).

In summary, CNT frameworks can be prepared through two strategies: direct growth by CVD and the solution treatment of CNT powders followed by freeze-drying or supercritical drying. The CNT frameworks prepared by the CVD method have better structural integrity and robustness. However, the CNT aerogels prepared from CNT suspensions have the advantages of low cost, scalability, adjustable functionalization, and the potential to tailor microstructures. However, the solution process creates new structural defects and shortens the raw CNTs, leading to the degradation of *k*. The weak interactions between the suspended nanotubes also result in inferior thermal conduction and mechanical properties. Furthermore, the CNT aerogels fabricated via solution assembly are fragile and can easily collapse under compression. Therefore, the CVD method is considered the best method for building 3D self-supporting CNT sponges.

4.3.2.2. CNT networks for thermal management. Despite the excellent out-of-plane thermal conduction properties of CNT arrays, in some cases, isotropic thermal conduction materials are required. The spaces between adjacent CNTs in the arrays hampers in-plane phonon transport, thus impeding the in-plane heat transfer of CNT array-based composites. Some researchers have attempted to construct isotropic CNT frameworks as heat conduction networks. Kong et al. [252] proposed a novel 3D CNT network by cross-linking a VACNT array with randomly oriented CNTs. The obtained CNT network had a *k* value of 5.4 ± 0.92 W m^{-1} K^{-1}, which was more than 300 % that of the primary VACNT array, and this network could be used to prepare high-performance TIMs. Choi et al. [253] fabricated PDMS/CNTs composites by coating PDMS layers on the inner and outer surfaces of a porous 3D sponge-like CNT structure. The *k* value of the composite with 8 vol% PDMS (92 mW m^{-1} K^{-1}) was 268 % higher than that of the pristine CNT sponge (25 mW m^{-1} K^{-1}) but still very low owing to the ultralight density and advanced pore structure of the sponge. Hsiao et al. [254,255] used sodium dodecyl sulfate@carboxymethyl cellulose as a functional surfactant and conductive poly(3,4-ethylenedioxythiophene)@poly(styrene sulfonate) as a thermally conductive bridge to cross-link MWCNTs and decrease the thermal resistance. A MWCNT foam was created using the freeze-drying

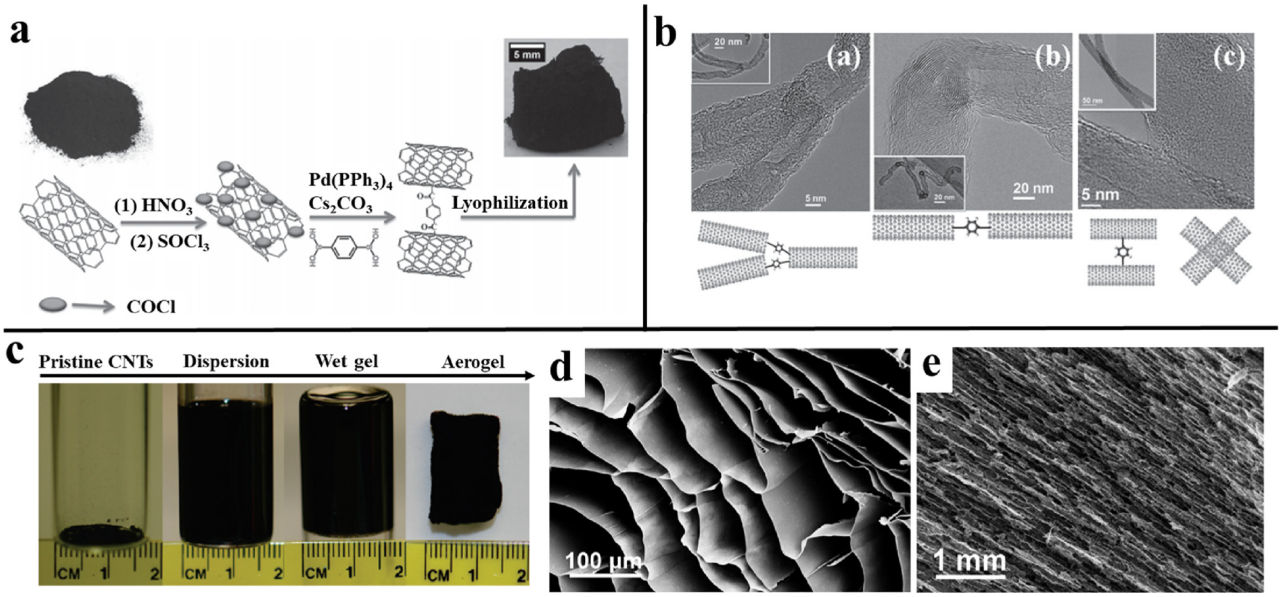

Fig. 20. (a) Preparation process for 3D CNT aerogels from CNT powders via a sol–gel method. (b) High-resolution TEM images of CNT aerogels with different junction structures [250]. Copyright 2015, Wiley-VCH. (c) Optical images for each preparation step during the fabrication of CNT aerogels. (d) Surface morphology of a CNT aerogel. (e) Vertical section image of a CNT aerogel [251]. Copyright 2010, American Chemical Society.

method, and after the introduction of PDMS, the *k* values of the composite reached 0.84 W m^{-1} K^{-1} and 1.16 W m^{-1} K^{-1}, respectively. However, these improvements in thermal conduction still fail to meet expectations, likely because of the huge thermal resistance inside the tubes.

4.3.2.2.1. Interfacial thermal resistance. Compared with the *k* values of individual CNTs (> 3000 W m^{-1} K^{-1} at ambient temperature) [213,256], the *k* values of isotropic CNT networks are much lower. Many studies have shown that CNT networks cannot achieve large improvements in *k*. In addition to the thermal resistance at the interface between the CNTs and the surrounding medium, which unavoidably limits the heat flow, the *k* of CNT–polymer composites is also degraded by the contact thermal resistance between adjacent nanotubes [257]. As shown in Fig. 21, a small contact area between adjacent CNTs leads to a high contact resistance. In polymer composites, phonon transmission between the CNTs is limited by high thermal resistance.

Because the CNT architecture has a loose structure and isotropic stacking, the thermal energy transfer between individual CNTs at the van der Waals contact distance is limited by the large contact resistance arising from weak bonding between the CNTs [219,258]. Malen et al. [259] studied phonon transport in a SWCNT aerogel prepared via the solution processing of purified SWCNTs. This SWCNT aerogel (8 kg m^{-3}) had a poor *k* value of 0.025 ± 0.010 W m^{-1} K^{-1}, which was attributed to the high porosity and the poor heat conduction at the tube–tube junctions. Based on molecular dynamics and mesoscale simulations, these authors suggested that thermal resistance at the junctions, which was due to the poor van der Waals interactions between the SWCNTs, seriously weakened the *k* of each SWCNT. Prasher et al. suggested that the *k* value of a packed bed of CNTs was smaller than those of typical isotropic polymers, with the *k* of the 3D tube network being reduced by the contact resistance at junctions formed between adjacent CNTs (Fig. 22a) [219]. Lukes and Zhong calculated the interfacial thermal resistance at CNT junctions using molecular dynamics and an analytical thermal model, as depicted in Fig. 22b. These calculations revealed that bringing nanotubes into intimate contact with one another decreased the contact thermal resistance by four orders of magnitude [258].

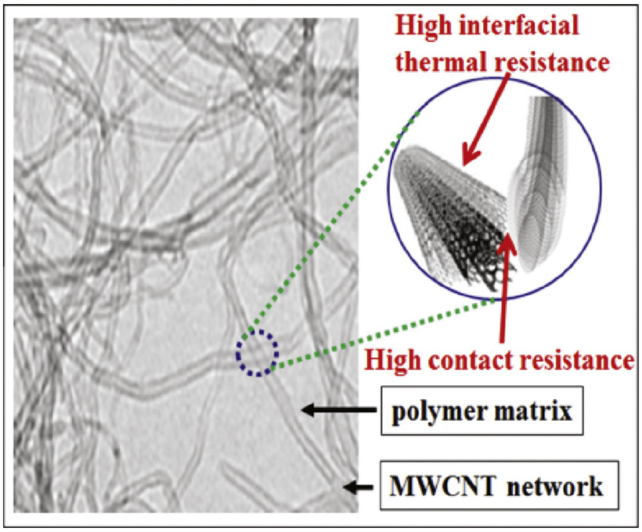

Fig. 21. Schematic diagram of the poor heat transfer in polymer/CNT composites [257]. Copyright 2012, Elsevier Ltd.

The EMT can be used to understand the reason for the *k* of a CNT aerogel being poor despite the individual CNTs having excellent thermal conductance. The *k* of a 3D network (with the density assumed to be 15 mg cm^{-3}) with perfect contact at tube–tube interfaces can be expressed as follows [82,219]:

$$k_{ef} = \langle \cos^2\theta \rangle k_{ECNTs} V_{CNTs} \tag{18}$$

where k_{ef} is the effective thermal conductivity of the macroscopic CNT framework; k_{ECNTs} is the thermal conductivity of the individual tubes in the CNT framework; V_{CNTs} is the volume fraction of the CNTs; and θ is the angle between a given direction and the tube axis. The angle brackets indicate an average over all the tubes in the CNT framework. For a perfectly isotropic structure, the value of $\langle \cos^2\theta \rangle$ is 1/3. The experimentally measured k_{ef} values for the CNT monolith were 0.025–0.15 W m^{-1} K^{-1} and the volume fraction of the CNTs in the sponge was 0.0083. Using these values yields k_{ECNTs} = 9.04–54.22 W m^{-1} K^{-1}, which is more than two orders of magnitude lower than the experimentally measured *k* values of individual MWCNTs (≥2000 W m^{-1} K^{-1}) [260]. This discrepancy is the result of the huge thermal resistance inside the CNT sponge. We define the total thermal resistance

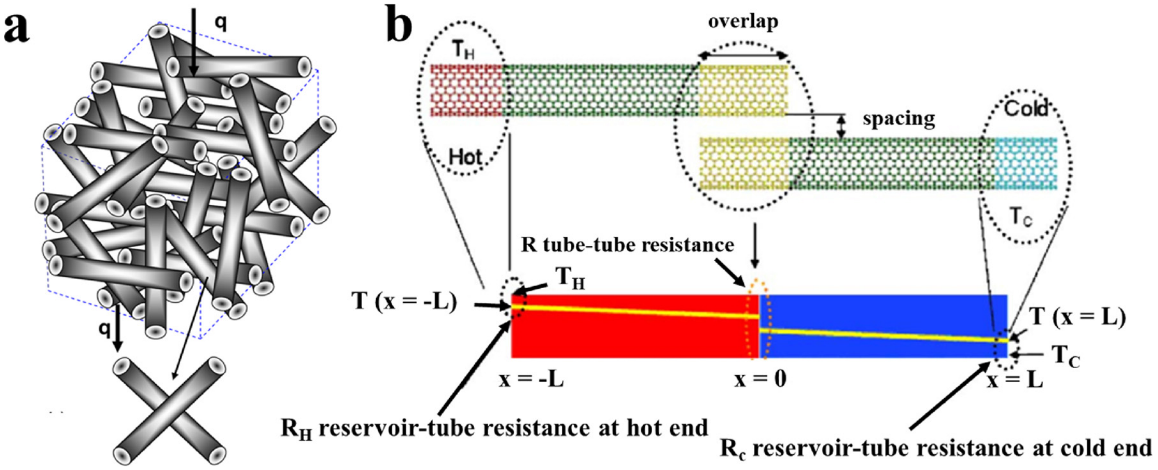

Fig. 22. (a) Schematic of the 3D random of CNT network and the crossed CNTs junctions [219]. Copyright 2009, The American Physical Society. (b) Molecular dynamics (upper) and finite difference models (lower) for investigating the effect of overlap and space on tube–tube and reservoir–tube resistances [258]. Copyright 2006, The American Physical Society.

of a CNT sponge, R_{total}, as:

$$R_{total} = R_{tube} + R_{junction} \tag{19}$$

where R_{tube} is the thermal resistance imposed by thermal transport along the individual CNTs; and $R_{junction}$ is the thermal resistance imposed by thermal transport through the CNT–CNT junctions. R_{total}, R_{tube}, and $R_{junction}$ are estimated separately according to the follow equations:

$$R_{total} = \frac{L}{k_{ef}A} = \frac{L}{k_{ef}(2\pi rn\delta - \pi n^2\delta^2)} \tag{20}$$

$$R_{tube} = \frac{L}{k_{ECNT}A} = \frac{L}{k_{ECNT}(2\pi rn\delta - \pi n^2\delta^2)} \tag{21}$$

$$R_{junction} = \frac{L}{k_{ef}(2\pi rn\delta - \pi n^2\delta^2)} - \frac{L}{k_{ECNT}(2\pi rn\delta - \pi n^2\delta^2)} \tag{22}$$

Here, A is the cross-sectional area of an individual MWCNTs; L is the average length of the MWCNTs (approximately 100 μm); r is the MWCNT radius (10 nm); δ is the layer distance in the MWCNTs (0.335 nm); and n is the number of layers in the MWCNTs (10). This thermal model is meant to estimate the order of magnitude for the thermal conductance. For the 15 mg cm^{-3} CNT sponges ($k \sim 0.081$ W m^{-1} K^{-1}), the calculated values are $R_{total} = 3.95 \times 10^{10}$ K W^{-1}, $R_{tube} = 2.85 \times 10^{8}$ K W^{-1}, and $R_{junction} = 3.92 \times 10^{10}$ K W^{-1}.

From the calculated results, the interface thermal resistance at the CNT–CNT junctions accounts for the majority of the thermal resistance in the CNT sponges, i.e., 99.3 % of the total thermal resistance. This value allows us to assess the effect of the interface resistance at CNT–CNT junctions on the heat flow in composites. Thus, the k of a 3D CNT network mainly results from the heat transfer behavior of the tube junctions [219]; therefore, connecting the surfaces of individual CNTs is crucial for improving heat transfer in macroscopic CNT networks.

4.3.2.2.2. Junction welding. To address the issue of discontinuity, an effective strategy is to construct a covalent structure by welding the joints between the CNTs using a high k material. To and Yang [261] investigated the effect of welding on the thermal conductance of a randomly oriented CNT network using molecular dynamics simulations. The results indicated that the heat conductance of intertube junctions was two orders of magnitude larger than the contact conductance between two adjacent CNTs in close contact (Fig. 23a). In our earlier work [260], we welded the junctions of CNTs by introducing a graphite structure and graphene sheets (Fig. 23b–d). The welding of discontinuous CNTs with graphite or graphene structures effectively decreased the interfacial thermal resistance between adjacent nanotubes and enhanced the heat and stress transfer through the junctions. This interconnected network structure of welded CNTs can be used as a thermally conductive network in polymer matrices to improve the heat transfer efficiency.

Based on the junction welding strategy, we presented a high-performance elastic thermally conductive PDMS composite. As shown in Fig. 24a, a 3D CNT network with welded interconnected graphitic layers was obtained by pyrolyzing polyacrylonitrile. Using this continuous welded 3D CNT framework as the heat conduction network, we prepared a w-CNT/PDMS composite with excellent heat conductivity and elasticity. The maximum k value of the composite was 8.46 W m^{-1} K^{-1} at a loading of 4.57 wt% welded CNTs, which was more than 62 % higher than that of a composite with an unwelded CNT sponge (Fig. 24b). Therefore, improving the continuity of the 3D CNT framework is an efficient way to decrease the thermal resistance and improve the heat transfer performance.

In addition, we also prepared an elastic graphene-strengthened CNT network/polyimide composite (G-CNT/PI) with controllable thermal and electrical conductance and resilience by constructing a 3D interconnected graphene-cross-linked CNT continuous framework (Fig. 24c) [260]. The 3D skeleton consisting of graphene and CNTs served as a conductive network and elastic template to provide rigid and insulating polyimide with good conductance and resilience. During the preparation process, graphene sheets were introduced to strengthen the integration between the tubes in the CNT sponge, thus significantly improving phonon, electron, and stress transmission between neighboring tubes. Subsequently, polyimide layers were uniformly coated on the carbon network via a layer-by-layer deposition process to produce polyimide composites with controllable densities (75.5–210 mg cm^{-3}). This cross-linked porous structure imparted the composite with regulable resilience and robust structural stability (Fig. 24d). This graphene–CNT hybrid skeleton provided transmission channels for phonons and electrons in the polyimide matrix. The k value of composite could be maintained at 0.325–10.89 W m^{-1} K^{-1} with electrical conductivities of 0.015–0.29 S m^{-1}. The elasticity and good heat conduction ability of this composite makes it suitable for flexible heat conductors, and the stress-sensitive conductivity makes it an ideal candidate for preparing piezoresistive sensors.

In summary, most macroscopic 3D CNT architectures are CNT arrays or CNT aerogels. As CNT arrays are parallelly connected networks of 1D tubes, all the tubes are aligned in a single direction and are separated from each other. This parallel network structure results in a high heat transfer capability in the axial direction (alignment direction) [4]. In contrast, CNT aerogels generally exhibit isotropic heat conductance, which is attributable to the random orientation in the

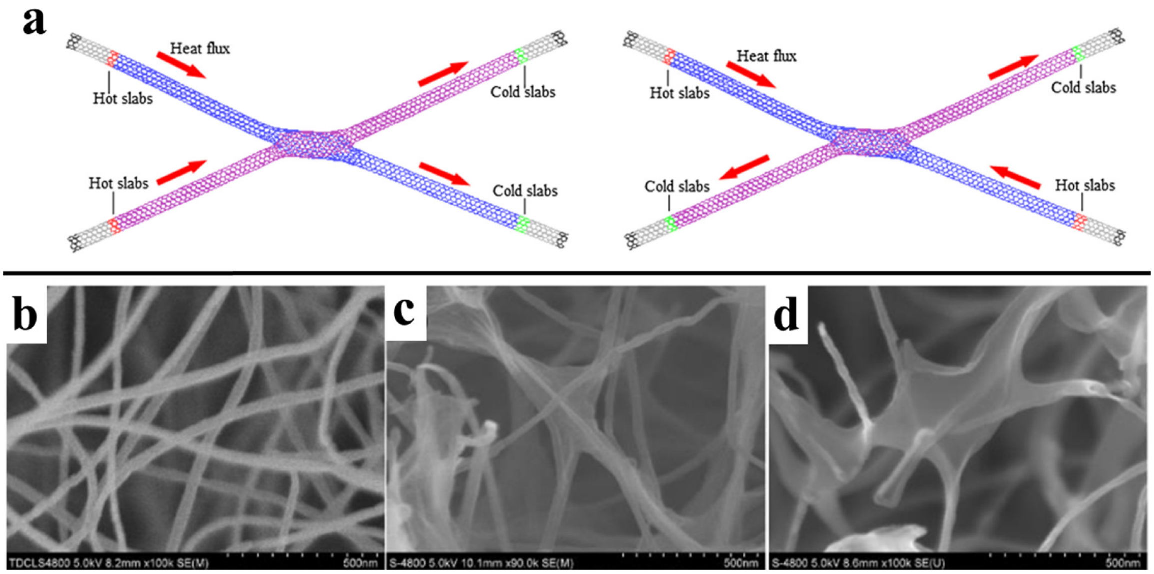

Fig. 23. (a) Effect of intertube junction welding on thermal conductance [261]. Copyright 2014, Elsevier Ltd. SEM images of (b) original CNT sponges and (c, d) CNT networks cross-linked with graphene layers [260]. Copyright 2019, Wiley-VCH.

network. Therefore, composites with either isotropic k or directional k can be prepared by choosing different structural networks according to the requirements. As an effective thermally conductive medium, the 3D CNT framework has the potential to improve the k of polymers. However, isotropic 3D CNT frameworks appear to provide no advantages owing to their loose structures and highly random orientations, which are not conducive to heat transfer. Only by strengthening the connections at the CNT junctions of the internal interfaces in a 3D

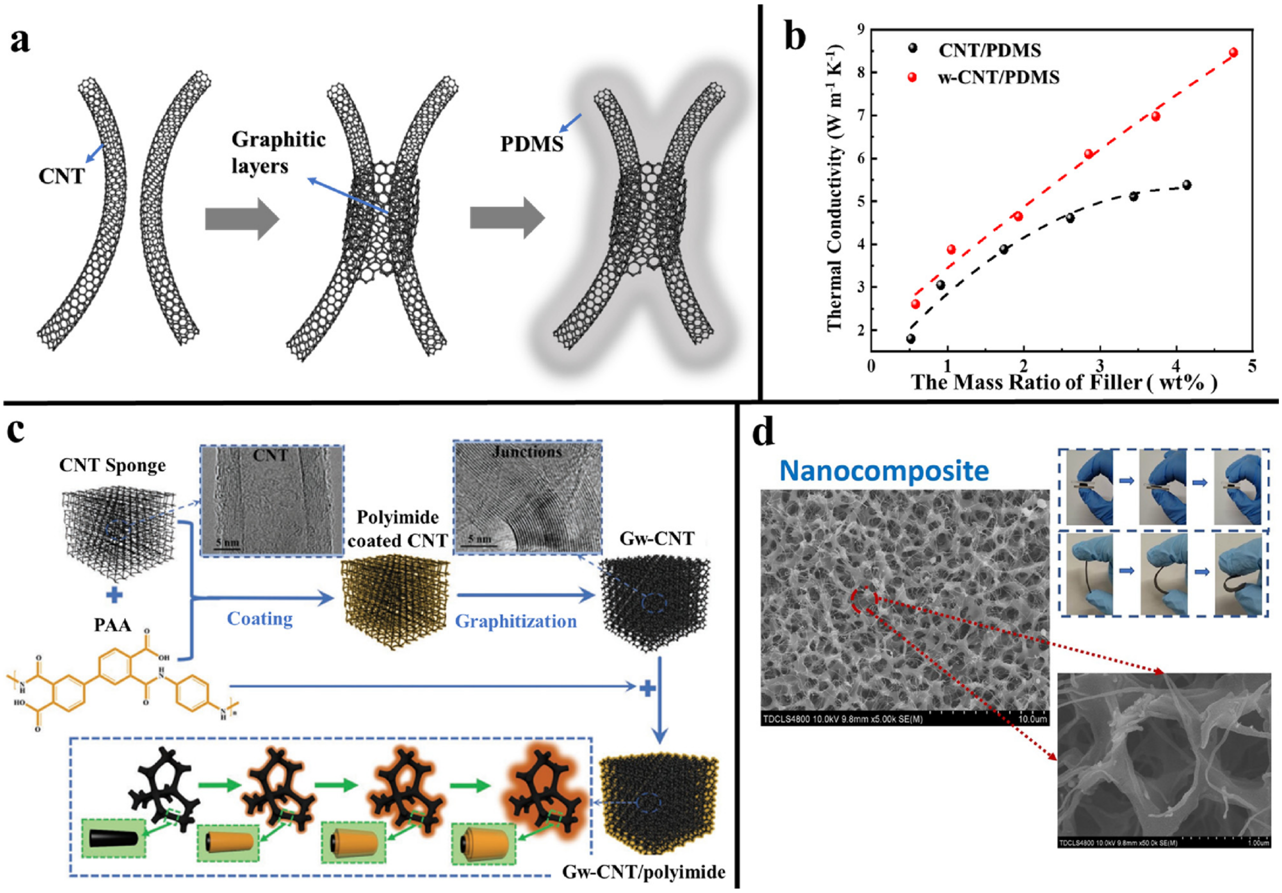

Fig. 24. (a) Schematic of the preparation process for PDMS composites with high thermal conductivities using a 3D CNT framework welded with graphite layers as a thermally conductive network. (b) Effect of graphite welding on the thermal conduction of various samples [262]. Copyright 2019, Elsevier Ltd. (c) Schematic of the preparation process for elastic and highly thermally conductive polyimide composites. (d) SEM images of the polyimide composite microstructures [260]. Copyright 2019, Wiley-VCH.

CNT framework can the heat transfer performance be effectively improved.

4.4. 3D BN frameworks

The intrinsically high electrical conductivities of graphene and CNTs limit their applications in microelectronics packaging, where electrically insulating materials are preferred. Thus, the *k* of polymers, which are typically electrically insulating materials, should be improved by being compounded with thermally conductive fillers that are also suitable electrical insulating materials. Some ceramics (i.e., Al_2O_3, AlN, and BN), which have high *k* values but are suitable electrical insulators [45,263–266]. are considered appropriate candidates for thermally conductive fillers. Among these, BN may be an ideal filler for enhancing the *k* of a polymer matrix owing to its peculiar 2D structure (similar to the graphene structure) and ultrahigh heat conduction ability in the in-plane direction [267].

BN has an analogous crystal structure to graphene and hence possesses similar material properties, good heat conduction, thermal stability, and outstanding mechanical properties. However, BN and graphene have contrasting electrical conductivities and permittivities. Owing to various desirable properties, such as high thermal conduction (more than 600 W m^{-1} K^{-1}), good electrical insulation properties, a relatively low dielectric constant, and a 2D structure, BN platelets are promising candidates for preparing polymer-based thermal conductors. BN has been widely used as a filler in the fabrication of composites with high thermal conductance. Because interfaces are a crucial factor in determining the *k* of composites, 3D BN frameworks have been constructed to connect BN platelets and act as a thermally conductive network in polymers.

4.4.1. Construction of 3D BN networks

3D BN networks exhibit a remarkable ability to increase the *k* of polymer composites without affecting the good insulating properties of polymers. Similar to 3D graphene networks, 3D BN networks are typically prepared using two basic strategies: self-assembly of BN nanosheets on a template [22,268–275]and in situ growth by CVD on Ni templates [275–280]. As shown in Fig. 25a–d, Zeng's group [22] created a 3D BN network using ice template assembly. This process usually includes three steps: (i) preparing an aqueous suspension of non-covalent functionalized BN nanosheets with an adhesive (such as PVA) being used as a bridge to link the BN sheets; (ii) freezing and freeze-casting of the aqueous suspension; and (iii) heat-temperature annealing to remove the adhesive. Similarly, Wang et al. use the NH_4HCO_3 as the structural constituent material to fabricate the 3D BN foam, the NH_4HCO_3 act as a template and can be removed by decomposing in gas at 80 °C [281]. In addition to the removable template (like ice), some existing 3D skeletons, such as melamine foam [282], graphene [81,275,283,284], and cellulose nanofiber aerogels (Fig. 25e) [269], have also been used as templates to form BN sheets into interconnected 3D architectures. However, the 3D networks formed via the template self-assembly of BN nanosheets are generally not completely continuous, and the discontinuities amplify phonon scattering at the interfaces between the BN sheets.

Depositing atomic hexagonal BN layers by CVD on 3D metallic templates is an effective method for preparing continuous, interface-free 3D BN structures, as shown in Fig. 26. Ashton et al. [277] grew a 3D BN foam on a nickel foam via low-pressure CVD using solid borazine as the precursor. Typically, the growth mechanism is similar to that for graphene preparation. In the preparation process, the precursor (borazine) was diffused into a quartz tube furnace. At a temperature of 1000 °C, borazine was converted to polyborazylene, which diffused onto the surface of the metallic foam, where cross-linking reactions occurred between B−H and NH− groups on adjacent chains. Finally, the unaligned chain branches of polyborazylene were dehydrogenated to obtain hexagonal BN [276]. To isolate the BN layers from the Ni template without causing damage or collapse, the BN surface was dip-coated with poly(methyl methacrylate) (PMMA) layers before etching the template (similar to the process used for GFs). In the final step, the PMMA layers were removed via high-temperature annealing in air. The obtained 3D BN networks, which were inherently interconnected and isotropic in nature, can substantially reduce or even eliminate the interfaces between BN sheets in composites.

Methods other than the two conventional preparation strategies have also been reported for preparing 3D BN. Hersam et al. [285] constructed BN architectures using 3D printing technology; these architectures were subsequently used as heat-conductive fillers to enhance the *k* of polymers. Zettl and co-workers [286] synthesized sp^2-bonded BN aerogels based on graphene frameworks via the carbothermal reduction of boron oxide and simultaneous nitridation. In this process, graphene was placed together with boron oxide in a graphite crucible and heated rapidly in a furnace under a nitrogen atmosphere. Under high-temperature conditions, the graphene sheets reacted with boron oxide and nitrogen to form sp^2-bonded BN, nominally according to the equation $B_2O_3 + 3C + N_2 \rightarrow 2BN + 3CO$ [287]. This reaction was one of the earliest synthetic routes for high-purity BN and has been used to prepare high-quality 3D continuous structures of BN. Similarly, Golberg et al. [288] created a BN nanorod-assembled

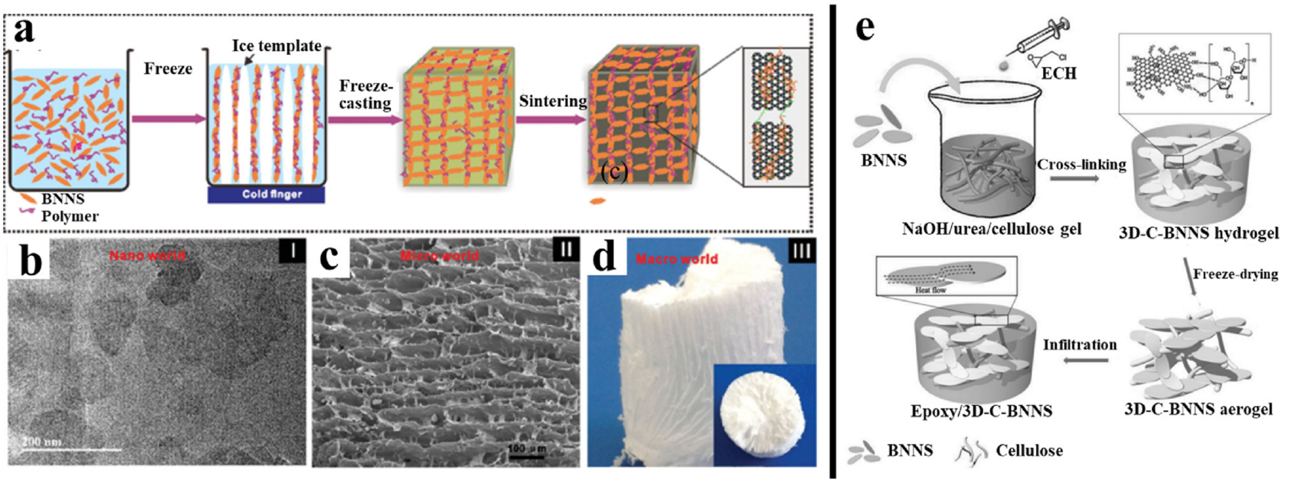

Fig. 25. (a) Schematic diagram of the construction of BN aerogels by a self-assembly strategy. (b, c) Microscope images and (d) photograph of the BN aerogel [22]. Copyright 2015, Wiley-VCH. (e) Schematic illustration of the preparation process for a 3D interconnected BN network using cellulose nanofibers as a template [269]. Copyright 2016, Wiley-VCH.

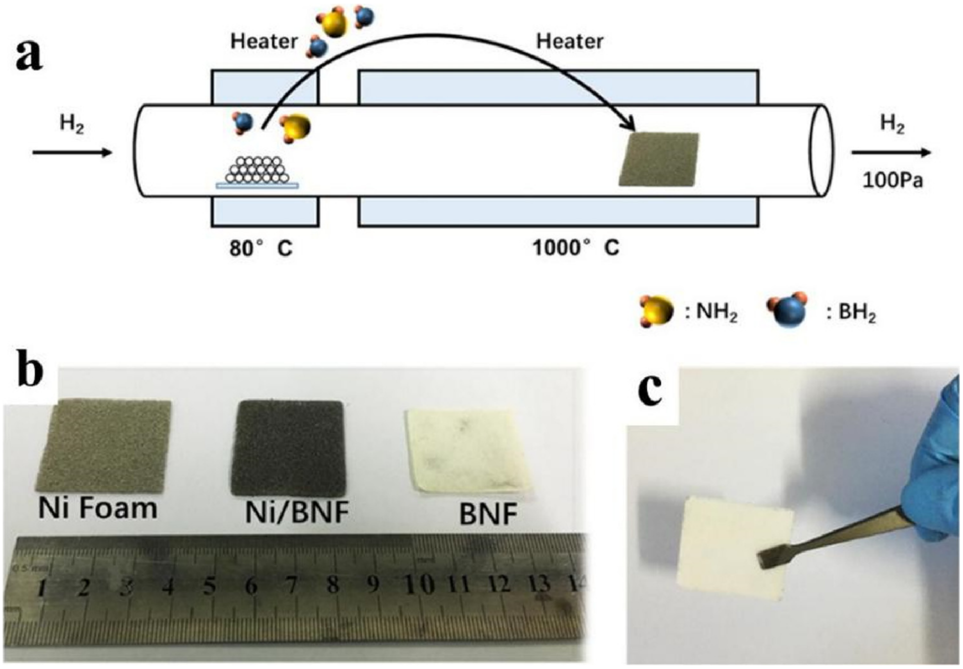

Fig. 26. (a) CVD growth of a BN foam using a nickel foam template. (b) Photographs of Ni foam, Ni/BN foam, and BN. (c) Photograph of the prepared freestanding 3D h-BN [277]. Copyright 2017, Elsevier Ltd.

framework and a nanosheet-interconnected framework via in situ carbothermal reduction CVD using a carbon-based network as the template. Cao et al. [289] fabricated bulk BN foams by pyrolyzing polyborazine foams. However, these BN foams exhibited poor thermal conduction (0.03–0.05 W m^{-1} K^{-1}) owing to their low densities and amorphous microstructures. Recently, Wong et al. [115] prepared an interconnected hierarchically porous BN network via direct foaming. In this approach for building an isotropic BN architecture, sodium dodecyl sulfate was used as both a foaming agent and a surfactant, and gelatin was used to protect the structural integrity of the BN architecture. Inspired by the jelly, Li et al. constructed the interconnected BN network by a foaming route using the curdlan as the gelling agent to immobilize the bubble-templated network [290]. Other authors also constructed a 3D architecture by stacking BN sheets reinforced with rGO via an ice template. The corresponding BN-rGO/epoxy composite presented a high in-plane k value of 5.05 W m^{-1} K^{-1}. Theoretical modeling demonstrated that the improvement in k could be attributed to a continuous BN-rGO network, which led to high rates of phonon transfer [81].

4.4.2. 3D BN/polymer composites

As the k value of BN is intrinsically inferior to those of carbon materials, higher loadings of BN are necessary to prepare thermally conductive composites. To maximize the heat conduction in a polymer matrix, it is necessary to assemble BN nanosheets into a 3D multilevel ordered structure and load the conductive network into the polymer matrix. Zeng et al. [22] reported a novel composite consisting of a 3D BN network infiltrated with an epoxy, which exhibited a high k value of 2.85 W m^{-1} K^{-1} at a relatively low BN content (9.29 vol%). This k value was 181 % higher than that of the composite with randomly dispersed BN nanosheets. The 3D BN architecture provides improved heat conduction by decreasing the interfacial thermal resistance among the BN sheets. Chen et al. [269] prepared a nanofiber-supported BN framework by assembling BN nanosheets on a 3D cellulose skeleton. The interconnected network structure of the 3D BN framework was preserved in the polymer matrix. The composite had an exceptionally high k value of approximately 3.13 W m^{-1} K^{-1} at a BN loading of 9.6 vol%, which is more than 14 times that of the neat polymer.

Furthermore, the heat transfer ability in different directions can be regulated by changing the orientation of the 3D BN skeleton. Bai et al. [291] used bidirectional freezing to build a 3D conduction network with long-range-aligned lamellar layers. This highly organized BN architecture offered extended phonon channels in parallel directions and achieved a considerable improvement in k (6.07 W m^{-1} K^{-1}) at a relatively low BN loading of 15 vol%. In addition, these authors also studied the effects of three different BN network structures on heat conduction in polymer composites (Fig. 27). This comparison of BN/polymer composites with “randomly distributed”, “uniaxially aligned”, and “nacre-mimetic long-range lamellar” BN networks revealed that the network with a regular orientation was the most favorable for heat transfer (Fig. 27d). The k values of these three composites were 1.00 ± 0.19, 1.9 ± 0.35, and 6.07 ± 0.2 W m^{-1} K^{-1} (Fig. 27e).

In addition to the directional freeze-drying method, a few other methods have been reported for assembling ordered 3D BN structures to prepare anisotropic thermally conductive materials. For instance, Kim et al. [292] presented a guided assembly technology in a tetrahedrally structured PDMS slab to construct a continuous 3D BN network. As shown in Fig. 28a, a BN dispersion was dropped between a blade and a tetrahedral PDMS slab. Blade movement resulted in immediate solvent evaporation and stacking of the BN sheets on the structured PDMS surface. These BN sheets, which were aligned on the PDMS slab, were transferred onto a polymer, which imparted an inverse shape to the aligned structures. As shown in Fig. 28b, the 3D thermal transfer pathways in different polymer composites (PDMS and acrylate adhesive) resulted in good k values of 1.15 W m^{-1} K^{-1} (through-plane) and 11.05 W m^{-1} K^{-1} (in-plane) at a low BN fraction (16 wt%). Recently, Hu and co-workers constructed the BN network by the salt template method using PVDF as the adhesive (Fig. 28c), which was used as the thermal conductive network to improve the k value of epoxy. The interconnected 3D BN network can be observed in the obtained epoxy/BN-PVDF composites (Fig. 28d). The composite exhibited a k of 1.227 W m^{-1} K^{-1} with 21 wt% BN, which can be further increased to 1.466 W m^{-1} K^{-1} by thermal treatment to convert the PVDF into carbon (Fig. 28e). As illustrated in Fig. 28f, the improvement is attributed from the conversion of PVDF into carbon can alleviate the phonon scattering and promote more phonons pass through the filler

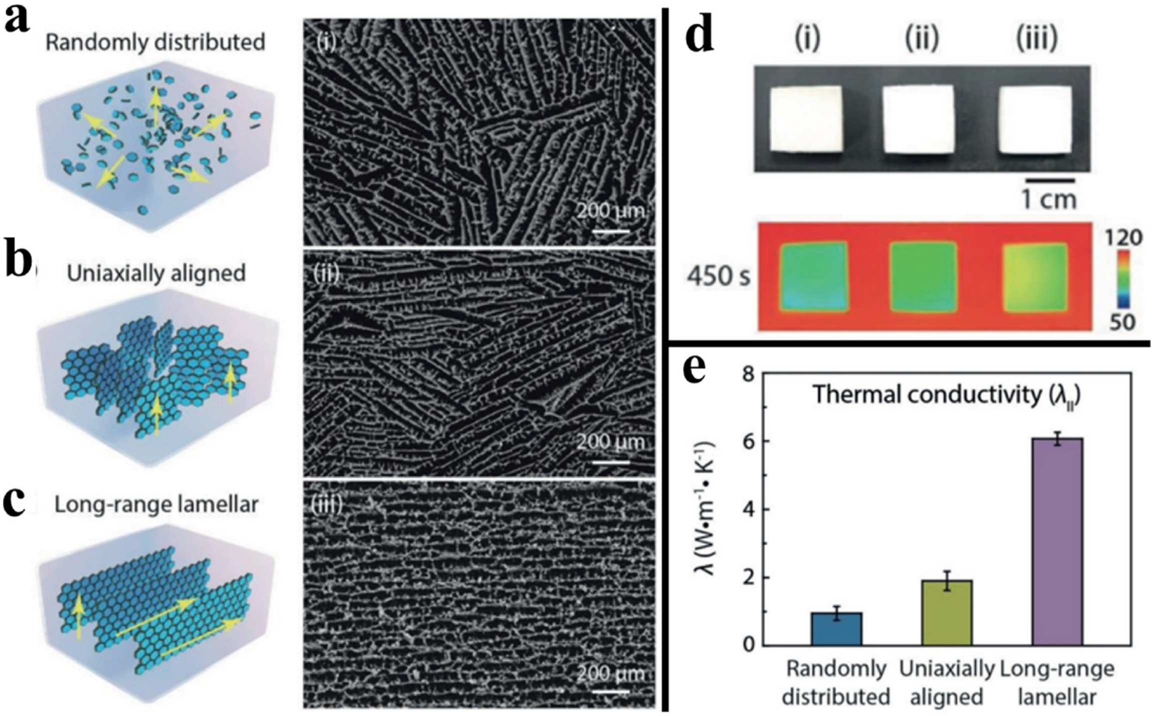

Fig. 27. Comparison of the microstructures and thermal behavior of composites filled with distinct BN frameworks: (a) randomly distributed network, (b) uniaxially aligned network, and (c) long-range lamellar network. (d) Optical and infrared thermal photographs of the three composites. (e) *k* values of the three composites [291]. Copyright 2019, Wiley-VCH.

interface [293].

In summary, owing to their good heat conductivity and electrical insulation properties, 3D networks composed of BN have become a viable option for the production of microelectronics packaging. 3D BN skeletons can be constructed via self-assembly of BN nanosheets or via in situ CVD growth. For the preparation of composites, the density of the 3D BN framework should be high enough to provide a sufficient number of channels for heat transfer. In thermally conductive composites, the *k* in different directions can be controlled by adjusting the orientation of the BN network.

4.5. *Metallic 3D networks*

The earliest commercial thermally conductive adhesives and other TIMs all used metal micro/nanoparticles as thermally conductive reinforcements [294–298]. As heat-conducting additives, metal fillers provide superior thermal transfer performance. In recent years, the use of 3D metallic networks as the heat transfer medium for polymer composites has received considerable attention owing to their low thermal resistance, low density, and mechanical strength. Commonly used 3D heat-conducting metallic networks include copper foams [299–302], aluminum foams [303,304], nickel foams [305,306], and silver skeletons [307]. For example, Fang and co-workers [23] used metal foams (Ni and Cu) as conductive skeletons to increase the *k* of PCMs. Future discoveries of new thermally conductive materials will provide more choices for building thermally conductive networks. Razeeb et al. prepared a TIM by embedding a silver nanowire array inside a polycarbonate template; the resulting composites exhibited a *k* value of 30.3 W m^{-1} K^{-1} [307]. As the majority of metal foams are commercially available, these polymer composites can be fabricated using the direct impregnation method. Although the *k* values of metals are inferior to those of graphene and CNTs, the internal continuity of 3D metal networks imparts a smaller interface thermal resistance, which is crucial for increasing the heat transfer ability of polymers.

Metallic fillers are generally used in combination with other fillers to form interconnected 3D hybrid heat-conducting networks [308]. Xu et al. fabricated the hybrid filler network by using the carbon felt (CFelt) as skeleton and electroplating the Cu on the CFelt surface (as shown in Fig. 29a). By impregnating the epoxy, the obtained composites (Cu-CFelt/epoxy) presented a high k of 30.69 W m^{-1} K^{-1}, which was 140 times higher than the pure epoxy (Fig. 29b, c) [116]. Zhu et al. constructed a CNT–Cu hybrid foam via a high-temperature tube furnace process. As a thermally conductive reinforcement, this hybrid foam improved the thermal transport properties of paraffin wax, increasing the *k* value to 3.49 W m^{-1} K^{-1} from 0.105 W m^{-1} K^{-1} [309]. Huang et al. fabricated epoxy composites with an rGO-wrapped nickel foam as the heat-conducting filler. The presence of rGO improved the compatibility between the nickel foam and the epoxy, resulting in a 2.6-fold enhancement of the *k* value [306]. Metallic nanoparticles are also widely used as junction connectors to bridge adjacent filler particles, and the resulting 3D conducting networks usually exhibit a reduced contact thermal resistance among filler particles [310,311]. For instance, Sun and co-workers prepared highly thermally conductive epoxy composites by introducing silver nanoparticles into a BN network to create additional contacts between the BN sheets [312].

In summary, owing to their superior thermal conductivity and excellent structural continuity, metallic networks are promising candidates for fabricating highly thermally conductive polymer composites. However, the poor flexibility, poor interfacial compatibility with polymer matrices and modification difficulties have limited the application of metallic fillers in the field of polymer-based TIMs.

4.6. *Other 3D filler frameworks*

Several other types of fillers with high thermal conductivity can also be constructed into 3D networks via self-assembly or CVD (e.g., diamond, Al_2O_3, and SiC). These fillers offer more options for producing heat-conductive polymer composites.

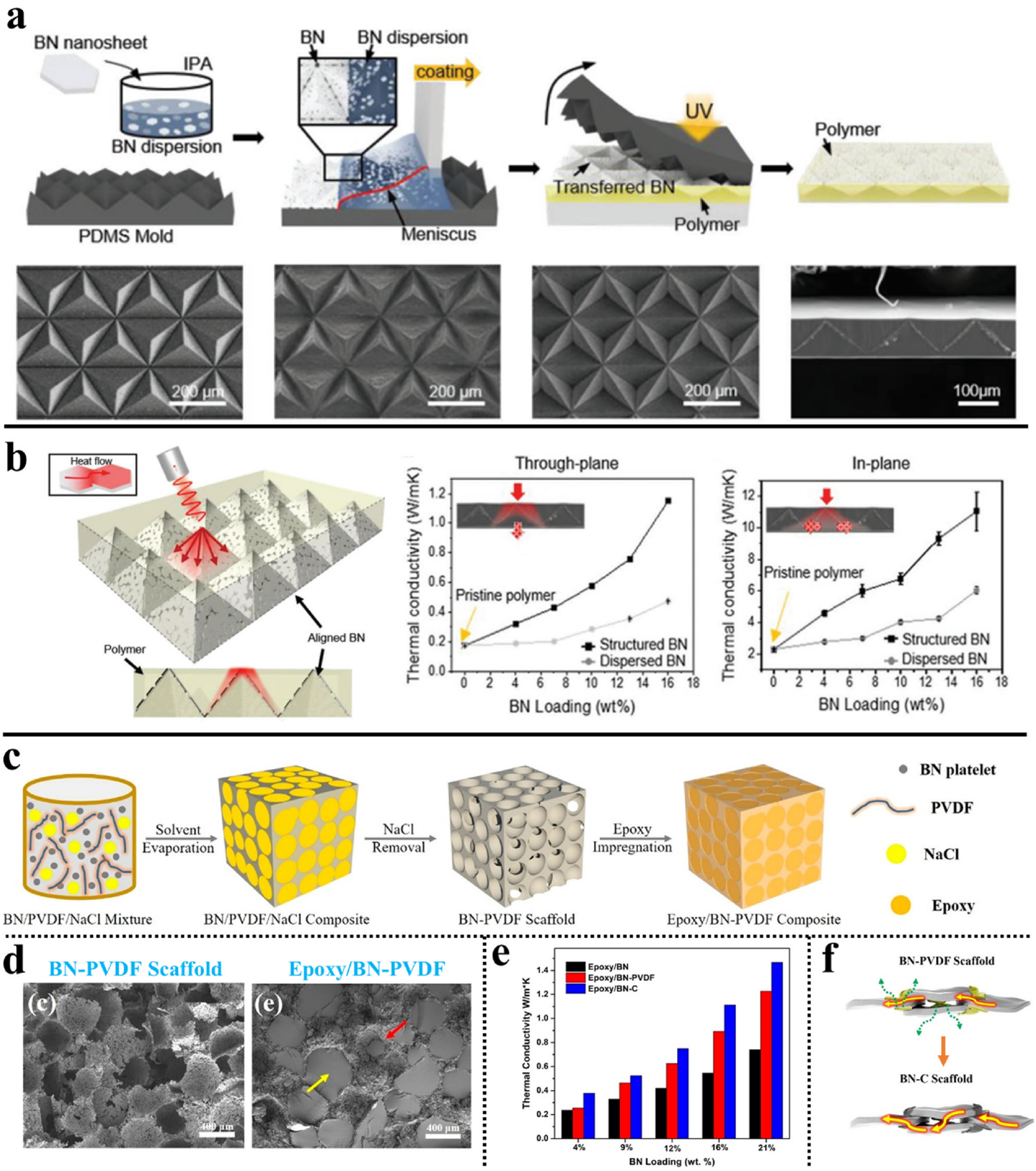

Fig. 28. (a) Schematic for the fabrication of an anisotropic heat-conducting polymer film via the guided assembly of BN sheets on a structured PDMS slab and corresponding SEM images of each fabrication step. (b) Schematic of a BN–epoxy composite film with continuous 3D thermal transfer pathways provided by the tetrahedral BN network and the heat transfer abilities of BN–epoxy composites with randomly dispersed filler sheets and a structured filler network [292]. Copyright 2019, Wiley-VCH. (c) Schematic for the preparation of BN-PVDF networks and epoxy composites by the salt template method. (d) SEM images of the obtained BN-PVDF networks and the Epoxy/BN-PVDF composites. (e) The *k* values of epoxy composites with different fillers. (f) Schematic illustration of thermal conduction mechanism at BN-PVDF interface and BN-C interface [293]. Copyright 2020, American Chemical Society.

4.6.1. Carbon-based heat-conductive networks

In addition to CNTs and graphene, other highly thermally conductive carbon materials, such as graphite foam, diamond foam, and other carbon foams, can be used to improve the *k* of polymers by constructing 3D networks [313–318]. Wei et al. [24] prepared a novel macroscopic porous structure of diamond foam by hot-filament CVD on a Cu foam substrate. This 3D diamond foam at a loading of 1.2 wt% significantly increased the *k* value of an epoxy from 0.23 to 2.28 W m^{-1} K^{-1}. 3D diamond foams have also been used in thermal energy storage applications to enhance the heat transfer ability of PCMs (Fig. 30) [313]. Karthik et al. [316,317] fabricated a highly interconnected 3D graphite foam with a moderate *k* value by pyrolyzing polymeric precursors and PU foam. This foam was used as a heat conduction matrix to improve the *k* of PCMs. Thus, the diversity of carbon materials expands

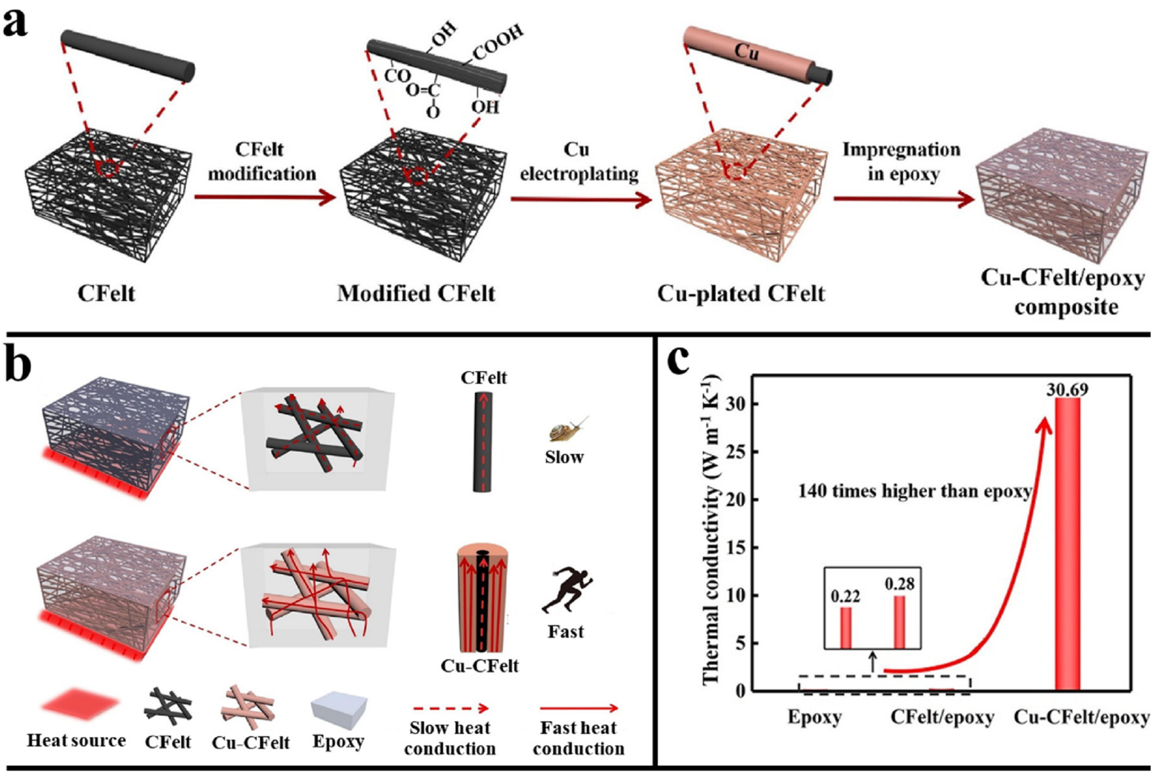

Fig. 29. (a) Schematic of preparation process of Cu-CFelt/epoxy composites. (b) Schematic illustration of the heat transfer behavior in CFelt/epoxy and Cu-CFelt/epoxy. (c) Comparison of the k value of epoxy composites with different filler network [116]. Copyright 2020, Elsevier Ltd.

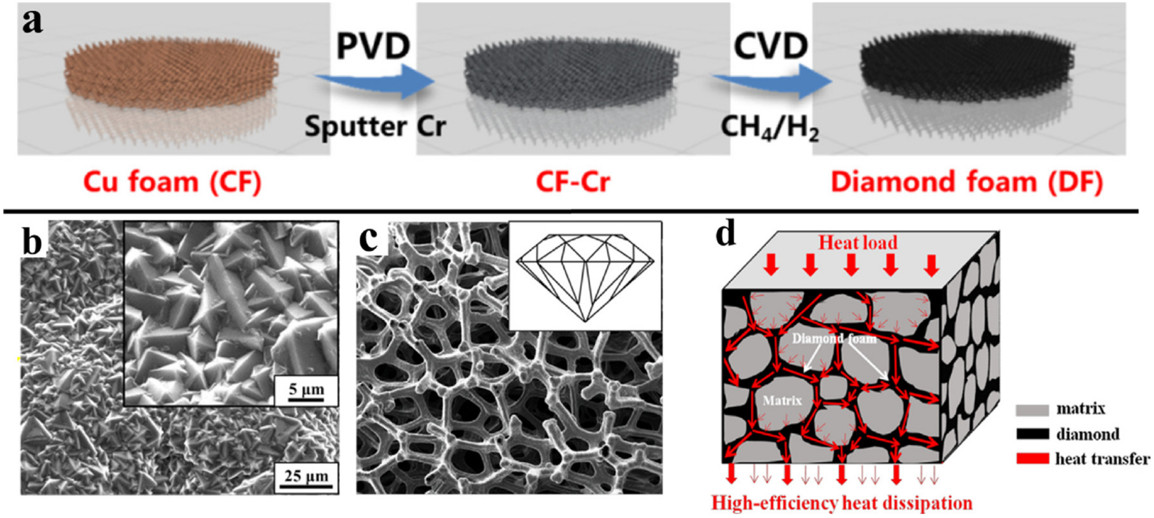

Fig. 30. (a) Procedure for the preparation of a 3D diamond network. (b) High-magnification SEM image of the diamond foam surface [24]. Copyright 2018, Elsevier Ltd. (c) SEM image of the diamond foam. (d) Diagram of a 3D continuous diamond structure as a high-efficiency thermally conductive network [313]. Copyright 2019, Elsevier Ltd.

the availability of 3D network structures for preparing highly thermally conductive composites.

4.6.2. Silicon carbide heat-conductive networks

Owing to its high *k*, chemical stability, and mechanical strength, SiC is considered an ideal thermally conductive filler. Wong et al. [21] used a SiC nanowire to build vertically oriented and interconnected frameworks to enhance the *k* of an epoxy. The obtained composite had a good through-plane *k* value of 1.67 $W\ m^{-1}\ K^{-1}$ with a loading of only 2.17 vol% SiC. The SiC frameworks were constructed via freeze-casting of nanowire aqueous suspensions, followed by thermal sintering to consolidate the junctions; this resulted in aligned honeycomb-like SiC layers. Jiang et al. [110] constructed a 3D-structured composite of SiC nanowires and graphene sheets by employing high-frequency heating. This 3D filler embedded in a polyimide matrix improved the heat conductance, with a *k* value of 2.63 $W\ m^{-1}\ K^{-1}$ obtained with 11 wt% filler. Feng et al. [319] prepared a thermally conductive composite network from preconstructed vertically oriented SiC microwires via unidirectional freeze-casting. This vertically aligned SiC network exhibited a significant *k* enhancement at a low loading.

4.6.3. Other thermally conductive networks

In recent years, other high-*k* materials have also been used to construct 3D thermally conductive networks. As a traditional conductor, Al_2O_3 has a relatively high *k* value (~ 36 W m^{-1} K^{-1}) and is inexpensive. Yuan et al. [320] constructed a continuous Al_2O_3 network using branched Al_2O_3, which substantially improved the thermal transfer ability of polymers. Hong et al. [321] used a polypropylene (PP) aerogel as a heat conduction network in a PP/PCM composite. This *k* value of this composite was 0.534 W m^{-1} K^{-1} at 25 °C, which was more than 100 % larger than that of pure paraffin. Huang et al. used the MXene ($Ti_3C_2T_x$) as filler to construct the aligning interconnected conductive network, which can achieve a 220 % improvement in *k* of PDMS with a low MXene content (2.5 vol%) [322]. The construction of heat conduction networks using various fillers provides more candidates for the preparation of polymer-based TIMs.

4.6.4. 3D hybrid thermally conductive networks

Many studies have indicated that the incorporation of multiple fillers into polymers is an effective strategy for realizing high-performance composites [51,323–325]. Compared with the enhancement achieved with a single filler, remarkable synergetic effects can be achieved by incorporating multiple filler materials, such as graphene and BN, via a well-designed process [326]. Coordination between multiple fillers can realize great improvements in the *k* of composites [46,48,323,324,327–332]. Yao et al. [81] constructed a 3D phonon transfer network consisting of stacked BN sheets and rGO. The resultant epoxy composite displayed a high *k* value of 5.5 W m^{-1} K^{-1} with 13.16 vol% filler, which is superior to the performance reported for BN-based composites. Kim et al. constructed a hybrid filler network by alternately stacking BN sheets and rGO in a well-aligned microsandwich structure. This orientated network provided an 11-fold increase in the *k* value of polyimide composites at a low filler content (2.5 vol%) [333]. Yu et al. [111] built a continuous rGO/BN thermally conductive network by hydrothermally treating a suspension of GO sheets and BN platelets. The resulting polymer composite exhibited a high *k* value of 11.01 W m^{-1} K^{-1} in the through-plane direction. Hybrid networks significantly enhance the diversity of available 3D structures and can endow materials with various interesting properties.

5. In situ construction of 3D interconnected networks

The formation of an interconnected network is essential for improving the heat transfer ability of polymers. While using preconstructed 3D networks as fillers is an effective method for forming continuous heat conduction networks in polymer matrices, other methods, such as adding a large volume fraction of particle fillers, are not widely successful. However, another simple and scalable approach has been proposed for preparing thermally conductive polymer composites via in situ construction of an interconnected conducting network [334–337]. In this process, polymer powders are precoated with a thermally conductive filler and then shaped into a monolith by hot pressing. As shown in Fig. 31a, Lin's group prepared the graphene/polymer composites by coating graphene on polymer powder first, followed by hot pressing [43]. Thus, a continuous graphene conducting network can be formed in the polymer matrix, and this approach can be used for almost all thermoplastic polymers (polyethylene, PP, PVA, and polyvinylidene fluoride). The *k* of PP composites with an in situ constructed interconnected graphene network was much higher than those of blended composites with randomly distributed graphene (Fig. 31b, c). Similarly, Wu and Wang prepared highly thermally conductive BN/polystyrene composites using this coating and hot-pressing method. The resultant sample had a *k* value of 8.0 W m^{-1} K^{-1} at a BN content of 13.4 vol% (Fig. 31d) [69]. Wang's group fabricated highly ordered 3D CNTs/polystyrene composites using this approach, as shown in Fig. 31e. CNTs were coated at the surfaces of polystyrene particles and a 3D CNT interconnected framework was formed in the polystyrene matrix after compression and heat treatment [335]. This process provides a new strategy for preparing unique composite structures with excellent properties.

However, there are several limitations to this approach. First, this thermoforming method is only suitable for the preparation of thermoplastic polymer materials, and it is often necessary to process the polymer into tiny particles in advance [43]. Second, it is difficult to construct anisotropic thermally conductive composites via this method because this stacking and assembly method strongly favors the formation of isotropic interconnected network structures [338]. Third, forming a perfect, even coating of the filler on the polymer microparticles is challenging. Moreover, completely coated filler particles could form discontinuous polymer phases in composites, thus affecting the mechanical properties of the macroscopic materials. Therefore, this in situ construction approach for 3D interconnected conducting network has narrow applicability.

6. Summary and outlook

Flexible, lightweight, and highly thermally conductivity polymer-based TIMs are significant for the development of next-generation high-power and highly integrated electronic devices. Because of the revolutionary progress in nanomaterials and materials processing technology, a variety of novel thermally conductive fillers and 3D architectures have been rapidly developed, providing numerous possibilities for the preparation of high-performance polymer-based TIMs. In this review, we provide distinctive perspectives on the current scientific research trends in 3D thermally conductive networks for applications in advanced polymer-based TIMs. The thermal conduction mechanisms, the factors affecting thermal conduction in polymers, and various strategies for improving heat transfer capacities are discussed. In addition, the construction methods and structural characteristics of different 3D structures, including GFs, CNT networks, BN networks, and other 3D interconnected architectures are discussed and contrasted. On this basis, the following main conclusions can be drawn:

(1) Phonon transport is the dominant mechanism of thermal conduction in polymers. Disordered polymer molecular chains and weak molecular interactions can cause intense phonon scattering and impede phonon transfer, which are responsible for the poor thermal conductivity of polymers. Strategies to improve the thermal conductivity of polymers include regulating molecules to reduce the disorder of polymer molecular chains and thus weaken phonon scattering or constructing phonon transport pathways in the polymer matrix by filling with thermally conductive fillers. Although engineering the chain orientation, crystallinity, and molecular interactions can improve the intrinsic thermal conduction of polymers, it is still extremely challenging to design and modify polymer molecular structures in a controllable manner. In contrast, strengthening with thermally conductive fillers is a widely applicable and effective method, as the phonons can be effectively transferred through the thermal conduction network formed by fillers in the polymer matrix.

(2) In polymer composites, the *k* value is mainly limited by the interfacial thermal resistance at various interfaces, including the filler–polymer and filler–filler interfaces. A great mismatch between the inherent phonon frequencies is responsible for the thermal resistance at the filler–polymer interface. This phenomenon is unavoidable and it is difficult to realize significant improvements. Thus, the interfacial thermal resistance at the filler–filler interfaces plays a decisive role in the *k* of polymer composites. In traditional polymer composites with dispersed filler particles, it is difficult to form an interconnected filler network, which limits the extent to which *k* can be improved. In contrast, constructing a 3D network in polymer composites has been shown to be an effective route for realizing high-efficiency heat transfer at relatively low filler

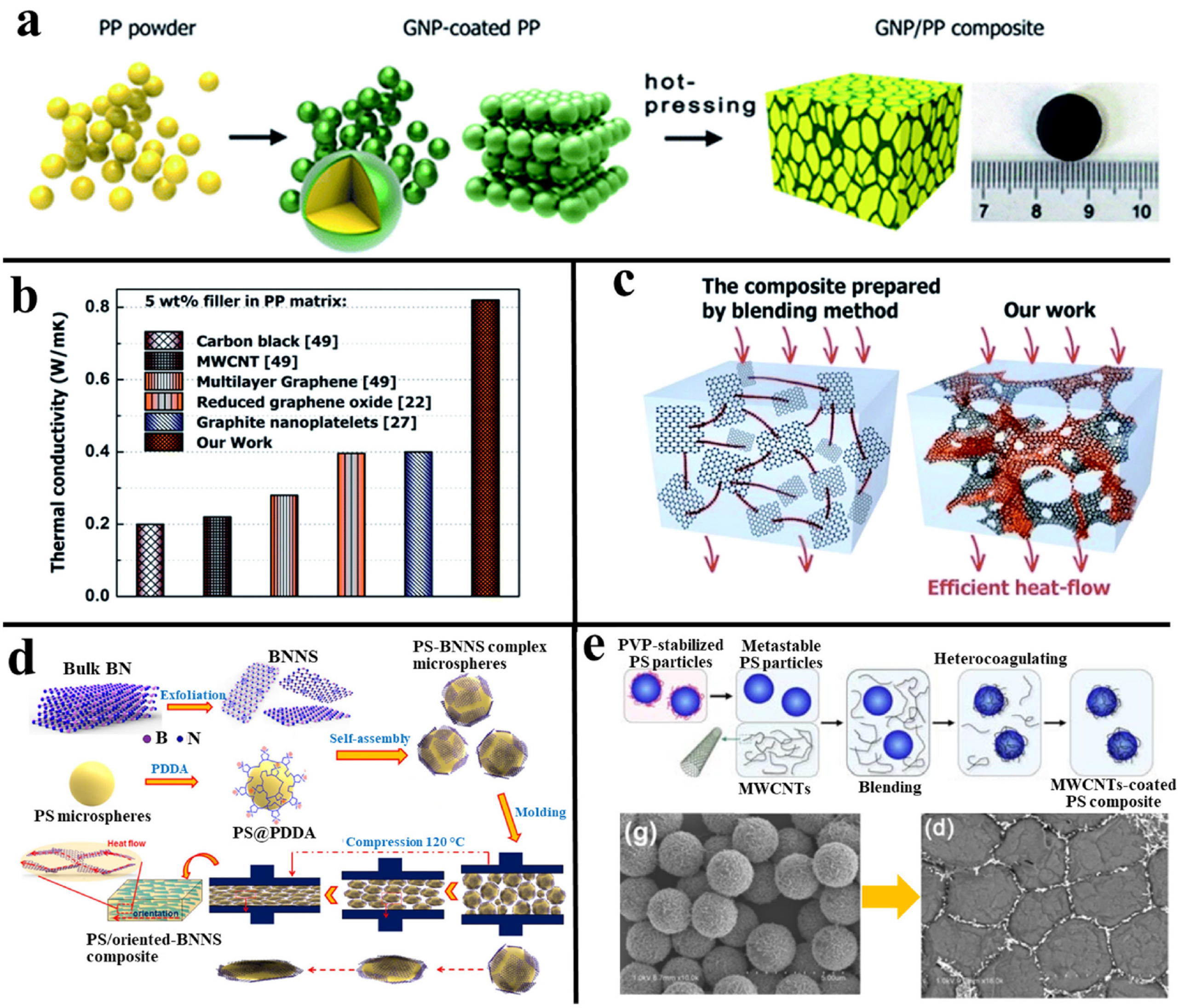

Fig. 31. (a) Schematic of the preparation process for thermal conducting composites via the in situ construction of a 3D interconnected network. (b) Comparison between the *k* values of these composites with those containing a randomly dispersed filler. (c) Schematic of efficient thermal conduction through an interconnected graphene network compared with that through dispersed graphene [43]. Copyright 2017, Royal Society of Chemistry. (d) Schematic of the formation mechanism for polystyrene composites with a continuous BN network [69]. Copyright 2017, American Chemical Society. (e) Schematic of the preparation of CNT-coated polystyrene particles and micrographs of CNT/polystyrene spheres and composites [335]. Copyright 2019, Science Publishing Group.

loadings owing to the low interface thermal resistance in the intrinsic interconnected 3D structure. Many studies have demonstrated that the improvement in thermal conduction achieved using 3D network fillers is far greater than that realized using dispersed filler particles.

(3) The most commonly studied 3D thermal conductivity networks include GFs, CNT frameworks, BN aerogels, and other 3D-structured thermal fillers. GF, the most widely used 3D structure for enhancing the *k* of polymers, is typically prepared via the CVD template growth method or the GO assembly method. Graphene grown via CVD has superior quality, high structural integrity, and better connectivity, whereas the GO assembly method offers advantages in terms of material preparation, economy, and large-scale production. The *k* values of polymer/3D graphene composites are affected by the quality of graphene and the density of its 3D structure; graphene networks with fewer defects and higher densities tend to achieve high *k* values. Interconnected 3D CNT frameworks, including CNT arrays and CNT aerogels, are also important thermally conductive fillers. CNT arrays with highly oriented structures can be fabricated using the CVD method and can endow composites with directional thermal conductivity. In contrast, CNT aerogels usually have isotropic properties and can be prepared by both the CVD method and the chemical/physical assembly method. The loose structure and ultralight density of CNT aerogels result in an inferior *k*. However, strengthening the connections at the junctions of individual CNTs has proven to be an effective method for improving the thermal conduction of CNT aerogels. BN foam is a promising new type of filler that is suitable for TIMs used in electronics owing to its good thermal conduction and electrical insulation properties. 3D BN networks can be constructed via CVD template dispersion and ice template assembly.

(4) In addition to graphene, CNTs, and BN, several other 3D interconnected structures have been proposed, such as graphite foam, SiC foam, diamond foam, and metallic foam. As efficient thermal conductivity networks, all of these materials have a significant effect on enhancing the *k* of polymers. Although graphene and CNTs have the best thermal conductivities, their ultrahigh electroconductivities make them unsuitable for applications in electronic products requiring electrical insulation. Owing to their excellent electrical insulation properties, BN and other inorganic heat-

conducting materials have greater applicability in the field of electronic devices. However, owing to strong interlayer forces in 2D BN, it is difficult to prepare BN sheets by stripping. As a result, small BN sheets are produced, causing abundant interfaces to be formed when building a 3D network, which seriously reduces the heat transfer efficiency. Therefore, methods for preparing large BN sheets are the key to improving the thermal conducting capabilities of 3D BN structures. Compared with the 2D structures of graphene and BN, the 1D nanostructure of CNTs results in more internal interfaces and thus a greater interface thermal resistance in 3D CNT networks. However, this linear structure also facilitates the assembly of CNTs into highly oriented structures (arrays), resulting in much higher anisotropy than can be achieved using 2D materials. Therefore, different heat conduction networks can be selected according to the properties of the materials and the application requirements.

Despite the great progress achieved over the past few years in improving the *k* of polymers by constructing 3D heat conduction networks, there is still significant scope for future work. In particular, we believe that the following aspects warrant exploration:

(1) The constructed 3D network can reduce the contact thermal resistance between the fillers in composites; however, the interfacial thermal resistance at the filler–polymer interface is still very large, which seriously damages the comprehensive properties of the composites. Owing to the tremendous mismatch between the inherent phonon spectra, improving the thermal resistance between two different media remains a difficult problem.
(2) The extent of heat transport is determined by the number of heat conduction channels. Because of weak van der Waals forces, the constructed 3D networks are always less dense, which hinders further improvements in the heat transfer capacity. Thus, improving the density of conductive 3D structures continues to be a challenging issue.
(3) Several theoretical models have been established to calculate and investigate the *k* values and thermal conduction mechanisms of polymer composites with dispersed filler particles. However, few models have been proposed for exploring the heat flow in 3D macroscopic networks. A universal theoretical simulation for thermal conduction in polymer composites with 3D filler networks has yet to be established. Such a model would be of great significance for studying the heat transfer behavior of 3D networks.
(4) Notwithstanding the production of 3D networks and the corresponding polymer composites in laboratories, most current methods cannot achieve large-scale continuous production. Therefore, the commercial applications of polymer-based composites with 3D heat conduction networks are far from being realized.

Declaration of Competing Interest

The authors report no declarations of interest.

Acknowledgements

This work was financially supported by National Key R&D Program of China (No. 2016YFA0202302), National Natural Science Funds for Distinguished Young Scholars (No. 51425306), the State Key Program of National Natural Science Foundation of China (No. 51633007), National Natural Science Foundation of China (Nos. 51773147, 51803151 and 51973152), National Outstanding Youth Talent Program (2019), and Scientific and Technological Commission of China.

References

[1] N. Burger, A. Laachachi, M. Ferriol, M. Lutz, V. Toniazzo, D. Ruch, Prog. Polym. Sci. 61 (2016) 1–28.
[2] Z. Yan, G.X. Liu, J.M. Khan, A.A. Balandin, Nat. Commun. 3 (2012) 1–8.
[3] M.T. Pettes, H.X. Ji, R.S. Ruoff, L. Shi, Nano Lett. 12 (2012) 2959–2964.
[4] T.X. Ji, Y.Y. Feng, M.M. Qin, W. Feng, Compos. Part A-Appl. Sci. Manuf. 91 (2016) 351–369.
[5] G.H. Kim, D. Lee, A. Shanker, L. Shao, M.S. Kwon, D. Gidley, J. Kim, K.P. Pipe, Nat. Mater. 14 (2015) 295–300.
[6] R. Prasher, Proc. IEEE 94 (2006) 1571–1586.
[7] X.Y. Huang, P.K. Jiang, T. Tanaka, IEEE Electr. Insul. Mag. 27 (2011) 8–16.
[8] A. Li, C. Zhang, Y.F. Zhang, Polymers 9 (2017) 437.
[9] X.F. Xu, J. Chen, B.W. Li, Journal Of Physics-Condensed Matter 28 (2016) 483001.
[10] D. Ma, A. Arora, S. Deng, G. Xie, J. Shiomi, N. Yang, Mater. Today Phys. 8 (2019) 56–61.
[11] Y. Zhang, Y.J. Heo, Y.R. Son, I. In, K.H. An, B.J. Kim, S.J. Park, Carbon 142 (2019) 445–460.
[12] C.L. Huang, X. Qian, R.G. Yang, Mater. Sci. Eng. R-Rep. 132 (2018) 1–22.
[13] X.F. Xu, J. Chen, J. Zhou, B.W. Li, Adv. Mater. 30 (2018) 1705544.
[14] A.A. Balandin, Nat. Mater. 10 (2011) 569–581.
[15] C.H. Yu, L. Shi, Z. Yao, D.Y. Li, A. Majumdar, Nano Lett. 5 (2005) 1842–1846.
[16] H.Y. Chen, V.V. Ginzburg, J. Yang, Y.F. Yang, W. Liu, Y. Huang, L.B. Du, B. Chen, Prog. Polym. Sci. 59 (2016) 41–85.
[17] Z.D. Han, A. Fina, Prog. Polym. Sci. 36 (2011) 914–944.
[18] H.X. Ji, L.L. Zhang, M.T. Pettes, H.F. Li, S.S. Chen, L. Shi, R. Piner, R.S. Ruoff, Nano Lett. 12 (2012) 2446–2451.
[19] X.F. Zhang, K.K. Yeung, Z.L. Gao, J.K. Li, H.Y. Sun, H.S. Xu, K. Zhang, M. Zhang, Z.B. Chen, M.M.F. Yuen, S.H. Yang, Carbon 66 (2014) 201–209.
[20] K. Hata, D.N. Futaba, K. Mizuno, T. Namai, M. Yumura, S. Iijima, Science 306 (2004) 1362–1364.
[21] Y.M. Yao, X.D. Zhu, X.L. Zeng, R. Sun, J.B. Xu, C.P. Wong, ACS Appl. Mater. Interfaces 10 (2018) 9669–9678.
[22] X.L. Zeng, Y.M. Yao, Z.Y. Gong, F.F. Wang, R. Sun, J.B. Xu, C.P. Wong, Small 11 (2015) 6205–6213.
[23] X. Huang, Y.X. Lin, G. Alva, G.Y. Fang, Sol. Energy Mater. Sol. Cells 170 (2017) 68–76.
[24] W.T. Ye, Q.P. Wei, L. Zhang, H.C. Li, J.T. Luo, L. Ma, Z.J. Deng, C.T. Lin, K.C. Zhou, Mater. Des. 156 (2018) 32–41.
[25] X.C. Gui, J.Q. Wei, K.L. Wang, A.Y. Cao, H.W. Zhu, Y. Jia, Q.K. Shu, D.H. Wu, Adv. Mater. 22 (2010) 617–621.
[26] A. Henry, G. Chen, Phys. Rev. Lett. 101 (2008) 235502.
[27] X.J. Wang, M. Kaviany, B.L. Huang, Nanoscale 9 (2017) 18022–18031.
[28] Y.F. Xu, D. Kraemer, B. Song, Z. Jiang, J.W. Zhou, J. Loomis, J.J. Wang, M.D. Li, H. Ghasemi, X.P. Huang, X.B. Li, G. Chen, Nat. Commun. 10 (2019) 1–8.
[29] S. Shen, A. Henry, J. Tong, R.T. Zheng, G. Chen, Nat. Nanotechnol. 5 (2010) 251–255.
[30] V. Singh, T.L. Bougher, A. Weathers, Y. Cai, K.D. Bi, M.T. Pettes, S.A. McMenamin, W. Lv, D.P. Resler, T.R. Gattuso, D.H. Altman, K.H. Sandhage, L. Shi, A. Henry, B.A. Cola, Nat. Nanotechnol. 9 (2014) 563-563.
[31] Y.F. Xu, X.X. Wang, J.W. Zhou, B. Song, Z. Jiang, E.M.Y. Lee, S. Huberman, K.K. Gleason, G. Chen, Sci. Adv. 4 (2018) eaar3031.
[32] X.J. Wang, V. Ho, R.A. Segalman, D.G. Cahill, Macromolecules 46 (2013) 4937–4943.
[33] Y. Guo, K. Ruan, X. Shi, X. Yang, J. Gu, Compos. Sci. Technol. 193 (2020) 108134.
[34] X.Y. Huang, T. Iizuka, P.K. Jiang, Y. Ohki, T. Tanaka, J. Phys. Chem. C 116 (2012) 13629–13639.
[35] Y. Huang, J.T. Hu, Y.M. Yao, X.L. Zeng, J.J. Sun, G.R. Pan, R. Sun, J.B. Xu, C.P. Wong, Adv. Mater. Interfaces 4 (2017) 1700446.
[36] Y. Agari, T. Uno, J. Appl. Polym. Sci. 30 (1984) 2225–2235.
[37] Z.H. Li, L. Wang, Y. Li, Y.Y. Feng, W. Feng, Compos. Sci. Technol. 179 (2019) 10–40.
[38] C.Y. Zhi, Y. Bando, C.C. Tang, H. Kuwahara, D. Golberg, Adv. Mater. 21 (2009) 2889–2893.
[39] P. Goli, S. Legedza, A. Dhar, R. Salgado, J. Renteria, A.A. Balandin, J. Power Sources 248 (2014) 37–43.
[40] K.M.F. Shahil, A.A. Balandin, Nano Lett. 12 (2012) 861–867.
[41] M. Shtein, R. Nadiv, M. Buzaglo, K. Kahil, O. Regev, Chem. Mater. 27 (2015) 2100–2106.
[42] X. Yang, X.Y. Yu, K. Naito, H.L. Ding, X.W. Qu, Q.X. Zhang, J. Nanosci. Nanotechnol. 18 (2018) 3291–3298.
[43] F.E. Alam, W. Dai, M.H. Yang, S.Y. Du, X.M. Li, J.H. Yu, N. Jiang, C.T. Lin, J. Mater. Chem. A 5 (2017) 6164–6169.
[44] S.Y. Wei, Q.X. Yu, Z.G. Fan, S.W. Liu, Z.G. Chi, X.D. Chen, Y. Zhang, J.R. Xu, RSC Adv. 8 (2018) 22169–22176.
[45] K. Sato, H. Horibe, T. Shirai, Y. Hotta, H. Nakano, H. Nagai, K. Mitsuishi, K. Watari, J. Mater. Chem. 20 (2010) 2749–2752.
[46] A.P. Yu, P. Ramesh, X.B. Sun, E. Bekyarova, M.E. Itkis, R.C. Haddon, Adv. Mater. 20 (2008) 4740–4744.
[47] Q.Q. Bai, X. Wei, J.H. Yang, N. Zhang, T. Huang, Y. Wang, Z.W. Zhou, Compos. Part A-Appl. Sci. Manuf. 96 (2017) 89–98.
[48] S.Q. Song, Y. Zhang, Carbon 123 (2017) 158–167.
[49] L.J. Fang, C. Wu, R. Qian, L.Y. Xie, K. Yang, P.K. Jiang, RSC Adv. 4 (2014) 21010–21017.
[50] L. Yu, J.S. Park, Y.S. Lim, C.S. Lee, K. Shin, H.J. Moon, C.M. Yang, Y.S. Lee,

J.H. Han, Nanotechnology 24 (2013) 155604.
[51] T.L. Li, S.L.C. Hsu, J. Phys. Chem. B 114 (2010) 6825–6829.
[52] J.P. Cao, X. Zhao, J. Zhao, J.W. Zha, G.H. Hu, Z.M. Dang, ACS Appl. Mater. Interfaces 5 (2013) 6915–6924.
[53] D. Yorifuji, S. Ando, J. Mater. Chem. 21 (2011) 4402–4407.
[54] T.L. Zhou, X. Wang, X.H. Liu, D.S. Xiong, Carbon 48 (2010) 1171–1176.
[55] B.H. Xie, X. Huang, G.J. Zhang, Compos. Sci. Technol. 85 (2013) 98–103.
[56] S.H. Song, K.H. Park, B.H. Kim, Y.W. Choi, G.H. Jun, D.J. Lee, B.S. Kong, K.W. Paik, S. Jeon, Adv. Mater. 25 (2013) 732–737.
[57] C.Y. Zhi, Y. Bando, T. Terao, C.C. Tang, H. Kuwahara, D. Golberg, Adv. Funct. Mater. 19 (2009) 1857–1862.
[58] F.M. Du, C. Guthy, T. Kashiwagi, J.E. Fischer, K.I. Winey, J. Polym. Sci. Part B-Polym. Phys. 44 (2006) 1513–1519.
[59] Z. Liu, J.H. Li, X.H. Liu, ACS Appl. Mater. Interfaces 12 (2020) 6503–6515.
[60] H.S. Kim, J.U. Jang, J. Yu, S.Y. Kim, Compos. Part B-Eng. 79 (2015) 505–512.
[61] H.S. Kim, H.S. Bae, J. Yu, S.Y. Kim, Sci. Rep. 6 (2016) 1–9.
[62] Y.Q. Guo, K.P. Ruan, X.T. Yang, T.B. Ma, J. Kong, N.N. Wu, J.X. Zhang, J.W. Gu, Z.H. Guo, J. Mater. Chem. C 7 (2019) 7035–7044.
[63] W. Yu, H.Q. Xie, L.Q. Yin, J.C. Zhao, L.G. Xia, L.F. Chen, Int. J. Therm. Sci. 91 (2015) 76–82.
[64] V. Goyal, A.A. Balandin, Appl. Phys. Lett. 100 (2012) 073113.
[65] H.S. Kim, J.U. Jang, H. Lee, S.Y. Kim, S.H. Kim, J. Kim, Y.C. Jung, B.J. Yang, Adv. Eng. Mater. 20 (2018) 1800204.
[66] M. Li, Y. Sun, H.Y. Xiao, X.J. Hu, Y.N. Yue, Nanotechnology 26 (2015) 105703.
[67] Y. Zhang, H.X. Han, N. Wang, P.T. Zhang, Y.F. Fu, M. Murugesan, M. Edwards, K. Jeppson, S. Volz, J.H. Liu, Adv. Funct. Mater. 25 (2015) 4430–4435.
[68] D. Li, M.B. Muller, S. Gilje, R.B. Kaner, G.G. Wallace, Nat. Nanotechnol. 3 (2008) 101–105.
[69] X.W. Wang, P.Y. Wu, ACS Appl. Mater. Interfaces 9 (2017) 19934–19944.
[70] V. Varshney, S.S. Patnaik, A.K. Roy, G. Froudakis, B.L. Farmer, ACS Nano 4 (2010) 1153–1161.
[71] M. Cao, C.Y. Du, H. Guo, S.S. Song, X.P. Li, B.A. Li, Compos. Sci. Technol. 173 (2019) 33–40.
[72] K. Gharagozloo-Hubmann, A. Boden, G.J.F. Czempiel, I. Firkowska, S. Reich, Appl. Phys. Lett. 102 (2013) 213103.
[73] H. Shen, J. Guo, H. Wang, N. Zhao, J. Xu, ACS Appl. Mater. Interfaces 7 (2015) 5701–5708.
[74] X. Shen, Z.Y. Wang, Y. Wu, X. Liu, J.K. Kim, Carbon 108 (2016) 412–422.
[75] B. Coto, I. Antia, M. Blanco, I. Martinez-De-Arenaza, E. Meaurio, J. Barriga, J.R. Sarasua, Comput. Mater. Sci. 50 (2011) 3417–3424.
[76] H. Park, J.J. Zhao, J.P. Lu, Nano Lett. 6 (2006) 916–919.
[77] J.Y. Kim, J.H. Lee, J.C. Grossman, ACS Nano 6 (2012) 9050–9057.
[78] B. Mortazavi, S. Ahzi, Carbon 63 (2013) 460–470.
[79] Y.A. Kim, S. Kamio, T. Tajiri, T. Hayashi, S.M. Song, M. Endo, M. Terrones, M.S. Dresselhaus, Appl. Phys. Lett. 90 (2007) 093125.
[80] R.J. Warzoha, A.S. Fleischer, Nano Energy 6 (2014) 137–158.
[81] Y.M. Yao, J.J. Sun, X.L. Zeng, R. Sun, J.B. Xu, C.P. Wong, Small 14 (2018) 1704044.
[82] C.-W. Nan, R. Birringer, D.R. Clarke, H. Gleiter, J. Appl. Phys. 81 (1997) 6692–6699.
[83] G.Q. Zhang, Y.P. Xia, H. Wang, Y. Tao, G.L. Tao, S.T. Tu, H.P. Wu, J. Compos. Mater. 44 (2010) 963–970.
[84] S.H. Xie, Y.Y. Liu, J.Y. Li, Appl. Phys. Lett. 92 (2008) 243121.
[85] J.E. Peters, D.V. Papavassiliou, B.P. Grady, Macromolecules 41 (2008) 7274–7277.
[86] K. Chu, C.C. Jia, X.B. Liang, H. Chen, W.J. Gao, Rare Metals 28 (2009) 646–650.
[87] V. Varshney, A.K. Roy, G. Froudakis, B.L. Farmer, Nanoscale 3 (2011) 3679–3684.
[88] J. Chen, J.H. Walther, P. Koumoutsakos, Adv. Funct. Mater. 25 (2015) 7539–7545.
[89] G.K. Dimitrakakis, E. Tylianakis, G.E. Froudakis, Nano Lett. 8 (2008) 3166–3170.
[90] B. Tang, S.L. Wang, J. Zhang, Z.W. Wang, Y.F. He, W.Q. Huang, Int. Mater. Rev. 63 (2018) 204–225.
[91] C. Zhang, A. Li, Y.H. Zhao, S.L. Bai, Y.F. Zhang, Compos. Part B-Eng. 135 (2018) 201–206.
[92] F. Irin, S. Das, F.O. Atore, M.J. Green, Langmuir 29 (2013) 11449–11456.
[93] Z.P. Chen, W.C. Ren, L.B. Gao, B.L. Liu, S.F. Pei, H.M. Cheng, Nat. Mater. 10 (2011) 424–428.
[94] M. Xu, D.N. Futaba, T. Yamada, M. Yumura, K. Hata, Science 330 (2010) 1364–1368.
[95] K. Zhang, Y. Chai, M.M.F. Yuen, D.G.W. Xiao, P.C.H. Chan, Nanotechnology 19 (2008) 215706.
[96] Z.L. Gao, K. Zhang, M.M.F. Yuen, Nanotechnology 22 (2011) 265611.
[97] Q.Z. Liang, X.X. Yao, W. Wang, Y. Liu, C.P. Wong, ACS Nano 5 (2011) 2392–2401.
[98] I. Kholmanov, J. Kim, E. Ou, R.S. Ruoff, L. Shi, ACS Nano 9 (2015) 11699–11707.
[99] M. Loeblein, A. Bolker, S.H. Tsang, N. Atar, C. Uzan-Saguy, R. Verker, I. Gouzman, E. Grossman, E.H.T. Teo, Small 11 (2015) 6425–6434.
[100] Y.H. Zhao, Z.K. Wu, S.L. Bai, Composites Part a-Applied Science and Manufacturing 72 (2015) 200–206.
[101] J. Yang, X.F. Li, S. Han, R.Z. Yang, P. Min, Z.Z. Yu, J. Mater. Chem. A 6 (2018) 5880–5886.
[102] F. An, X.F. Li, P. Min, P.F. Liu, Z.G. Jiang, Z.Z. Yu, ACS Appl. Mater. Interfaces 10 (2018) 17383–17392.
[103] Z. Fan, F. Gong, S.T. Nguyen, H.M. Duong, Carbon 81 (2015) 396–404.
[104] G. Lian, C.C. Tuan, L.Y. Li, S.L. Jiao, Q.L. Wang, K.S. Moon, D.L. Cui, C.P. Wong, Chem. Mater. 28 (2016) 6096–6104.
[105] J. Yang, X.F. Li, S. Han, Y.T. Zhang, P. Min, N. Koratkar, Z.Z. Yu, J. Mater. Chem. A 4 (2016) 18067–18074.
[106] H. Hou, W. Dai, Q.W. Yan, L. Lv, F.E. Alam, M.H. Yang, Y.G. Yao, X.L. Zeng, J.B. Xu, J.H. Yu, N. Jiang, C.T. Lin, J. Mater. Chem. A 6 (2018) 12091–12097.
[107] Z.D. Liu, D.Y. Shen, J.H. Yu, W. Dai, C.Y. Li, S.Y. Du, N. Jiang, H.R. Li, C.T. Lin, RSC Adv. 6 (2016) 22364–22369.
[108] H.X. Ji, D.P. Sellan, M.T. Pettes, X.H. Kong, J.Y. Ji, L. Shi, R.S. Ruoff, Energy Environ. Sci. 7 (2014) 1185–1192.
[109] J. Yang, E.W. Zhang, X.F. Li, Y.T. Zhang, J. Qu, Z.Z. Yu, Carbon 98 (2016) 50–57.
[110] W. Dai, J.H. Yu, Y. Wang, Y.Z. Song, F.E. Alam, K. Nishimura, C.T. Lin, N. Jiang, J. Mater. Chem. A 3 (2015) 4884–4891.
[111] F. An, X.F. Li, P. Min, H.F. Li, Z. Dai, Z.Z. Yu, Carbon 126 (2018) 119–127.
[112] J. Yang, G.Q. Qi, Y. Liu, R.Y. Bao, Z.Y. Liu, W. Yang, B.H. Xie, M.B. Yang, Carbon 100 (2016) 693–702.
[113] R. Wang, L.X. Wu, D.X. Zhuo, J.H. Zhang, Y.D. Zheng, Ind. Eng. Chem. Res. 57 (2018) 10967–10976.
[114] X. Shen, Z.Y. Wang, Y. Wu, X. Liu, Y.B. He, Q.B. Zheng, Q.H. Yang, F.Y. Kang, J.K. Kim, Mater. Horiz. 5 (2018) 275–284.
[115] Z.L. Tian, J.J. Sun, S.G. Wang, X.L. Zeng, S. Zhou, S.L. Bai, N. Zhao, C.P. Wong, J. Mater. Chem. A 6 (2018) 17540–17547.
[116] F. Xu, Y. Cui, D. Bao, D. Lin, S. Yuan, X. Wang, H. Wang, Y. Sun, Chem. Eng. J. 388 (2020) 124287.
[117] P. Lv, X.W. Tan, K.H. Yu, R.L. Zheng, J.J. Zheng, W. Wei, Carbon 99 (2016) 222–228.
[118] T.X. Ji, Y.Y. Feng, M.M. Qin, S.W. Li, F. Zhang, F. Lv, W. Feng, Carbon 131 (2018) 149–159.
[119] J.K. Ma, T.Y. Shang, L.L. Ren, Y.M. Yao, T. Zhang, J.Q. Xie, B.T. Zhang, X.L. Zeng, R. Sun, J.B. Xu, C.P. Wong, Chem. Eng. J. 380 (2020) 122550.
[120] Z. Wang, Y. Cao, D. Pan, S. Hu, Polymers 12 (2020) 1121.
[121] Y. Lin, J. Chen, P.K. Jiang, X.Y. Huang, Chem. Eng. J. 389 (2020) 123467.
[122] M. Foygel, R.D. Morris, D. Anez, S. French, V.L. Sobolev, Phys. Rev. B 71 (2005) 104201.
[123] M.A. Schuetz, L.R. Glicksman, J. Cell. Plast. 20 (1984) 114–121.
[124] M. Qin, Y. Xu, R. Cao, W. Feng, L. Chen, Adv. Funct. Mater. 28 (2018) 1805053.
[125] H.M. Fang, S.L. Bai, C.P. Wong, Compos. Part A-Appl. Sci. Manuf. 112 (2018) 216–238.
[126] Nat. Nanotechnol. 5 (2010) 755-755.
[127] A.K. Geim, K.S. Novoselov, Nat. Mater. 6 (2007) 183–191.
[128] S. Stankovich, D.A. Dikin, G.H.B. Dommett, K.M. Kohlhaas, E.J. Zimney, E.A. Stach, R.D. Piner, S.T. Nguyen, R.S. Ruoff, Nature 442 (2006) 282–286.
[129] X.L. Pan, L.H. Shen, A.P.H.J. Schenning, C.W.M. Bastiaansen, Adv. Mater. 31 (2019) 1904348.
[130] A.K. Geim, Science 324 (2009) 1530–1534.
[131] L. Hu, T. Desai, P. Keblinski, J. Appl. Phys. 110 (2011) 033517.
[132] J.J. Jia, X.Y. Sun, X.Y. Lin, X. Shen, Y.W. Mai, J.K. Kim, ACS Nano 8 (2014) 5774–5783.
[133] C.B. Liang, H. Qiu, Y.Y. Han, H.B. Gu, P. Song, L. Wang, J. Kong, D.P. Cao, J.W. Gu, J. Mater. Chem. C 7 (2019) 2725–2733.
[134] X.H. Cao, Z.Y. Yin, H. Zhang, Energy Environ. Sci. 7 (2014) 1850–1865.
[135] Z.P. Chen, C. Xu, C.Q. Ma, W.C. Ren, H.M. Cheng, Adv. Mater. 25 (2013) 1296–1300.
[136] M. Loeblein, R.Y. Tay, S.H. Tsang, W.B. Ng, E.H.T. Teo, Small 10 (2014) 2992–2999.
[137] L.C. Tang, Y.J. Wan, D. Yan, Y.B. Pei, L. Zhao, Y.B. Li, L.B. Wu, J.X. Jiang, G.Q. Lai, Carbon 60 (2013) 16–27.
[138] L.Z. Guan, Y.J. Wan, L.X. Gong, D. Yan, L.C. Tang, L.B. Wu, J.X. Jiang, G.Q. Lai, J. Mater. Chem. A 2 (2014) 15058–15069.
[139] L.Z. Guan, L. Zhao, Y.J. Wan, L.C. Tang, Nanoscale 10 (2018) 14788–14811.
[140] K.W. Chen, L.B. Chen, Y.Q. Chen, H. Bai, L. Li, J. Mater. Chem. 22 (2012) 20968–20976.
[141] Y.X. Xu, K.X. Sheng, C. Li, G.Q. Shi, ACS Nano 4 (2010) 4324–4330.
[142] Z.Q. Niu, J. Chen, H.H. Hng, J. Ma, X.D. Chen, Adv. Mater. 24 (2012) 4144–4150.
[143] F. Zhang, C. Ye, W. Dai, L. Lv, Q.L. Yuan, K.W.A. Chee, K. Yang, N. Jiang, C.T. Lin, Z.L. Zhan, D. Dai, H. Li, Chin. Chem. Lett. 31 (2020) 244–248.
[144] W.Q. Chen, P.S. Xiao, H.H. Chen, H.T. Zhang, Q.C. Zhang, Y.S. Chen, Adv. Mater. 31 (2019) 1802403.
[145] X. Zhang, K.S. Ziemer, K. Zhang, D. Ramirez, L. Li, S.R. Wang, L.J. Hope-Weeks, B.L. Weeks, ACS Appl. Mater. Interfaces 7 (2015) 1057–1064.
[146] H.C. Bi, K.B. Yin, X. Xie, Y.L. Zhou, N. Wan, F. Xu, F. Banhart, L.T. Sun, R.S. Ruoff, Adv. Mater. 24 (2012) 5124–5129.
[147] W.F. Chen, S.R. Li, C.H. Chen, L.F. Yan, Adv. Mater. 23 (2011) 5679–5683.
[148] L. Qiu, J.Z. Liu, S.L.Y. Chang, Y.Z. Wu, D. Li, Nat. Commun. 3 (2012) 1–7.
[149] Z.H. Tang, S.L. Shen, J. Zhuang, X. Wang, Angew. Chem.-Int. Ed. 49 (2010) 4603–4607.
[150] H. Bai, C. Li, X.L. Wang, G.Q. Shi, J. Phys. Chem. C 115 (2011) 5545–5551.
[151] A. Kudo, P.G. Campbell, J. Biener, Chemnanomat 4 (2018) 338–342.
[152] B. Sun, X.D. Huang, S.Q. Chen, P. Munroe, G.X. Wang, Nano Lett. 14 (2014) 3145–3152.
[153] H. Wang, D.S. Zhang, T.T. Yan, X.R. Wen, J.P. Zhang, L.Y. Shi, Q.D. Zhong, J. Mater. Chem. A 1 (2013) 11778–11789.
[154] X.L. Zhao, W.Q. Yao, W.W. Gao, H. Chen, C. Gao, Adv. Mater. 29 (2017) 1701482.
[155] A.E. Jakus, E.B. Secor, A.L. Rutz, S.W. Jordan, M.C. Hersam, R.N. Shah, ACS Nano 9 (2015) 4636–4648.
[156] C. Zhu, T.Y. Liu, F. Qian, T.Y.J. Han, E.B. Duoss, J.D. Kuntz, C.M. Spadaccini, M.A. Worsley, Y. Li, Nano Lett. 16 (2016) 3448–3456.
[157] Q.Q. Zhang, F. Zhang, S.P. Medarametla, H. Li, C. Zhou, D. Lin, Small 12 (2016) 1702–1708.
[158] X.W. Tang, H. Zhou, Z.C. Cai, D.D. Cheng, P.S. He, P.W. Xie, D. Zhang, T.X. Fan, ACS Nano 12 (2018) 3502–3511.

[159] Z.X. Zhang, J.Y. Qu, Y.Y. Feng, W. Feng, Compos. Commun. 9 (2018) 33–41.
[160] H. Bai, C. Li, X.L. Wang, G.Q. Shi, Chem. Commun. 46 (2010) 2376–2378.
[161] J.K. Han, Y.T. Shen, W. Feng, Nanoscale 8 (2016) 14139–14145.
[162] Y.X. Xu, Q.O. Wu, Y.Q. Sun, H. Bai, G.Q. Shi, ACS Nano 4 (2010) 7358–7362.
[163] H.P. Cong, X.C. Ren, P. Wang, S.H. Yu, ACS Nano 6 (2012) 2693–2703.
[164] Y.H. Chang, J. Li, B. Wang, H. Luo, H.Y. He, Q. Song, L.J. Zhi, J. Mater. Chem. A 1 (2013) 14658–14665.
[165] S.T. Sun, P.Y. Wu, J. Mater. Chem. 21 (2011) 4095–4097.
[166] P.M. Sudeep, T.N. Narayanan, A. Ganesan, M.M. Shaijumon, H. Yang, S. Ozden, P.K. Patra, M. Pasquali, R. Vajtai, S. Ganguli, A.K. Roy, M.R. Anantharaman, P.M. Ajayan, ACS Nano 7 (2013) 7034–7040.
[167] J.H. Li, S.F. Zhao, G.P. Zhang, Y.J. Gao, L.B. Deng, R. Sun, C.P. Wong, J. Mater. Chem. A 3 (2015) 15482–15488.
[168] Y.R. Li, J. Chen, L. Huang, C. Li, J.D. Hong, G.Q. Shi, Adv. Mater. 26 (2014) 4789–4793.
[169] H.Y. Sun, Z. Xu, C. Gao, Adv. Mater. 25 (2013) 2554–2560.
[170] H. Zhuo, Y.J. Hu, X. Tong, Z.H. Chen, L.X. Zhong, H.H. Lai, L.X. Liu, S.S. Jing, Q.Z. Liu, C.F. Liu, X.W. Peng, R.C. Sun, Adv. Mater. 30 (2018) 1706705.
[171] T. Liu, M.L. Huang, X.F. Li, C.J. Wang, C.X. Gui, Z.Z. Yu, Carbon 100 (2016) 456–464.
[172] Y. Zhao, J. Liu, Y. Hu, H.H. Cheng, C.G. Hu, C.C. Jiang, L. Jiang, A.Y. Cao, L.T. Qu, Adv. Mater. 25 (2013) 591–595.
[173] Z. Han, Z.H. Tang, P. Li, G.Z. Yang, Q.B. Zheng, J.H. Yang, Nanoscale 5 (2013) 5462–5467.
[174] W.Y. Zhang, Q.Q. Kong, Z.C. Tao, J.C. Wei, L.J. Xie, X.Y. Cui, C.M. Chen, Adv. Mater. Interfaces 6 (2019) 1900147.
[175] W.F. Chen, L.F. Yan, Nanoscale 3 (2011) 3132–3137.
[176] K.X. Sheng, Y.X. Xu, C. Li, G.Q. Shi, New Carbon Mater. 26 (2011) 9–15.
[177] L.B. Zhang, G.Y. Chen, M.N. Hedhili, H.N. Zhang, P. Wang, Nanoscale 4 (2012) 7038–7045.
[178] S. Korkut, J.D. Roy-Mayhew, D.M. Dabbs, D.L. Milius, I.A. Aksay, ACS Nano 5 (2011) 5214–5222.
[179] X.H. Cao, Y.M. Shi, W.H. Shi, G. Lu, X. Huang, Q.Y. Yan, Q.C. Zhang, H. Zhang, Small 7 (2011) 3163–3168.
[180] I. Jung, H.Y. Jang, S. Park, Appl. Phys. Lett. 103 (2013) 023105.
[181] M. Zhou, T.Q. Lin, F.Q. Huang, Y.J. Zhong, Z. Wang, Y.F. Tang, H. Bi, D.Y. Wan, J.H. Lin, Adv. Funct. Mater. 23 (2013) 2263–2269.
[182] G.Q. Ning, Z.J. Fan, G. Wang, J.S. Gao, W.Z. Qian, F. Wei, Chem. Commun. 47 (2011) 5976–5978.
[183] H.N. Huang, H. Bi, M. Zhou, F. Xu, T.Q. Lin, F.X. Liu, L.Y. Zhang, H. Zhang, F.Q. Huang, J. Mater. Chem. A 2 (2014) 18215–18218.
[184] F. Xu, T.Q. Lin, H. Bi, F.Q. Huang, Carbon 111 (2017) 128–132.
[185] H. Bi, T.Q. Lin, F. Xu, Y.F. Tang, Z.Q. Liu, F.Q. Huang, Nano Lett. 16 (2016) 349–354.
[186] J. Yan, G.Q. Qi, R.Y. Bao, K.Y. Yi, M.L. Li, L. Peng, Z. Cai, M.B. Yang, D.C. Wei, W. Yang, Energy Storage Mater. 13 (2018) 88–95.
[187] Y.J. Zhong, M. Zhou, F.Q. Huang, T.Q. Lin, D.Y. Wan, Sol. Energy Mater. Sol. Cells 113 (2013) 195–200.
[188] J. Liu, Y.F. Liu, H.B. Zhang, Y. Dai, Z.S. Liu, Z.Z. Yu, Carbon 132 (2018) 95–103.
[189] Z.D. Liu, Y.P. Chen, Y.F. Li, W. Dai, Q.W. Yan, F.E. Alam, S.Y. Du, Z.W. Wang, K. Nishimura, N. Jiang, C.T. Lin, J.H. Yu, Nanoscale 11 (2019) 17600–17606.
[190] Y.A. Samad, Y.Q. Li, A. Schiffer, S.M. Alhassan, K. Liao, Small 11 (2015) 2380–2385.
[191] C. Zhu, T.Y.J. Han, E.B. Duoss, A.M. Golobic, J.D. Kuntz, C.M. Spadaccini, M.A. Worsley, Nat. Commun. 6 (2015) 1–8.
[192] D.X. Luong, A.K. Subramanian, G.A.L. Silva, J. Yoon, S. Cofer, K. Yang, P.S. Owuor, T. Wang, Z. Wang, J. Lou, P.M. Ajayan, J.M. Tour, Adv. Mater. 30 (2018) 1707416.
[193] M.K. Smith, D.X. Luong, T.L. Bougher, K. Kalaitzidou, J.M. Tour, B.A. Cola, Appl. Phys. Lett. 109 (2016) 253107.
[194] J. Lin, Z.W. Peng, Y.Y. Liu, F. Ruiz-Zepeda, R.Q. Ye, E.L.G. Samuel, M.J. Yacaman, B.I. Yakobson, J.M. Tour, Nat. Commun. 5 (2014) 1–8.
[195] R.Q. Ye, D.K. James, J.M. Tour, Adv. Mater. 31 (2019) 1803621.
[196] N. Kurra, Q. Jiang, P. Nayak, H.N. Alshareef, Nano Today 24 (2019) 81–102.
[197] X.Y. Xiao, T.E. Beechem, M.T. Brumbach, T.N. Lambert, D.J. Davis, J.R. Michael, C.M. Washburn, J. Wang, S.M. Brozik, D.R. Wheeler, D.B. Burckel, R. Polsky, ACS Nano 6 (2012) 3573–3579.
[198] S.B. Ye, J.C. Feng, P.Y. Wu, ACS Appl. Mater. Interfaces 5 (2013) 7122–7129.
[199] H. Xiao, P. Xie, S.J. Qiu, M.Z. Rong, M.Q. Zhang, Carbon 139 (2018) 648–655.
[200] S.L. Chen, G.H. He, H. Hu, S.Q. Jin, Y. Zhou, Y.Y. He, S.J. He, F. Zhao, H.Q. Hou, Energy Environ. Sci. 6 (2013) 2435–2439.
[201] A. Li, C. Zhang, Y.F. Zhang, Compos. Part A-Appl. Sci. Manuf. 103 (2017) 161–167.
[202] P. Thiyagarajan, Z. Yan, J.C. Yoon, M.W. Oh, J.H. Jang, RSC Adv. 5 (2015) 99394–99397.
[203] Y.H. Zhao, Y.F. Zhang, Z.K. Wu, S.L. Bai, Compos. Part B-Eng. 84 (2016) 52–58.
[204] G.Q. Xin, T.K. Yao, H.T. Sun, S.M. Scott, D.L. Shao, G.K. Wang, J. Lian, Science 349 (2015) 1083–1087.
[205] Y.W. Zhu, S. Murali, W.W. Cai, X.S. Li, J.W. Suk, J.R. Potts, R.S. Ruoff, Adv. Mater. 22 (2010) 3906–3924.
[206] G.Q. Xin, H.T. Sun, S.M. Scott, T.K. Yao, F.Y. Lu, D.L. Shao, T. Hu, G.K. Wang, G. Ran, J. Lian, ACS Appl. Mater. Interfaces 6 (2014) 15262–15271.
[207] L. Song, F. Khoerunnisa, W. Gao, W.H. Dou, T. Hayashi, K. Kaneko, M. Endo, P.M. Ajayan, Carbon 52 (2013) 608–612.
[208] Y.P. Zhang, D.L. Li, X.J. Tan, B. Zhang, X.F. Ruan, H.J. Liu, C.X. Pan, L. Liao, T. Zhai, Y. Bando, S.S. Chen, W.W. Cai, R.S. Ruoff, Carbon 54 (2013) 143–148.
[209] M.H. Jin, T.H. Kim, S.C. Lim, D.L. Duong, H.J. Shin, Y.W. Jo, H.K. Jeong, J. Chang, S.S. Xie, Y.H. Lee, Adv. Funct. Mater. 21 (2011) 3496–3501.
[210] P. Min, J. Liu, X.F. Li, F. An, P.F. Liu, Y.X. Shen, N. Koratkar, Z.Z. Yu, Adv. Funct. Mater. 28 (2018) 1805365.
[211] X.H. Li, P.F. Liu, X.F. Li, F. An, P. Min, K.N. Liao, Z.Z. Yu, Carbon 140 (2018) 624–633.
[212] Y.H. Zhao, Y.F. Zhang, S.L. Bai, Compos. Part A-Appl. Sci. Manuf. 85 (2016) 148–155.
[213] P. Kim, L. Shi, A. Majumdar, P.L. McEuen, Phys. Rev. Lett. 87 (2001) 215502.
[214] S. Berber, Y.K. Kwon, D. Tomanek, Phys. Rev. Lett. 84 (2000) 4613–4616.
[215] M.J. Biercuk, M.C. Llaguno, M. Radosavljevic, J.K. Hyun, A.T. Johnson, J.E. Fischer, Appl. Phys. Lett. 80 (2002) 2767–2769.
[216] M.L. Bauer, Q.N. Pham, C.B. Saltonstall, P.M. Norris, Appl. Phys. Lett. 105 (2014) 151909.
[217] M.B. Jakubinek, M.A. White, G. Li, C. Jayasinghe, W.D. Cho, M.J. Schulz, V. Shanov, Carbon 48 (2010) 3947–3952.
[218] Q.W. Liao, Z.C. Liu, W. Liu, C.C. Deng, N. Yang, Sci. Rep. 5 (2015) 1–7.
[219] R.S. Prasher, X.J. Hu, Y. Chalopin, N. Mingo, K. Lofgreen, S. Volz, F. Cleri, P. Keblinski, Phys. Rev. Lett. 102 (2009) 105901.
[220] Y. Chalopin, S. Volz, N. Mingo, J. Appl. Phys. 108 (2010) 039902.
[221] T. Kimura, H. Ago, M. Tobita, S. Ohshima, M. Kyotani, M. Yumura, Adv. Mater. 14 (2002) 1380–1383.
[222] C.M. Seah, S.P. Chai, A.R. Mohamed, Carbon 49 (2011) 4613–4635.
[223] L.Q. Liu, W.J. Ma, Z. Zhang, Small 7 (2011) 1504–1520.
[224] C. Kocabas, M.A. Meitl, A. Gaur, M. Shim, J.A. Rogers, Nano Lett. 4 (2004) 2421–2426.
[225] H.S. Kim, B. Kim, B. Lee, H. Chung, C.J. Lee, H.G. Yoon, W. Kim, J. Phys. Chem. C 113 (2009) 17983–17988.
[226] B. Kim, H. Chung, W. Kim, J. Phys. Chem. C 114 (2010) 15223–15227.
[227] M. Xu, D.N. Futaba, M. Yumura, K. Hata, ACS Nano 6 (2012) 5837–5844.
[228] T. Yamada, T. Namai, K. Hata, D.N. Futaba, K. Mizuno, J. Fan, M. Yudasaka, M. Yumura, S. Iijima, Nat. Nanotechnol. 1 (2006) 131–136.
[229] H.Q. Hou, A.K. Schaper, Z. Jun, F. Weller, A. Greiner, Chem. Mater. 15 (2003) 580–585.
[230] R. Andrews, D. Jacques, A.M. Rao, F. Derbyshire, D. Qian, X. Fan, E.C. Dickey, J. Chen, Chem. Phys. Lett. 303 (1999) 467–474.
[231] T. Tong, Y. Zhao, L. Delzeit, A. Kashani, M. Meyyappan, A. Majumdar, Ieee Trans. Compon. Packag. Technol. 30 (2007) 92–100.
[232] A.M. Marconnett, N. Yamamoto, M.A. Panzer, B.L. Wardle, K.E. Goodson, ACS Nano 5 (2011) 4818–4825.
[233] I. Ivanov, A. Puretzky, G. Eres, H. Wang, Z.W. Pan, H.T. Cui, R.Y. Jin, J. Howe, D.B. Geohegan, Appl. Phys. Lett. 89 (2006) 223110.
[234] T. Borca-Tasciuc, M. Mazumder, Y. Son, S.K. Pal, L.S. Schadler, P.M. Ajayan, J. Nanosci. Nanotechnol. 7 (2007) 1581–1588.
[235] X. Wang, Q. Jiang, W.Z. Xu, W. Cai, Y. Inoue, Y.T. Zhu, Carbon 53 (2013) 145–152.
[236] N. Mingo, D.A. Broido, Phys. Rev. Lett. 95 (2005) 096105.
[237] M.B. Jakubinek, M.B. Johnson, M.A. White, C. Jayasinghe, G. Li, W.D. Cho, M.J. Schulz, V. Shanov, Carbon 50 (2012) 244–248.
[238] Z.L. Wang, D.W. Tang, X.H. Zheng, W.G. Zhang, Y.T. Zhu, Nanotechnology 18 (2007) 475714.
[239] X.C. Gui, Z.Q. Lin, Z.P. Zeng, K.L. Wang, D.H. Wu, Z.K. Tang, Nanotechnology 24 (2013) 085705.
[240] M. Xu, D.N. Futaba, M. Yumura, K. Hata, Adv. Mater. 23 (2011) 3686–3691.
[241] M. Xu, D.N. Futaba, M. Yumura, K. Hata, Nano Lett. 11 (2011) 3279–3284.
[242] G. Yang, W. Choi, X. Pu, C. Yu, Energy Environ. Sci. 8 (2015) 1799–1807.
[243] D.P. Hashim, N.T. Narayanan, J.M. Romo-Herrera, D.A. Cullen, M.G. Hahm, P. Lezzi, J.R. Suttle, D. Kelkhoff, E. Munoz-Sandoval, S. Ganguli, A.K. Roy, D.J. Smith, R. Vajtai, B.G. Sumpter, V. Meunier, H. Terrones, M. Terrones, P.M. Ajayan, Sci. Rep. 2 (2012) 363.
[244] C.S. Shan, W.J. Zhao, X.L. Lu, D.J. O'Brien, Y.P. Li, Z.Y. Cao, A.L. Elias, R. Cruz-Silva, M. Terrones, B.Q. Wei, J. Suhr, Nano Lett. 13 (2013) 5514–5520.
[245] F.T. Jiang, Y.Z. Fang, Y. Liu, L. Chen, Q.S. Xue, Y. Lu, J.X. Lu, M.Y. He, J. Mater. Chem. 19 (2009) 3632–3637.
[246] K.H. Kim, Y. Oh, M.F. Islam, Nat. Nanotechnol. 7 (2012) 562–566.
[247] K.H. Kim, Y. Oh, M.F. Islam, Adv. Funct. Mater. 23 (2013) 377–383.
[248] M.B. Bryning, D.E. Milkie, M.F. Islam, L.A. Hough, J.M. Kikkawa, A.G. Yodh, Adv. Mater. 19 (2007) 661–664.
[249] R.R. Kohlmeyer, M. Lor, J. Deng, H.Y. Liu, J. Chen, Carbon 49 (2011) 2352–2361.
[250] S. Ozden, T.N. Narayanan, C.S. Tiwary, P. Dong, A.H.C. Hart, R. Vajtai, P.M. Ajayan, Small 11 (2015) 688–693.
[251] J.H. Zou, J.H. Liu, A.S. Karakoti, A. Kumar, D. Joung, Q.A. Li, S.I. Khondaker, S. Seal, L. Zhai, ACS Nano 4 (2010) 7293–7302.
[252] Q.Y. Kong, L. Bodelot, B. Lebental, Y.D. Lim, L.L. Shiau, B. Gusarov, C.W. Tan, K. Liang, C.X. Lu, C.S. Tan, P. Coquet, B.K. Tay, Carbon 132 (2018) 359–369.
[253] W. Choi, K. Choi, C. Yu, Adv. Funct. Mater. 28 (2018) 1704877.
[254] C.W. Chang-Jian, E.C. Cho, K.C. Lee, J.H. Huang, P.Y. Chen, B.C. Ho, Y.S. Hsiao, Compos. Part B-Eng. 136 (2018) 46–54.
[255] E.C. Cho, C.W. Chang-Jian, Y.S. Hsiao, K.C. Lee, J.H. Huang, Compos. Part A-Appl. Sci. Manuf. 90 (2016) 678–686.
[256] J. Hone, M. Whitney, C. Piskoti, A. Zettl, Phys. Rev. B 59 (1999) R2514–R2516.
[257] S.Y. Pak, H.M. Kim, S.Y. Kim, J.R. Youn, Carbon 50 (2012) 4830–4838.
[258] H.L. Zhong, J.R. Lukes, Phys. Rev. B 74 (2006) 125403.
[259] S.N. Schiffres, K.H. Kim, L. Hu, A.J.H. McGaughey, M.F. Islam, J.A. Malen, Adv. Funct. Mater. 22 (2012) 5251–5258.
[260] F. Zhang, Y.Y. Feng, M.M. Qin, L. Gao, Z.Y. Li, F.L. Zhao, Z.X. Zhang, F. Lv,

W. Feng, Adv. Funct. Mater. 29 (2019) 1901383.
[261] X.M. Yang, D.C. Chen, Z.H. Han, X.S. Ma, A.C. To, Int. J. Heat Mass Transf. 70 (2014) 803–810.
[262] F. Zhang, Y. Feng, M. Qin, T. Ji, F. Lv, Z. Li, L. Gao, P. Long, F. Zhao, W. Feng, Carbon 145 (2019) 378–388.
[263] J.F. Fu, L.Y. Shi, D.S. Zhang, Q.D. Zhong, Y. Chen, Polym. Eng. Sci. 50 (2010) 1809–1819.
[264] B.L. Zhu, J. Ma, J. Wu, K.C. Yung, C.S. Xie, J. Appl. Polym. Sci. 118 (2010) 2754–2764.
[265] M. Loeblein, S.H. Tsang, M. Pawlik, E.J.R. Phua, H. Yong, X.W. Zhang, C.L. Gan, E.H.T. Teo, ACS Nano 11 (2017) 2033–2044.
[266] Y.K. Kim, J.Y. Chung, J.G. Lee, Y.K. Baek, P.W. Shin, Compos. Part A-Appl. Sci. Manuf. 98 (2017) 184–191.
[267] V. Guerra, C.Y. Wan, T. McNally, Prog. Mater. Sci. 100 (2019) 170–186.
[268] H. Shen, C. Cai, J. Guo, Z.C. Qian, N. Zhao, J. Xu, RSC Adv. 6 (2016) 16489–16494.
[269] J. Chen, X.Y. Huang, Y.K. Zhu, P.K. Jiang, Adv. Funct. Mater. 27 (2017) 1604754.
[270] Z.C. Qian, H. Shen, X. Fang, L.W. Fan, N. Zhao, J. Xu, Energy Build. 158 (2018) 1184–1188.
[271] X.L. Zeng, J.J. Sun, Y.M. Yao, R. Sun, J.B. Xu, C.P. Wong, ACS Nano 11 (2017) 5167–5178.
[272] J.T. Hu, Y. Huang, Y.M. Yao, G.R. Pan, J.J. Sun, X.L. Zeng, R. Sun, J.B. Xu, B. Song, C.P. Wong, ACS Appl. Mater. Interfaces 9 (2017) 13544–13553.
[273] J. Yang, L.S. Tang, R.Y. Bao, L. Bai, Z.Y. Liu, W. Yang, B.H. Xie, M.B. Yang, J. Mater. Chem. A 4 (2016) 18841–18851.
[274] X.L. Zeng, L. Ye, S.H. Yu, R. Sun, J.B. Xu, C.P. Wong, Chem. Mater. 27 (2015) 5849–5855.
[275] J. Yang, L.S. Tang, L. Bai, R.Y. Bao, Z.Y. Liu, B.H. Xie, M.B. Yang, Y.G. Wei, ACS Sustain. Chem. Eng. 6 (2018) 6761–6770.
[276] J. Yin, X.M. Li, J.X. Zhou, W.L. Guo, Nano Lett. 13 (2013) 3232–3236.
[277] T.S. Ashton, A.L. Moore, J. Mater. Sci. 50 (2015) 6220–6226.
[278] H.M. Fang, S.L. Bai, C.P. Wong, Composites Part a-Applied Science and Manufacturing 100 (2017) 71–80.
[279] T.S. Ashton, A.L. Moore, Int. J. Heat Mass Transf. 115 (2017) 273–281.
[280] Y.X. Song, B. Li, S.W. Yang, G.Q. Ding, C.R. Zhang, X.M. Xie, Sci. Rep. 5 (2015) 10337.
[281] X. Xu, R. Hu, M. Chen, J. Dong, B. Xiao, Q. Wang, H. Wang, Chem. Eng. J. (2020) 125447.
[282] X.W. Wang, P.Y. Wu, Chem. Eng. J. 348 (2018) 723–731.
[283] H.M. Fang, X. Zhang, Y.H. Zhao, S.L. Bai, Compos. Sci. Technol. 152 (2017) 243–253.
[284] L.B. Shao, L.Y. Shi, X.H. Li, N. Song, P. Ding, Compos. Sci. Technol. 135 (2016) 83–91.
[285] L.M. Guiney, N.D. Mansukhani, A.E. Jakus, S.G. Wallace, R.N. Shah, M.C. Hersam, Nano Lett. 18 (2018) 3488–3493.
[286] M. Rousseas, A.P. Goldstein, W. Mickelson, M.A. Worsley, L. Woo, A. Zettl, ACS Nano 7 (2013) 8540–8546.
[287] R.T. Paine, C.K. Narula, Chem. Rev. 90 (1990) 73–91.
[288] Y.M. Xue, X. Zhou, T.Z. Zhan, B.Z. Jiang, Q.S. Guo, X.W. Fu, K. Shimamura, Y.B. Xu, T. Mori, P.C. Dai, Y. Bando, C.C. Tang, D. Golberg, Adv. Funct. Mater. 28 (2018) 1801205.
[289] F. Cao, Y. Ding, L. Chen, C. Chen, Z.Y. Fang, Mater. Des. 54 (2014) 610–615.
[290] J. Li, F. Li, X. Zhao, W. Zhang, S. Li, Y. Lu, L. Zhang, ACS Appl. Electron. Mater. (2020) 0c00227.
[291] J.K. Han, G.L. Du, W.W. Gao, H. Bai, Adv. Funct. Mater. 29 (2019) 1900412.
[292] H. Hong, Y.H. Jung, J.S. Lee, C. Jeong, J.U. Kim, S. Lee, H. Ryu, H. Kim, Z. Ma, T.I. Kim, Adv. Funct. Mater. 29 (2019) 1902575.
[293] X.L. Chen, J.S.K. Lim, W.L. Yan, F. Guo, Y.N. Liang, H. Chen, A. Lambourne, X. Hu, ACS Appl. Mater. Interfaces 12 (2020) 16987–16996.
[294] T.H. Chiang, Y.C. Lin, Y.F. Chen, E.Y. Chen, J. Appl. Polym. Sci. 133 (2016) 43587.
[295] H. Yu, L.L. Li, Y.J. Zhang, Scr. Mater. 66 (2012) 931–934.
[296] K. Pashayi, H.R. Fard, F.Y. Lai, S. Iruvanti, J. Plawsky, T. Borca-Tasciuc, J. Appl. Phys. 111 (2012) 104310.
[297] S.L. Wang, Y. Cheng, R.R. Wang, J. Sun, L. Gao, ACS Appl. Mater. Interfaces 6 (2014) 6481–6486.
[298] A. Bjorneklett, L. Halbo, H. Kristiansen, Int. J. Adhes. Adhes. 12 (1992) 99–104.
[299] W.Q. Li, H. Wan, H.J. Lou, Y.L. Fu, F. Qin, G.Q. He, Energy 127 (2017) 671–679.
[300] P. Zhang, Z.N. Meng, H. Zhu, Y.L. Wang, S.P. Peng, Appl. Energy 185 (2017) 1971–1983.
[301] A. Siahpush, J. O'Brien, J. Crepeau, J. Heat Transfer-Trans. Asme 130 (2008) 082301.
[302] P. Chen, X.N. Gao, Y.Q. Wang, T. Xu, Y.T. Fang, Z.G. Zhang, Sol. Energy Mater. Sol. Cells 149 (2016) 60–65.
[303] K. Lafdi, O. Mesalhy, S. Shaikh, J. Appl. Phys. 102 (2007) 083549.
[304] F. Zhu, C. Zhang, X.L. Gong, Appl. Therm. Eng. 109 (2016) 373–383.
[305] X. Xiao, P. Zhang, M. Li, Appl. Energy 112 (2013) 1357–1366.
[306] L. Huang, P.L. Zhu, G. Li, R. Sun, Appl. Phys. A-Mater. Sci. Process. 122 (2016) 515.
[307] J. Xu, A. Munari, E. Dalton, A. Mathewson, K.M. Razeeb, J. Appl. Phys. 106 (2009) 124310.
[308] X.T. Yang, S.G. Fan, Y. Li, Y.Q. Guo, Y.G. Li, K.P. Ruan, S.M. Zhang, J.L. Zhang, J. Kong, J.W. Gu, Compos. Part A-Appl. Sci. Manuf. 128 (2020) 105670.
[309] W. Zhu, N.X. Hu, Q.P. Wei, L. Zhang, H.C. Li, J.T. Luo, C.T. Lin, L. Ma, K.C. Zhou, Z.M. Yu, Mater. Des. 172 (2019) 107709.
[310] J. Dong, L. Cao, Y. Li, Z. Wu, C. Teng, Compos. Sci. Technol. 196 (2020) 108242.
[311] S.D. Yang, B. Xue, Y. Li, X.J. Li, L. Xie, S.H. Qin, K.H. Xu, Q. Zheng, Chem. Eng. J. 383 (2020) 123072.
[312] F.F. Wang, X.L. Zeng, Y.M. Yao, R. Sun, J.B. Xu, C.P. Wong, Sci. Rep. 6 (2016) 1–9.
[313] L. Zhang, K.C. Zhou, Q.P. Wei, L. Ma, W.T. Ye, H.C. Li, B. Zhou, Z.M. Yu, C.T. Lin, J.T. Luo, X.P. Gan, Appl. Energy 233 (2019) 208–219.
[314] L. Chen, N. Song, L.Y. Shi, P. Ding, Compos. Part A-Appl. Sci. Manuf. 112 (2018) 18–24.
[315] J. Klett, R. Hardy, E. Romine, C. Walls, T. Burchell, Carbon 38 (2000) 953–973.
[316] M. Karthik, A. Faik, P. Blanco-Rodriguez, J. Rodriguez-Aseguinolaza, B. D'Aguanno, Carbon 94 (2015) 266–276.
[317] M. Karthik, A. Faik, B. D'Aguanno, Sol. Energy Mater. Sol. Cells 172 (2017) 324–334.
[318] Y.J. Zhao, X. Min, Z.H. Huang, Y.G. Liu, X.W. Wu, M.H. Fang, Energy Build. 158 (2018) 1049–1062.
[319] Z.M. Shen, J.C. Feng, Compos. Sci. Technol. 170 (2019) 135–140.
[320] Y.G. Ouyang, G.L. Hou, L.Y. Bai, B.Q. Li, F.L. Yuan, Compos. Sci. Technol. 165 (2018) 307–313.
[321] H.Z. Hong, Y. Pan, H.X. Sun, Z.Q. Zhu, C.H. Ma, B. Wang, W.D. Liang, B.P. Yang, A. Li, Sol. Energy Mater. Sol. Cells 174 (2018) 307–313.
[322] D.Z. Wang, Y. Lin, D.W. Hu, P.K. Jiang, X.Y. Huang, Compos. Part A-Appl. Sci. Manuf. 130 (2020) 105754.
[323] X.Y. Huang, C.Y. Zhi, P.K. Jiang, J. Phys. Chem. C 116 (2012) 23812–23820.
[324] S.Y. Yang, W.N. Lin, Y.L. Huang, H.W. Tien, J.Y. Wang, C.C.M. Ma, S.M. Li, Y.S. Wang, Carbon 49 (2011) 793–803.
[325] L. Tang, M.K. He, X.Y. Na, X.F. Guan, R.H. Zhang, J.L. Zhang, J.W. Gu, Compos. Commun. 16 (2019) 5–10.
[326] J.C. Li, X.Y. Zhao, W.J. Wu, Z.X. Zhang, Y. Xian, Y.T. Lin, Y.L. Lu, L.Q. Zhang, Carbon 162 (2020) 46–55.
[327] H. Im, J. Kim, Carbon 50 (2012) 5429–5440.
[328] C.C. Teng, C.C.M. Ma, K.C. Chiou, T.M. Lee, Y.F. Shih, Mater. Chem. Phys. 126 (2011) 722–728.
[329] L. Chen, Y.Y. Sun, J. Lin, X.Z. Du, G.S. Wei, S.J. He, S. Nazarenko, Int. J. Heat Mass Transf. 81 (2015) 457–464.
[330] J.J. Che, M.F. Jing, D.Y. Liu, K. Wang, Q. Fu, Compos. Part A-Appl. Sci. Manuf. 112 (2018) 32–39.
[331] Z.G. Wang, F. Gong, W.C. Yu, Y.F. Huang, L. Zhu, J. Lei, J.Z. Xu, Z.M. Li, Compos. Sci. Technol. 162 (2018) 7–13.
[332] F. Yan, L. Liu, M. Li, M.J. Zhang, L.H. Xiao, Y.H. Ao, J. Mater. Sci. 53 (2018) 8108–8119.
[333] F.M. Guo, X. Shen, J.M. Zhou, D. Liu, Q.B. Zheng, J.L. Yang, B.H. Jia, A.K.T. Lau, J.K. Kim, Adv. Funct. Mater. 30 (2020) 1910826.
[334] J. Yue, J.K. Pan, Y.H. Deng, J. Li, J.J. Bao, J. Appl. Polym. Sci. 136 (2019) 47118.
[335] L. Yang, Y. Zhng, M. Hou, W.Y. Chen, Z.Q. Wang, Am. J. Polym. Sci. Technol. 5 (2019) 9–15.
[336] P. Wang, H.D. Chong, J.J. Zhang, H.B. Lu, ACS Appl. Mater. Interfaces 9 (2017) 22006–22017.
[337] A. Li, C. Zhang, Y.F. Zhang, Compos. Part A-Appl. Sci. Manuf. 101 (2017) 108–114.
[338] H. Yuan, Y. Wang, T. Li, Y.J. Wang, P.M. Ma, H.J. Zhang, W.J. Yang, M.Q. Chen, W.F. Dong, Nanoscale 11 (2019) 11360–11368.

Fei Zhang received his BS degree (2012) and MS degree (2015) in the Department of Chemistry and Chemical Engineering from Hunan University of Science and Technology. He obtained his PhD degree from the group of Prof. Wei Feng at the School of Materials Science and Engineering, Tianjin University in 2019. He held an academic position at The Chinese University of Hong Kong, Shenzhen in 2020. His current research is focus on the field of carbon based thermal conductive composite and its integrated applications.

Prof. Yiyu Feng is a research professor at the School of Materials Science and Engineering, Tianjin University. He obtained his PHD degree form Tianjin University in 2009 and held an academic position at Tianjin University in 2009. He has authored and co-authored over 90 academic articles and reviews. Currently, his research is focused on solar-thermal conversion and thermal interfacial materials and composites, as well as their application in heat-control systems.

Prof. Wei Feng is a full professor at School of Materials Science and Engineering of Tianjin University (China). He obtained his Ph.D. from the Xi'an Jiaotong University (China) in 2000. Then, he worked at Osaka University and Tsinghua University as a Japan Society for the Promotion of Science (JSPS) fellow and a postdoctoral researcher, respectively. His research interests include photo-responsive organic molecules or their derivatives, thermal-conductive and high-strength carbon-based composites, and two-dimensional fluorinated carbon materials or polymers. He was a recipient of the program for New Century Excellent Talents in University of Ministry of Education of China (2006), the "Ten-Thousand Talent Program" leading innovators of China (2018), the Young and middle-aged leading scientists of Ministry of Science and Technology of China (2017), the "131" Innovative Talent of Tianjin (2015), and senior visiting scholar of JSPS (2008). He has authored or coauthored 160 peer-reviewed SCI publication and recently published articles/reviews in Chem. Soc. Rev., Nat. Commun., Prog. Mater. Sci., Adv. Funct. Mater., Adv. Sci., J. Mater. Chem. A, etc., as a corresponding author. He holds over 60 Chinese patents and received the First Prize of Technical Innovation Award in Tianjin at 2015 and 2017, and the Second Prize of Natural Science Award in Tianjin at 2007 and 2011. As for the professional offices and services, he is serving as member of Science & Technology Commission of Ministry of Education, Evaluation Expert of National Found Program, and Chairman of Committee on thermal conductive Composite Materials, Chinese Society for Composite Materials.